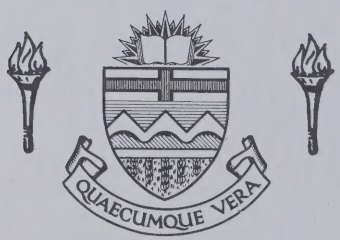

THE UNIVERSITY OF ALBERTA

POLARIZED FLUORESCENCE FROM THE CYTOPLASM OF LYMPHOCYTES

by

© ROBIN BRUCE BARNETT

A THESIS

SUBMITTED TO THE FACULTY OF GRADUATE STUDIES AND RESEARCH

IN PARTIAL FULFILMENT OF THE REQUIREMENTS FOR THE DEGREE

OF MASTER OF SCIENCE

DEPARTMENT OF PHYSICS

EDMONTON, ALBERTA

FALL, 1977

To my Mother and Father . . .

for their encouragement

ABSTRACT

Polarized fluorescence from the cytoplasm of human lymphocytes was studied using a modified fluorescence spectrophotometer. This technique was developed by Cercek for measuring antigen/mitogen-induced changes in the average microviscosity of the cytoplasm and has been proposed as a diagnostic test for cancer (5).

Experiments were performed with a Perkin-Elmer MPF-4 fluorescence spectrophotometer equipped with a thermostatted sample holder and a polarization accessory.

The spectrophotometer method was found to be unreliable for accurately determining the polarization of fluorescence from the cytoplasm. Specifically, filtrate fluorescence was found to vary with the method of filtration. Syringe, suction and gravitational filtration techniques were tried.

A semi-analytical technique was then developed for determining the polarization from the cytoplasm. This method was found to be more consistent than the former but had limited application for antigen/mitogen-stimulated systems. The method assumes that the polarization from the cytoplasm remains constant and that the rate of diffusion of fluorescein across the cell membrane is directly proportional to the intracellular concentration. Using the analytical method, the variation of the polarization of fluorescence from the cytoplasm with the pH, osmolarity and temperature of the supporting medium were found.

ACKNOWLEDGEMENTS

I would very much like to thank Dr. T. A. McPherson and the Research Unit at the Dr. W. W. Cross Cancer Institute. Without their financial and technical assistance this project would not have been possible.

I am indebted to Dr. Andrew Shaw for a tremendous amount of individual assistance and advice.

I would also like to thank Chairman John Charnock and the Department of Pharmacology for the use of their fluorescence spectrophotometer and other facilities.

I would especially like to thank Dr. Sid Usiskin, my supervisor, and Dr. John Scrimger for their encouragement and personal help throughout my program at the University of Alberta.

I wish to thank Diana Zaiffdeen for her immaculate typing of this manuscript.

Finally, I would like to thank Jan, for her patience and perseverance throughout the course of this work.

TABLE OF CONTENTS

LIST OF TABLES

LIST OF FIGURES

CHAPTER ONE

INTRODUCTION

1.1 CANCER DIAGNOSIS AND THE SCM TEST

A test which reliably distinguishes cancer patients from those suffering from nonmalignant disorders, is simple to perform, and requires only a few milliliters of peripheral blood, would revolutionize cancer diagnosis. Such a test has been reported by L. Cercek, B. Cercek and C. I. V. Franklin (5), and L. Cercek, B. Cercek and J. V. Garrett (8), and is known as the structuredness of cytoplasmic matrix or SCM test.

The SCM test was developed by the Cerceks (9-14) and employs the technique of fluorescence polarization. Using this technique, cells are irradiated with plane polarized light, and the polarization of fluorescence is simultaneously measured from fluorescein molecules in the cytoplasm. According to a classical theory by Einstein and Perrin (35), the polarization of fluorescence is related to the viscosity (η) by $1/P \propto 1/\eta$ (a complete description is given in Appendix C). However, since the cytoplasm is a heterogeneous, polyphasic medium, the polarization of fluorescence from the cytoplasm more accurately represents the average microviscosity or so-called "structuredness." The extent of the cytoplasm for a typical mammalian cell is shown in Figure 1.

The application of the SCM test is based on the principle that stimulatory molecules interacting with receptors on the cell surface induce changes in the average microviscosity of the cytoplasm. Cercek

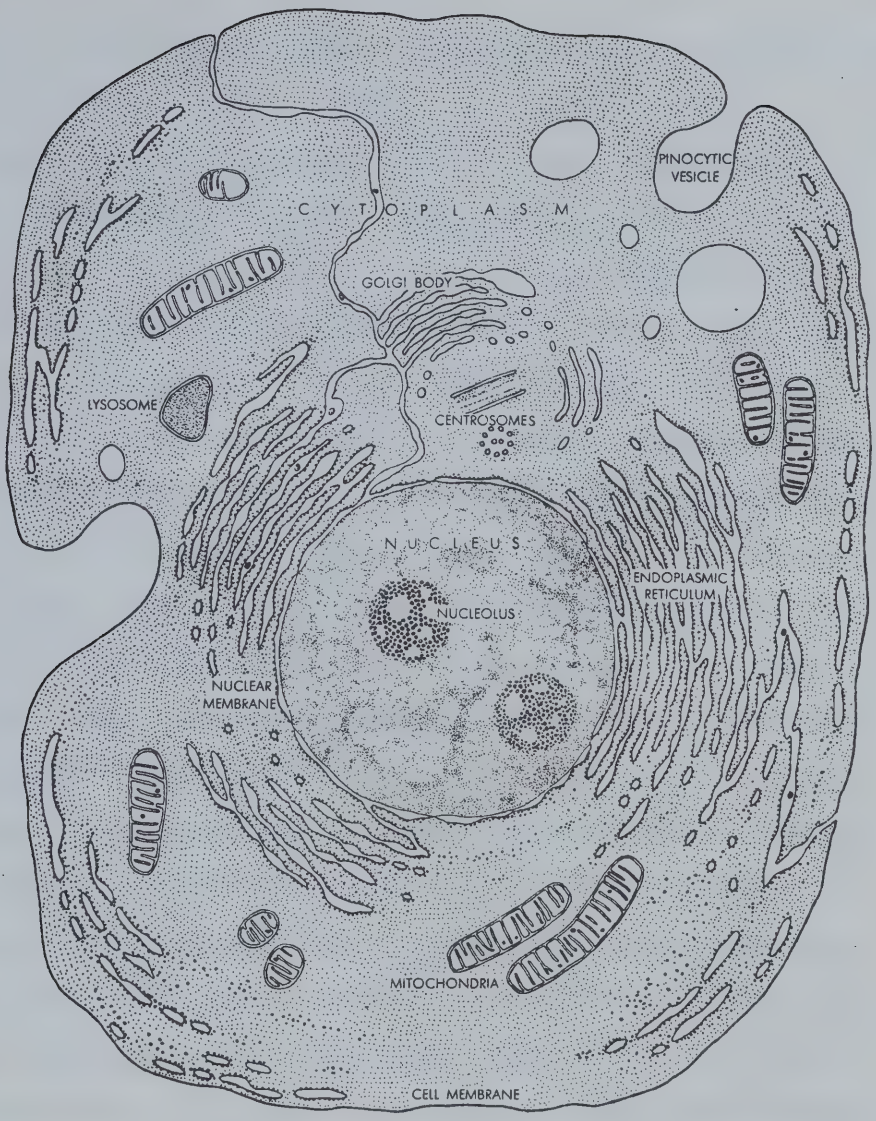

FIGURE 1. The extent of the cytoplasm for a typical mammalian cell.

(From Brachet: Scientific American, 55 :205,1961)

et al. (8) found that they could distinguish between normal subjects and those suffering from chronic lymphatic leukemia on the basis of differences in the SCM following exposure of their lymphocytes to the mitogen phytohaemagglutinin (PHA). Normal subjects showed reduced SCM whereas cancer patients did not. Extending their studies to other malignancies, they demonstrated that lymphocytes from 41 patients known to have neoplastic disease of breast, bladder, bone, brain, ovary, uterus, larynx, oral cavity, lung or skin showed no decrease in SCM in response to PHA while lymphocytes from 70 of 71 healthy donors, and all of 17 patients with non-neoplastic diseases responded with a characteristic decrease (5). Field and Caspary (20) had previously shown that encephalitogenic factor (EF) and cancer basic protein (CaBP) could distinguish cancer patients from healthy volunteers using the macrophage electrophoretic mobility (MEM) test. Their assay also utilised small quantities of peripheral blood but was extremely difficult to perform and had the added disadvantage of failing to discriminate between malignancy, and neurodegenerative disorders. The Cerceks employed EF and CaBP in the SCM test and found the reciprocal effect to PHA: cancer patients lymphocytes showed a reduction in SCM but cells from normal volunteers did not. This prompted the Cerceks to combine the responses to PHA and CaBP as a single parameter, the SCM response ratio (RR_{SCM}). The RR_{SCM} is the ratio of the polarization of fluorescence from the cytoplasm following exposure to CaBP to that following exposure to PHA (5). The ratio for donors without neoplastic disease ranges from 1.2 to 1.7, whereas cancer patients have values between 0.6 and 0.9. Although either response appears to reliably detect malignancy, the Cerceks felt

the response ratio sharpened resolution. RR_{SCM} values were used to monitor patients' lymphocytes after surgical removal of malignant tissues (6). Values were determined before and after operation. Surprisingly, 5 out of 6 patients showed a progressive increase in RR_{SCM} which reached the healthy range within two weeks of operation. This suggests that the test could be a useful monitor of the adequacy of surgery. A further claim is the possible application of the test to screen for premalignant conditions (6). In 8 out of 12 patients with histologically declared benign growths of the breast, the RR_{SCM} values were typical of malignant conditions. It was suggested that these might represent premalignant lesions. That the aberrant values from benign lesions questioned the interpretation placed on the results from malignant cases was not entertained. More recently, the Cerceks have demonstrated that decreased SCM can be elicited by stimulation with known tissue of the appropriate histological type (7). The specificity of response is illustrated by the demonstration that lymphocytes from patients with basal cell carcinoma responded to basal cell carcinoma tissue but not to squamous cell tissue. This suggests that the cells recognise tumour-specific antigens and broadens the diagnostic potential of the test enabling the type of malignancy to be determined.

Although the Cerceks have not attempted a mechanistic explanation of the SCM phenomenon they clearly imply it has an immunological basis. By studying SCM values in single cells (15) with a microscope-fluorometer equipped with plane polarising filters, they have been able to show that 15-23% of the lymphocytes from cancer patients respond to CaBP compared to 3-5% of the lymphocytes from healthy donors. The magnitude of the

response would appear to exclude participation of T (thymus-derived) lymphocytes through direct stimulation of membrane receptors for antigen, but could be compatible with the stimulation of cells having "passively" adsorbed antibody with antigen affinity. The difference in percentage response to PHA is less dramatic, normals having 45-54% of their lymphocytes showing decreased SCM compared to 36-45% of the lymphocytes from cancer patients. Since the overall response to PHA in cancer patients is negligible the degree of response per cell must be very small. Cancer patients frequently show normal PHA responses in the more conventional thymidine incorporation assay, suggesting that the SCM test is measuring a parameter unrelated to the blastogenic response.

Despite the uncertainty surrounding the underlying principles, the diagnostic potential of the test is clear and warrants a stringent investigation. As of yet, no critical evaluation of the SCM test has been reported. It was therefore the purpose of this study to investigate the methodology of the SCM test and to standardize the procedure for possible clinical implementation. Specific objectives were:

(i) To provide a standard procedure for measuring the polarization of fluorescence from the cytoplasm.

(ii) To measure the average polarization of fluorescence from the cytoplasm of human lymphocytes and to obtain the normal variation.

(iii) To establish the sensitivity of the average polarization of fluorescence with respect to variation in the temperature, pH, and osmolarity of the supporting medium.

CHAPTER TWO

INSTRUMENTATION AND EXPERIMENTAL TECHNIQUE

2.1 INSTRUMENTATION

2.1.1 General Requirements

The main difficulty in measuring polarized fluorescence from the cytoplasm of cells is due to Förster transfer (Appendix C.2). Förster transfer is an energy exchange between molecules that depolarizes fluorescence and occurs when the concentration of fluorescent solute exceeds a certain critical value. In order to attain a measurable polarization from a system of cells, it is therefore important that the intracellular dye concentration does not exceed the critical amount. In general, this concentration is low (10^{-4} M) and polarization measurement requires high optical sensitivity.

The study of polarized fluorescence from biological systems is relatively recent and, as such, there are no instruments available specifically for this purpose. There are several existing devices that can be modified, however, and these include the fluorescence microscope, the cytofluorograf, and the fluorescence spectrophotometer.

The fluorescence microscope enables the user to observe and quantitatively measure fluorescence from the cytoplasm of cells. This instrument can be modified for polarization study by adding two plane polarizing filters to the original optics. A schematic is shown in Figure 2. With the modified microscope, it is possible to measure the

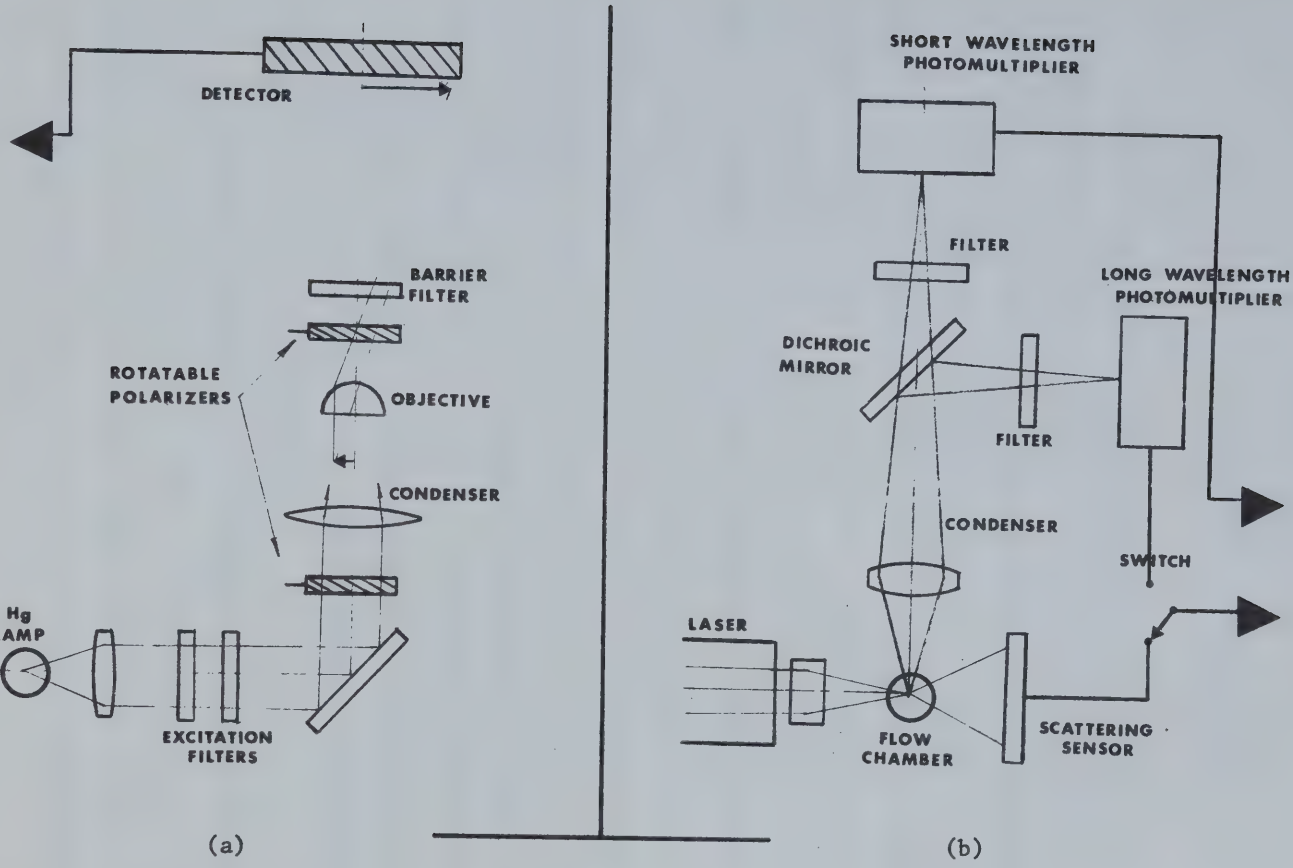

FIGURE 2 . Optical layouts for: (a) Fluorescence microscope (b) Cytofluorograf

polarization of fluorescence from single cells. Cercek (15) has recently done this with human lymphocytes using a modified Zeiss microscope-flourometer/01.

The disadvantage with this technique is that the microscope must be realigned for every cell that is examined. Consequently, the analysis of a large number of cells becomes tedious and impractical.

The cytofluorograf, as an alternative, is designed to analyse cells rapidly and automatically. A built-in laminar flow system provides typical sampling rates of 10^5 cells/minute (Bio/Physics Systems Inc.). The cytofluorograf is optically bi-functional and is primarily used for cell differentiation and counting. A diagram of the instrument is shown in Figure 2. To provide maximum sensitivity, a laser is used for excitation and, as each cell traverses the laser beam, it absorbs and scatters light relative to its morphology and stain uptake. At the choice of the user, the cytofluorograf simultaneously records either the fluorescent intensity at two different wavelengths (red and green), or the fluorescent intensity at one wavelength and forward angle scatter. In this way each cell is stored with two separate co-ordinates and can be later displayed on an oscilloscope.

In spite of its potential usefulness for polarization studies, the cytofluorograf has limited optical sensitivity. This can be directly attributed to the rate of sampling and to the amount of signal obtainable from individual cells. For this reason, the cytofluorograf was not chosen for instrumentation.[1]

---

[1]A group headed by Dr. A. Norman at the University of California is currently using a modified cytofluorograf to measure the polarization of fluorescence from cells. Direct correspondence (32) with this group confirms the sensitivity limitation of the instrument.

2.1.2 Fluorescence Spectrophotometer

The most feasible method of measuring the polarization of fluorescence from a large number of cells is using a fluorescence spectrophotometer. Although this instrument is mainly used for luminescence spectroscopy, it is readily extensible to fluorescing biological systems. The spectrophotometer is designed so that for sufficiently dilute solutions (where secondary absorption is negligible) the recorded fluorescence intensity is directly proportional to sample concentration,

$$\text{i.e.} \quad I = I_0 \cdot K \cdot \ell \cdot \varepsilon \cdot \phi_F \cdot c \qquad (2.1.1)$$

where K is a constant of the instrument, I_0 is the incident intensity, ℓ is the optical path length of the cuvette, and where ε, ϕ_F and C are the extinction coefficient, quantum efficiency, and concentration, respectively, of the sample. The quantities ε and ϕ_F depend on molecular structure and this topic is discussed in Appendix B.2. Most spectrophotometers employ right angle optics (emission recorded at right angles to the direction of excitation) and these can easily be modified for polarization study by inserting a plane polarizing filter before and after the sample holder.

The main advantage in using the spectrophotometer is that the fluorescent intensity from a large number of cells (10^6) can be measured simultaneously. This means that the average intracellular dye concentration can be far lower than for single cell measurement which alleviates the problem of depolarization by Förster transfer. Additional advantages of the instrument include the optical versatility of separate excitation and emission monochromators and the facility of temperature control.

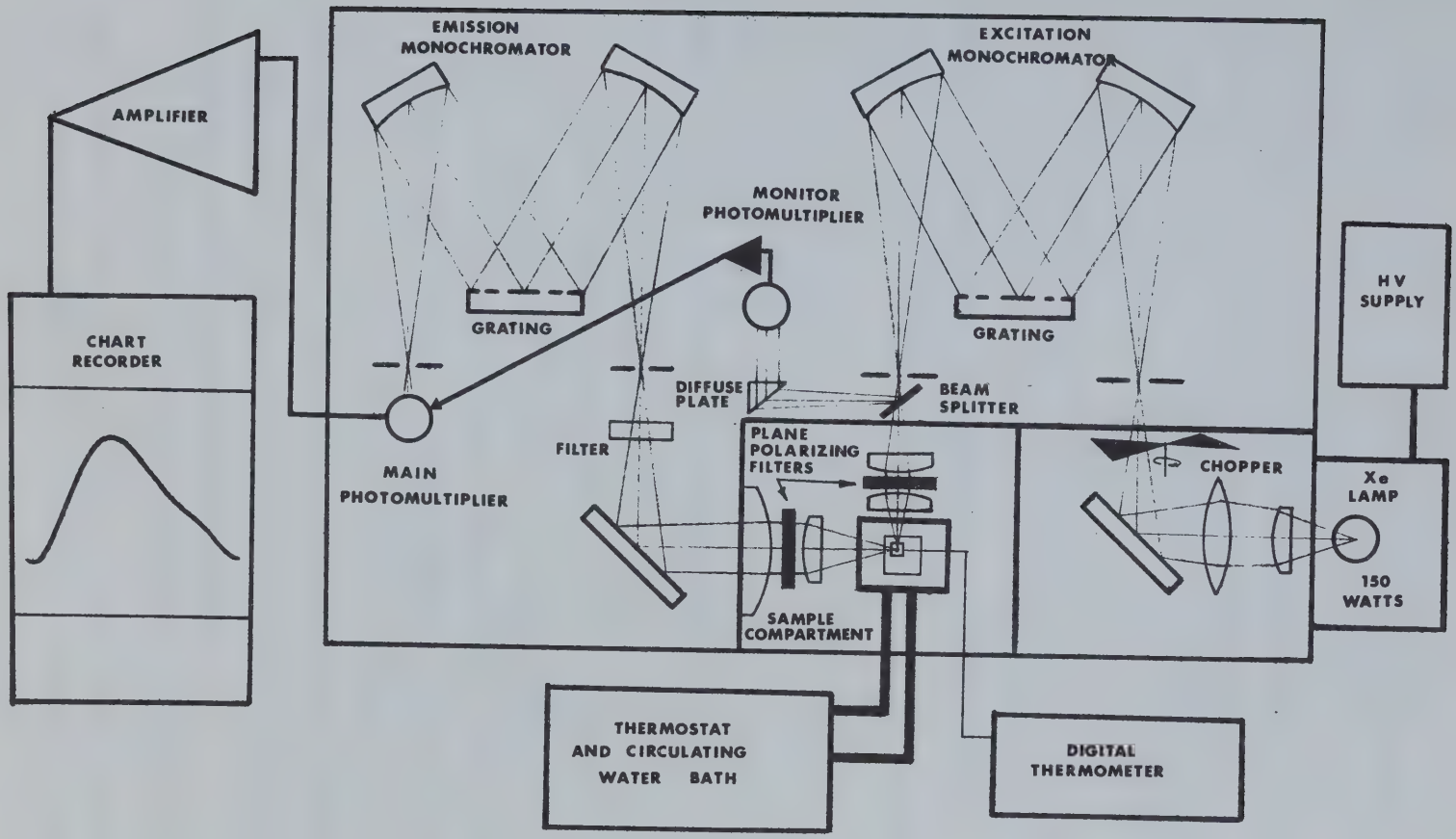

FIGURE 3 . Fluorescence Spectrophotometer

The difficulty with this method is that it introduces a background fluorescence comparable to the signal emitted by the cells. This is due to the amount of fluorescent dye that diffuses from the cells into the supporting medium. Consequently, considerable analysis must be performed to determine the polarization of fluorescence from the cytoplasm (Sections 2.4 and 2.5).

Of the spectrophotometers commercially available, a Perkin-Elmer MPF-4 was chosen because of its sensitivity and overall versatility. This instrument was generously provided by Dr. John Charnock of the Department of Pharmacology. A diagram of the complete apparatus is shown in Figure 3.

The source of excitation in the MPF-4 is a 150 watt continuous Xe arc. This light source is modulated at 56 HZ by an optical chopper to prevent 60 cycle interference during signal amplification. To enable monochromatic excitation and emission analysis, the instrument utilizes two precision Czerny-Turner monochromators. The reflection gratings comprising these are ruled vertically at 1200 lines/mm and are blazed at 300 nm. Each monochromator was calibrated with the 450.1 nm peak of the Xe source and both were accurate to within .5 nm. The entrance and exit slits for both excitation and emission monochromators are continuously adjustable and provide a spectral bandwidth from 0 to 20 nm. To eliminate scattered second order radiation, a selection of filters are provided preceding the emission monochromator.

The photometric part of the instrument is designed so that a small portion of the excitation light is reflected by the beam splitter to a reference photomultiplier. The resulting electrical signal is then

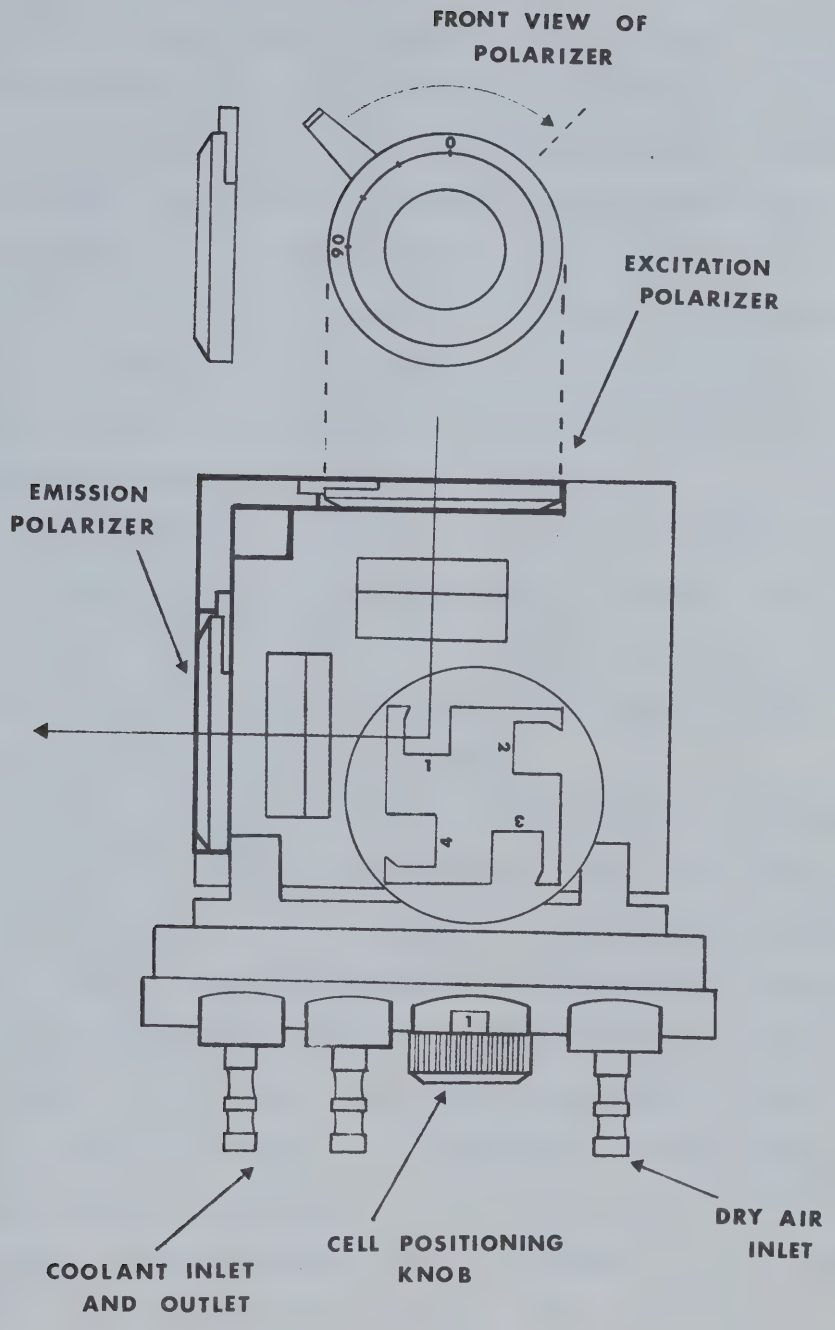

FIGURE 4 . Sample compartment and polarization accessory for the fluorescence spectrophotometer.

amplified and becomes part of a negative feedback circuit that controls the dynode voltage of the main photomultiplier. This feature enables the instrument to compensate for source intensity fluctuation. The main photomultiplier in the MPF-4 is an R446F wide range (200-900 nm) with a high red response. A separate amplifier controls the sensitivity of the instrument and amplifies the signal from the main photomultiplier. This unit also supplies the high voltage to the photomultipliers and contains the dynode voltage feedback circuitry. The output of the amplifier was displayed on a Perkin-Elmer 056 chart recorder.

The temperature of the sample compartment was controlled with an external ethylene-glycol reservoir which was continuously pumped through the base of the sample holder. A Haake regulator was used to maintain the temperature of the external bath and cuvette temperature was monitored by a Fluke digital thermometer.

The polarizing filters that were fitted in the sample compartment are manufactured by Polacoat and consist of a transparent quartz substrate coated with a 16 micron layer of a dichroic film. These filters provide a large working aperture (1" diameter) and are designed to polarize efficiently through wide angles of incidence. An "L" shaped holder positions the filters in the sample compartment and allows them to rotate through 90° (Figure 4). Each polarizer is calibrated in 30° increments from the pass direction which is indicated by a "0" on the outer edge. A restraining lever, which is fastened at 45° to the pass direction, allows the filters to transmit either vertically or horizontally polarized light in their extreme positions. The actual filter transmission is about 30% in the visible range.

For all measurements done with the spectrophorometer, fused silica (SiO_2), fluorescence free cuvettes were used. The cuvettes have a sample path length of 10 mm and are designed to hold a volume of 4 ml (12.5 mm x 12.5 mm x 45 mm outside dimensions).

2.2 PREPARATION OF LYMPHOCYTES

A normal adult has approximately 7×10^6 leukocytes per milliliter of blood. Since lymphocytes make up about 30% of all the white blood cells (Table I), this represents a maximum possible yield of 2.1×10^6 lymphocytes per milliliter. The most common method of preparing lymphocytes is using a density-gradient separation (23). With this technique, the cells are separated by centrifugation according to their sedimentation rates.

In general, the sedimentation rates of cells are determined by size rather than density and sedimentation is greatly enhanced if a cell type can be induced to aggregate. Solutions of Ficoll 400 are used for lymphocyte preparation because of its ability to promote erythrocyte aggregation. There are several Ficoll solutions commercially available and of these Ficoll-Paque (Pharmacia) was found to be the most effective. Ficoll-Paque is an aeuqous solution of density $1.077 \pm .001$ g/cm^3 containing 5.7 g Ficoll and 9 g diatrizoate sodium in every 100 ml. The function of diatrizoate sodium is to provide the optimal density and osmolarity necessary for the efficient removal of other cells from the lymphocytes.

To obtain the most homogeneous lymphocyte preparations, the following procedure was used:

AVERAGE WHITE BLOOD CELL PERCENTAGES FOR NORMAL ADULT (FROM GUYTON(22))	
CELL TYPE	% FROM TOTAL OF 7×10^3 WBC/mm^3
POLYMORPHONUCLEAR NEUTROPHILS	62.0 %
EOSINOPHILS	2.3 %
BASOPHILS	.4 %
MONOCYTES	5.3 %
LYMPHOCYTES	30.0 %
IN ADDITION THERE ARE: 3×10^5 PLATELETS/mm^3 BLOOD 5.4×10^6 RBC/mm^3 BLOOD	

TABLE I

Whole blood (10-20 ml) was collected in sterile vials and swirled over glass beads to catalyze clotting. Upon formation, the clots (and thus platelets) were removed and the remaining blood was added to test tubes containing carbonyl iron (10 mg iron/ml blood). These tubes were agitated at 37° C for 10 minutes allowing granulocytes, monocytes, and macrophages to phagocytize the iron particles. The blood was then mixed with 3% plasma gelatin (75% blood, 25% gelatin) and left to stand at 37° C for approximately 30 minutes. During this time the plasma gel causes the erythrocytes to aggregate and these, along with the iron-saturated leukocytes, settle out under the force of gravity.

The supernatant of the resulting suspension was gently layered onto Ficoll-Paque (3 ml Ficoll-Paque/3.5 ml blood in 1.5 cm diameter siliconized glass test tubes) and centrifuged at 400 g for 35 minutes at 18° C. This process forces out the remaining erythrocytes and granulocytes and causes the lymphocytes to collect at the interface of the suspension system.

The lymphocytes were then carefully extracted with a pasteur pipette and washed with Hank's balanced salt solution (3 ml lymphocytes/ 7 ml Hank's). To complete the wash, the cells were recentrifuged at 300 g for 10 minutes and finally suspended at room temperature in Medium 199 (Gibco).

Cell counts were done with an autocytometer (Fischer) and were periodically checked with a haemocytometer. Cell viability was determined using the technique of fluorochromasia (37) and cell purity was determined by direct examination with a microscope. Typical yields of $.7 \times 10^6$ lymphocytes/ml whole blood were obtained with this method and cell viability and purity were usually greater than 95%.

2.3 HYDROLYSIS KINETICS OF FDA BY LYMPHOCYTES

2.3.1 Staining Technique

In order to measure the polarization of fluorescence from a suspension of cells, it is necessary to stain the cytoplasm with a fluorescent dye. This can be done by immersing the cells in a solution containing a non-fluorescent flurogenic substrate. As the substrate diffuses into the cells, it is degraded by enzymes to yield a fluorescent end product. Rotman and Papermaster (37) have studied this process using various fluorescein esters of fatty acids. They found that the best substrate for staining was fluorescein diacetate (FDA). This ester is non-polar and rapidly diffuses across the cell membrane where it is enzymatically hydrolised to produce the fluorescent anion fluorescein^{--} (21). Because of its polarity, the outward diffusion of fluorescein is a much slower process than the inward flux of FDA. Consequently, the rate of production of fluorescein exceeds the rate of outward diffusion and the difference between these rates results in a net intracellular accumulation.

Fluorescein is extensively used for staining because it has a high quantum efficiency (ϕ_F = .80) and because it is not harmful to cells. This dye is particularly good for polarization studies because it does not complex to structures in the cell and is found uniformly distributed throughout the cytoplasm. Furthermore, fluorescein can be excited by visible light (470-475 nm) and irradiating cells in this range produces no damaging photolytic effects.

2.3.2 Michaelis-Menten Kinetics

The enzymatic hydrolysis of FDA can be described by:

$$FDA + E \underset{K_2}{\overset{K_1}{\rightleftharpoons}} (FDA)E \xrightarrow{K_3} F + E + 2A \qquad (2.3.1)$$

where (FDA)E is an intermediate enzyme-substrate complex and where F and A represent fluorescein and acetic acid respectively. For most enzyme reactions, the rate of formation of the enzyme-substrate complex is directly proportional to the free enzyme and substrate concentrations. Thus, the rate of change in the concentration of (FDA)E can be written:

$$\frac{d[(FDA)E]}{dt} = K_1 \cdot [E - (FDA)E] \cdot [FDA] - (K_2 + K_3) \cdot [(FDA)E] \qquad (2.3.2)$$

where [E - (FDA)E] is the free enzyme concentration.

According to the Michaelis-Menten formulation (31), the reaction described by equation (2.3.1) quickly reaches a steady state. This occurs when $\frac{d[(FDA)E]}{dt} = 0$, and the steady state concentration of (FDA)E is given by:

$$[(FDA)E]_{ss} = \frac{[FDA] \cdot [E]}{[FDA] + \frac{K_2 + K_3}{K_1}} = \frac{[FDA] \cdot [E]}{[FDA] + K_m} \qquad (2.3.3)$$

where $K_m = \frac{K_2 + K_3}{K_1}$ is defined as the Michaelis-Menten constant. During the steady state, the rate of formation of fluorescein is described by:

$$\frac{d[F]}{dt} = K_3 \cdot [(FDA)E]_{ss} \qquad (2.3.4)$$

and using equation (2.3.3):

$$\frac{d[F]}{dt} = \frac{K_3 \cdot [FDA] \cdot [E]}{[FDA] + K_m} \qquad (2.3.5)$$

Defining

$$V_{max} = \lim_{[FDA] \to \infty} \frac{d[F]}{dt} = K_3 \cdot [E] \qquad (2.3.6)$$

equation (2.3.5) can be modified to give:

$$\frac{d[F]}{dt} = \frac{V_{max} \cdot [FDA]}{[FDA] + K_m} \qquad (2.3.7)$$

or:

$$\frac{1}{\frac{d[F]}{dt}} = \frac{K_m}{V_{max}} \cdot \frac{1}{[FDA]} + \frac{1}{V_{max}} \qquad (2.3.8)$$

(Lineweaver-Burk modification (31))

Thus, for systems obeying Michaelis-Menten kinetics, the enzymatic hydrolysis of FDA can be completely described by the parameters K_m and V_{max} (equation 2.3.8), and these quantities can be obtained from a linear plot of $\left(\frac{d[F]}{dt}\right)^{-1}$ against $[FDA]^{-1}$. For cell systems, K_m and V_{max} depend on the number of cells (enzyme) that are used for the hydrolysis reaction. However, having calculated K_m and V_{max} for a particular number of cells, the kinetics can be determined for any number by knowing the substrate/cell ratio.

2.3.3 Experimental Determination of K_m and V_{max} for Lymphocytes

Because FDA is insoluble in water, stock solutions of 2.5×10^{-3} M FDA/acetone were prepared and stored at 4° C. Recrystallized FDA (Sigma) and 99% pure acetone (Fisher) were used for this purpose. Aqueous solutions (pH = 7.4) of FDA were made up by dissolving small volumes of the FDA/acetone solution in sterile phosphate buffered saline (PBS). Dilutions of approximately 1 in 10^4 produced minimal flocculation. Complete PBS (34, Table V) was used as a solvent for FDA/acetone because FDA is unstable in media with high amino acid content (Medium 199) and immediately forms a highly fluorescent background. This effect makes it impossible to detect the fluorescein produced by the cells. A similar problem occurs when penicillin streptomycin is added to FDA/PBS and for this reason the antibiotic was deleted from the medium.

Lymphocytes were prepared as in Section 2.2 and suspended in Medium 199 (Gibco) at concentrations of 5×10^6 cells/ml. Prior to incubation with FDA/PBS, the lymphocytes were kept in a water bath at 37° C.

For the kinetic study, the substrate concentration was varied from .25 μM to 10 μM FDA/PBS. Aliquots of .2 ml from the lymphocyte suspension were mixed with 2.8 ml of FDA/PBS and rapidly transferred in a cuvette to the sample holder of the spectrophotometer. The formation of fluorescein was recorded by irradiating the cells at 473 nm and monitoring the fluorescent intensity at 511 nm on the chart recorder. Measurements were taken for four minutes at 27° C. To determine the actual concentrations of fluorescein that were produced, a calibration curve was constructed using four fluorescein/PBS solutions of known

concentration. Since fluorescein is also insoluble in water, these solutions were prepared by first dissolving the fluorescein (Baker) in acetone and then dissolving small amounts of the acetone solution in PBS.

The formation of fluorescein for five different substrate concentrations is shown in Figure 5. As can be seen from the diagram, the curves are not exactly linear and therefore Michaelis-Menten kinetics do not strictly apply. By fitting the experimental curves to various analytical functions, and using the "minimum chi-squared" criterion, it was found that the best fit was a quadratic polynomial.[2] The quadratic coefficient of these polynomials is most significant for the higher substrate concentrations ($>10^{-6}$ M FDA/PBS) and this indicates that the hydrolysis reaction is inhibited when the intracellular fluorescein concentration becomes too high.

Rather than deleting the kinetics for substrate concentrations $> 10^{-6}$ M, K_m and V_{max} were determined by plotting $\left(\frac{d[F]}{dt}\right)^{-1}_{t=0}$ against $[FDA]^{-1}$. A least squares fit to the data is shown in Figure 6 and from the X and Y intercepts $K_m = 5.65 \times 10^{-6}$ M and $V_{max} = 6.89 \times 10^{-13}$ moles/s.

In Section 2.6.2, it is shown that after a four-minute incubation in FDA/PBS, and for a substrate/cell ratio of 7×10^{-15} moles FDA/cell, about 50% of the total fluorescein produced remains inside the cells. From Figures 5 and 6, this represents 2.02×10^{-11} moles of fluorescein, or for a population of 10^6 lymphocytes, about 2.02×10^{-17} moles/cell.

---

[2]For the analysis of the fluorescent intensity curves (Figure 5) a computer algorithm designed by Bevington (3) was used which provides a least squares fit to an arbitrary function. This program is listed in Fortran in Appendix D (Subroutine CURF). The experimental data were fitted to five different analytical functions including first, second, and third order polynomials, an exponential of the form $I(t) = A(1 - e^{-Bt})$, and the product of an exponential and a quadratic polynomial.

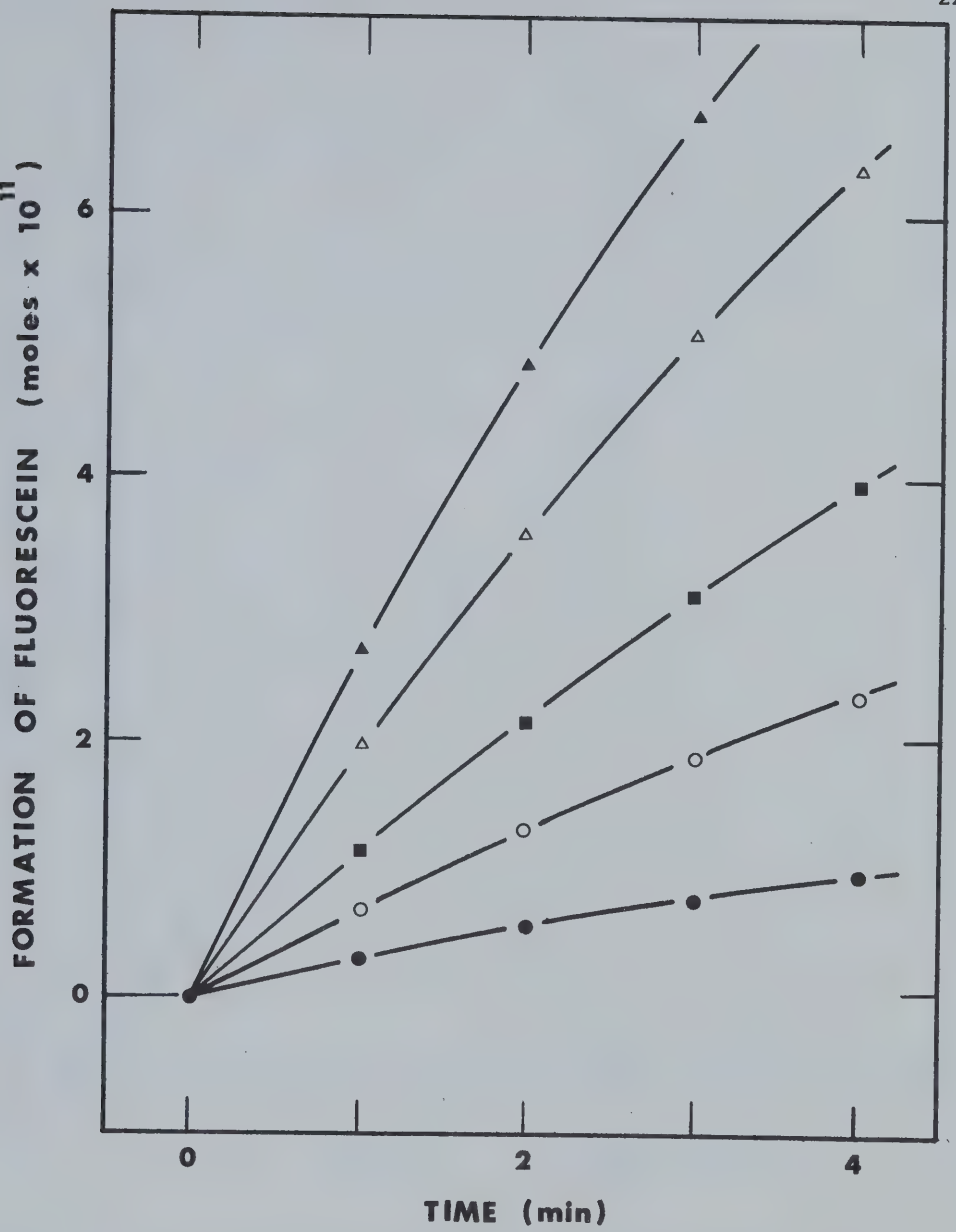

FIGURE 5 . Hydrolysis of FDA by lymphocytes. The reaction was observed at 27° C for substrate/cell ratios of; (●) 1.4×10^{-15}, (○) 2.8×10^{-15}, (■) 7×10^{-15}, (△) 1.4×10^{-14}, and (▲) 2.8×10^{-14} moles FDA/cell .

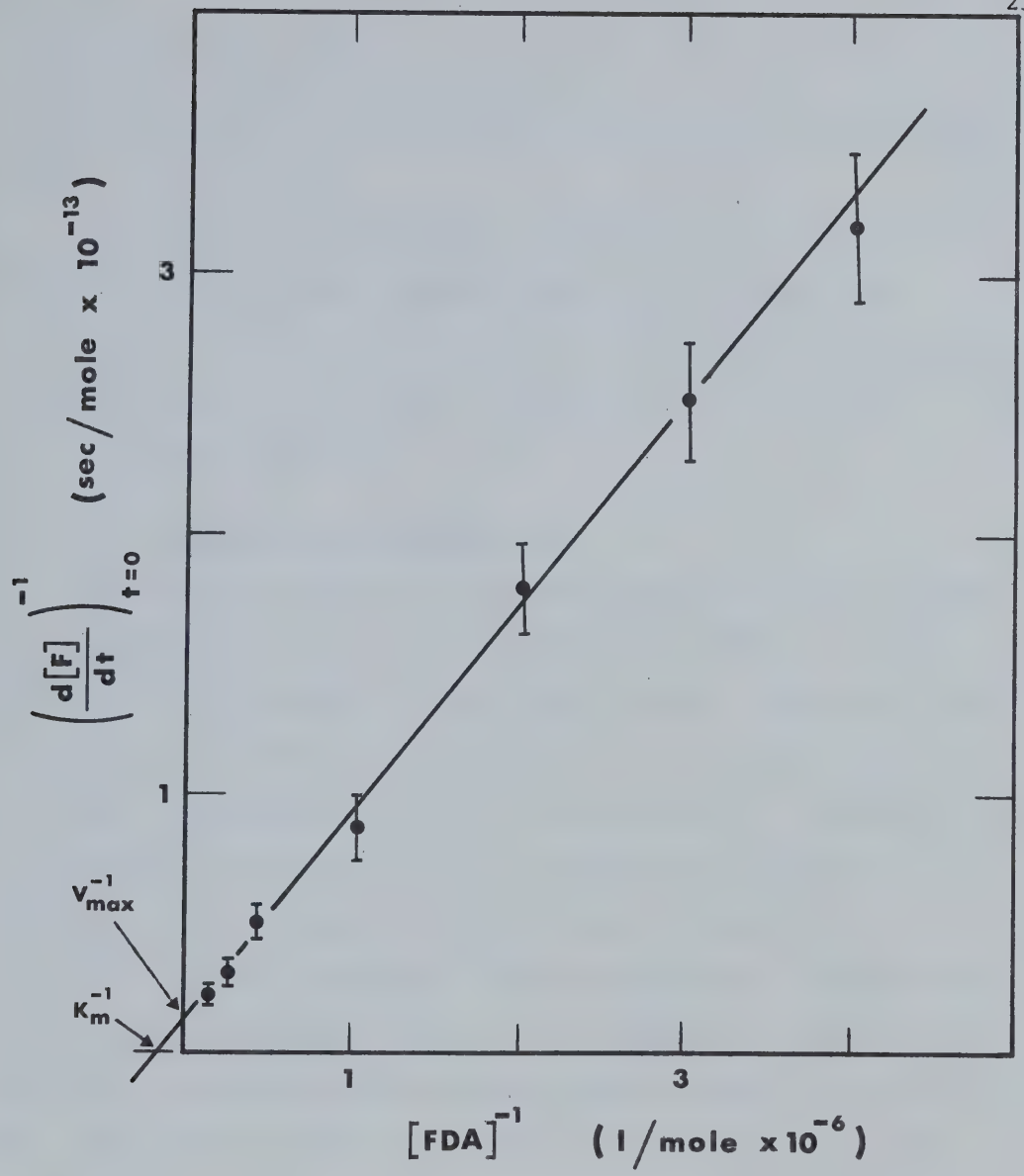

FIGURE 6 . Lineweaver-Burk plot for data appearing in Figure 5. K_m is the Michaelis-Menten constant and V_{max} is the maximum rate of hydrolysis of FDA .

Since the effective volume of a lymphocyte is 1.73×10^{-13} l, this amount of fluorescein corresponds to an average intracellular concentration of 1.17×10^{-4} M.[3]

As discussed in Appendix C.2, the polarization of fluorescence from fluorescein solutions begins to decrease for concentrations $> .3 \times 10^{-4}$ M. Thus, in order to attain an intracellular concentration below this value it is necessary to choose a substrate/cell ratio $\leq 7 \times 10^{-15}$ moles FDA/cell.

2.3.4 Relative Fluorescence Yield

Because of the relatively high cell concentrations that were used in these experiments, the fluorescence yield was studied to determine the effect of cell number. For this study, the cell concentration was varied from 1.67×10^5 to 1.33×10^6 lymphocytes/ml and the substrate/cell ratio was maintained at 7×10^{-15} moles FDA/cell. In each case the total amount of fluorescein that was produced from a four-minute incubation was appropriately scaled and compared to that for the 3.33×10^5 cells/ml concentration (arbitrary standard). The results of the experiment are shown in Figure 7. From Figure 7, it appears that the fluorescent intensity decreases for concentrations $> .67 \times 10^6$ cells/ml. It should be pointed out, however, that the data include a 3-5% scaling error and that the maximum loss in fluorescent intensity due to scattering was only 5%.

---

[3]The average diameter of a lymphocyte is approximately 10 μm and assuming the cells are spherical, this represents a volume of 5.24×10^{-13} l/cell. However, because the nucleus of a typical lymphocyte occupies 2/3 of the total volume, the actual volume of the cytoplasm is 1.73×10^{-13} l/cell.

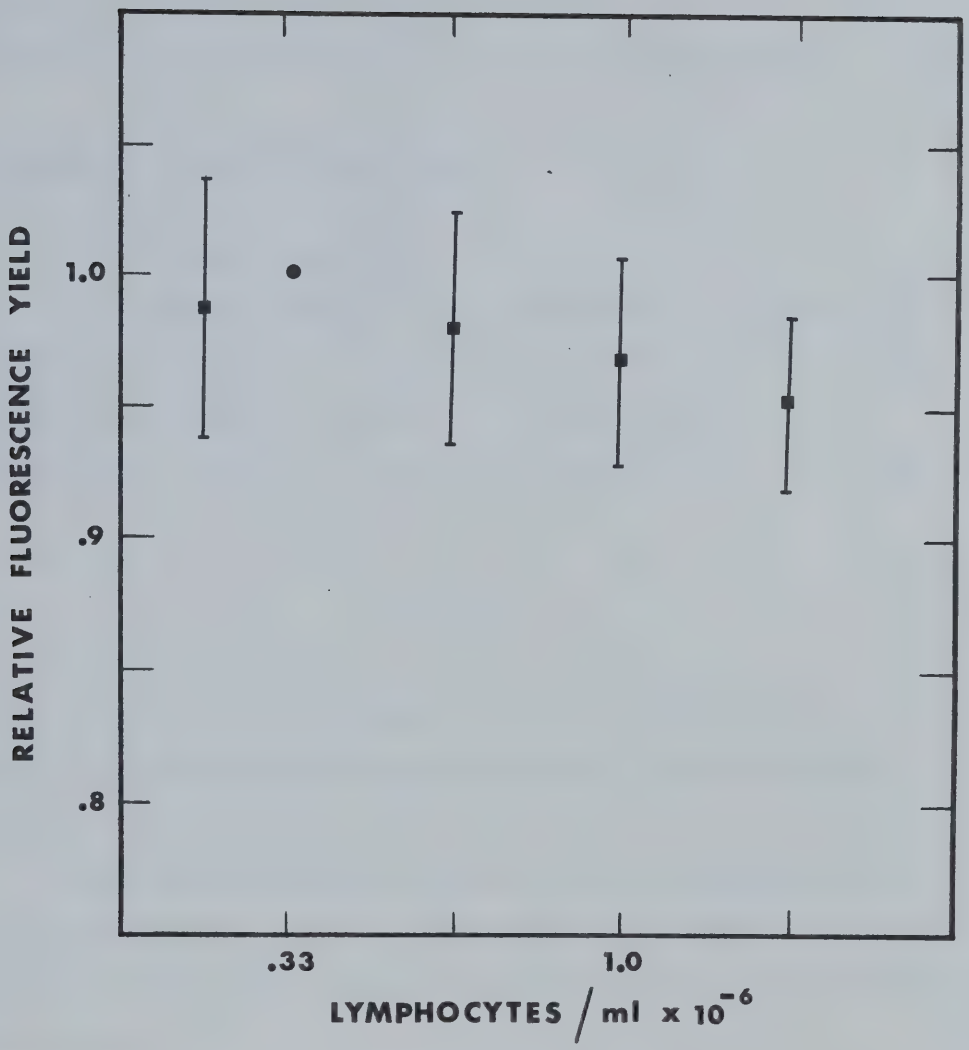

FIGURE 7 . Relative fluorescence yield. A cell concentration of $.33 \times 10^6$ lymphocytes/ml was chosen as an arbitrary standard.

The combined results of Figures 5, 6, and 7 indicate that the optimum substrate/cell ratio and cell concentration for polarization study are 7×10^{-15} ml/cell and 3.33×10^{5} cell/ml respectively.

2.4 MEASURING POLARIZED FLUORESCENCE

2.4.1 Grating Polarization

As described in Appendix C, the polarization of fluorescence is determined by exciting a sample with plane polarized light and analyzing the fluorescent intensity transmitted by a plane polarizing filter. More explicitly, the degree of polarization (equation (C.1.1)) is given by:

$$P = \frac{I_{\parallel} - I_{\perp}}{I_{\parallel} + I_{\perp}}$$

where $I_{\parallel}$ and $I_{\perp}$ are the fluorescent intensities transmitted by a polarizer whose pass direction is aligned parallel and perpendicular, respectively, to the electric field vector ($\vec{E}_0$) of the incident light.

To obtain the maximum polarization using the spectrophotometer, excitation is done with vertically polarized light. Hence, the reference directions for measuring $I_{\parallel}$ and $I_{\perp}$ are along the vertical and horizontal axes respectively.

There is a minor difficulty using the spectrophotometer in that both $I_{\parallel}$ and $I_{\perp}$ must pass through a grating monochromator before reaching the main photomultiplier (Figure 3). Consequently, $I_{\parallel}$ is significantly attenuated (relative to $I_{\perp}$) by the vertical rulings of the grating. To compensate for the asymmetric attenuation Azumi and McGlynn (1) have devised a simple procedure for obtaining a grating correction factor.

Their method is to excite with horizontally polarized light and to record the ratio of the vertical and horizontal fluorescent intensities transmitted by an emission polarizer. Designating these components as I_{HV} and I_{HH} respectively, the grating factor is defined by $G = I_{HV}/I_{HH}$. Because of the symmetry arising from horizontally polarized excitation (Appendix C) G should ideally be equal to 1 and any discrepancy is directly attributable to the grating. In practice G is always less than 1 and depends on the wavelength setting of the emission monochromator and to a lesser extent on the emission bandwidth (slit width). For a particular value of G, the degree of polarization is correctly given by:

$$P = \frac{I_{\parallel} - G \cdot I_{\perp}}{I_{\parallel} + G \cdot I_{\perp}} \qquad (2.4.1)$$

2.4.2 Experimental Procedure

The general procedure for measuring polarized fluorescence from a suspension of lymphocytes was the same as for the kinetics study done in Section 2.3.3.

Lymphocytes were prepared as in Section 2.2 and suspended in Medium 199 at a concentration of 5×10^6 cells/ml. Prior to incubation in FDA/PBS the cells were kept in a water bath at 37° C.

To minimize depolarization by Förster transfer a substrate/cell ratio of 7×10^{-15} moles FDA/cell was used. Aliquots of .2 ml of the lymphocyte suspension were added to 2.8 ml of 2.5×10^{-6} M FDA/PBS and transferred in a cuvette to the sample holder of the spectrophotometer. The cell suspension was irradiated at 473 nm with vertically polarized light (excitation polarizer in the "0" position as in Figure 4) and the fluorescent intensity components $I_{\parallel}$ and $I_{\perp}$ were recorded at 511 nm on

the chart recorder. Since $I_{\parallel}$ and $I_{\perp}$ could not be recorded simultaneously the emission polarizer was alternated at regular intervals between the "0" and "90" positions. Measurements were taken for approximately four minutes at 27° C.

A typical recorder printout is shown in Figure 8 where the data have been precorrected for grating attenuation. The solid segments of the $I_{\parallel}$ and $I_{\perp}$ curves represent the actual experimental data and the complete curves were obtained by fitting the data to quadratic polynomials (best least squares fit). The $I_{\parallel}^{e}$ and $I_{\perp}^{e}$ curves are hypothetical extracellular components to be described in Section 2.4.3.

Figure 8 also shows that there is a small naturally occurring background fluorescence from the FDA/PBS solution. This component provided a convenient means of determining the grating correction factor and the background polarization. With the emission monochromator set at 511 nm and using an emission bandwidth of 20 nm, G was calculated from the method of Azumi and McGlynn (1) to be .469 ± .002. The value of G was checked periodically over the course of an experiment.

From the $I_{\parallel}$ and $I_{\perp}$ data the total polarization of fluorescence as a function of time can be calculated by:

$$P(t) = \frac{I_{\parallel}(t) - I_{\perp}(t)}{I_{\parallel}(t) + I_{\perp}(t)}$$

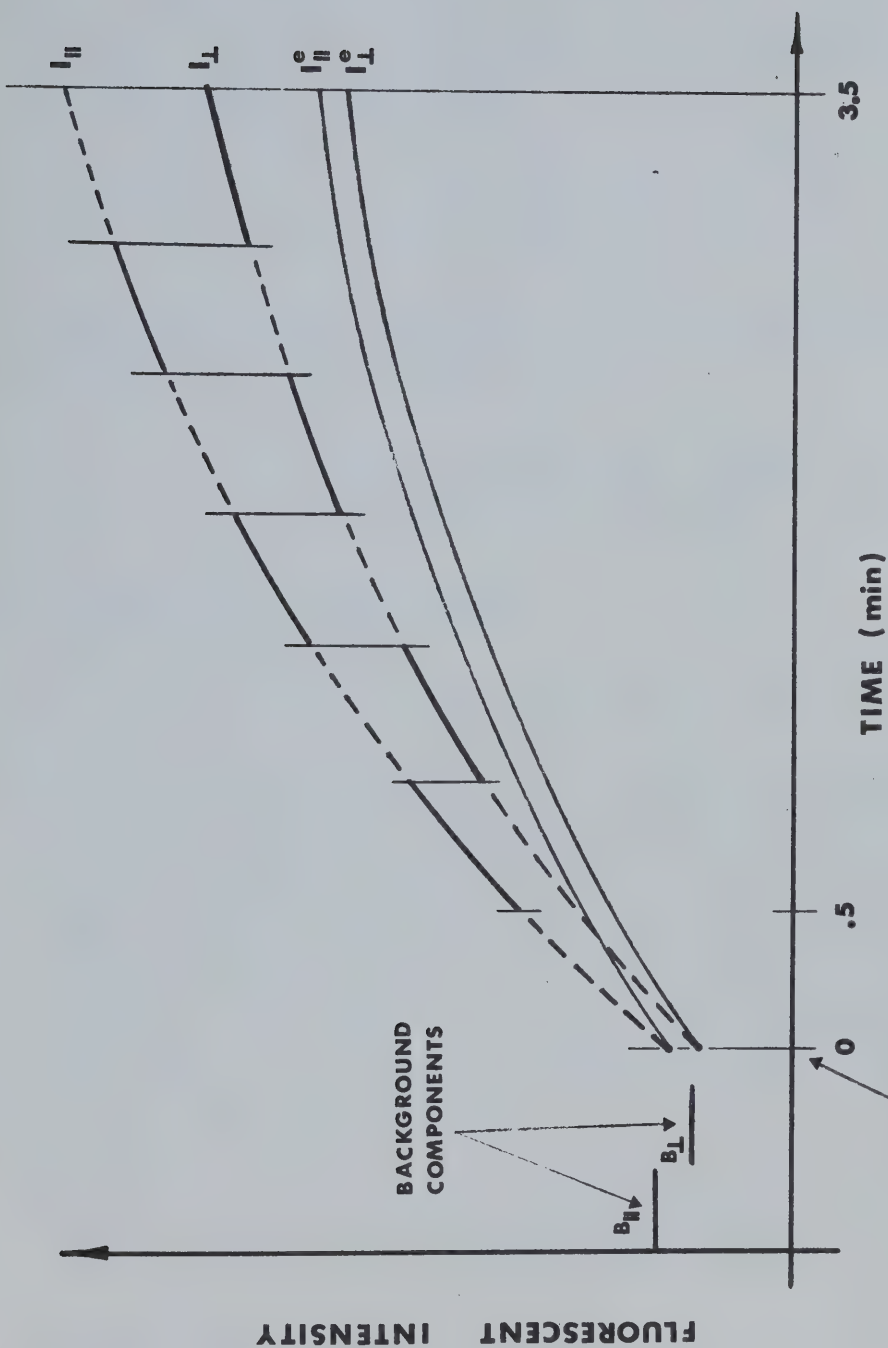

FIGURE 8 . A typical recorder printout. Data has been precorrected for grating attenuation.

2.4.3 Determination of the Polarization from the Cytoplasm

Because of the diffusion of fluorescein into the supporting medium the total fluorescent intensity consists of an intracellular and extracellular component. By defining:

$$I_{\parallel} = I^{e}_{\parallel} + I^{i}_{\parallel} \qquad (2.4.2a)$$

$$\text{and} \quad I_{\perp} = I^{e}_{\perp} + I^{i}_{\perp} \qquad (2.4.2b)$$

where e and i indicate extracellular and intracellular respectively, equation (C.1.1) can be expanded to give:

$$P = \frac{I^{i}_{\parallel} - I^{i}_{\perp}}{I^{i}_{\parallel} + I^{i}_{\perp}} \cdot \frac{I^{i}_{\parallel} + I^{i}_{\perp}}{I_{\parallel} + I_{\perp}} + \frac{I^{e}_{\parallel} - I^{e}_{\perp}}{I^{e}_{\parallel} + I^{e}_{\perp}} \cdot \frac{I^{e}_{\parallel} + I^{e}_{\perp}}{I_{\parallel} + I_{\perp}} \qquad (2.4.3)$$

This equation can be rewritten as:

$$P = P_c \cdot R_i + P_b \cdot R_e \qquad (2.4.4)$$

where P_c is the polarization from the cytoplasm, P_b is the background polarization, and where $R_n = \frac{I^{n}_{\parallel} + I^{n}_{\perp}}{I_{\parallel} + I_{\perp}}$ such that $\sum_n R_n = 1$. It is tempting to consider R_n as the ratio of the intensity of the "n"th component to the total intensity. However, because $I_t = I_{\parallel} + 2I_{\perp}$ (equation (C.1.12)) this is not exactly the case. To express the total polarization in terms of the actual component fractions, equation (C.1.10) can be expanded to give:

$$\frac{3 - P}{P} = \frac{(3 - P_c)\cdot(3 - P_b)}{3(P_c \cdot C_i + P_b \cdot C_e) - P_c \cdot P_b} \qquad (2.4.5)$$

where $C_n = \frac{I^n}{I_t} = \frac{I^{n}_{\parallel} + 2I^{n}_{\perp}}{I_{\parallel} + 2I_{\perp}}$ and $\sum_n C_n = 1$.

Equations (2.4.4) and (2.4.5) show that in order to calculate the polarization from the cytoplasm it is necessary to determine $I_{\parallel}^{e}$ and $I_{\perp}^{e}$.

2.4.4 Difficulties Obtaining P_c by Filtration

According to a method proposed by Cercek (12), P_c can be experimentally determined by filtering the cell suspension at the end of a run and obtaining $I_{\parallel}^{e}$ and $I_{\perp}^{e}$ from the filtrate. By marking the time at which the cells are filtered on the chart paper and extrapolating $I_{\parallel}$ and $I_{\perp}$ to the time of filtration (t_f), P_c can be calculated from:

$$P_c(t_f) = \frac{(I_{\parallel} - I_{\parallel}^{e}) - (I_{\perp} - I_{\perp}^{e})}{(I_{\parallel} - I_{\parallel}^{e}) + (I_{\perp} - I_{\perp}^{e})} \qquad (2.4.6)$$

Although this technique appears straightforward, considerable difficulty was encountered in applying it to the lymphocyte system. By trying various filtering techniques it was found that filtrate fluorescence ($I_{\parallel}^{e}$ and $I_{\perp}^{e}$) is a function of the method of filtration.[4] Consequently, different values of P_c are obtained corresponding to identical sets of $I_{\parallel}$ and $I_{\perp}$ curves. This inconsistency is the major difficulty in trying to determine P_c by filtration. In addition to the filtering problem there is also significant error introduced by extrapolating $I_{\parallel}$ and $I_{\perp}$. Because of these difficulties, the experimental method for determining P_c was abandoned.

---

[4]Filtration was performed with 1" diameter Swinney filter holders (Canlab) containing 2 μm polyvinylchloride filters (Millipore). Three separate techniques were tried including gravitational, syringe (3-5 ml), and suction filtration. For each method of filtration the filtrate fluorescence at t_f = 4 min was distinctly different. The values of $I_{\parallel}^{e}$ and $I_{\perp}^{e}$ were highest from the gravitational filtration followed by those from the suction filtration and finally from those obtained by the syringe filtration. This indicated that the filtrate fluorescence depends partly on the force of filtration and also on chemical factors.

2.5 ANALYTICAL DETERMINATION OF P_c

Since it was experimentally impossible to accurately determine $I_{\parallel}^{e}$ and $I_{\perp}^{e}$, an analytical method was developed.

Extracellular fluorescein is the result of diffusion across the cell membrane and this process can be examined independently. Rotman and Papermaster (37) have studied fluorescein diffusion from various mammalian cells including human lymphocytes, and have found that the diffusion rate of intracellular fluorescein is proportional to the concentration remaining in the cell;

$$\text{i.e.,} \qquad -\frac{d[F]_i}{dt} = \frac{d[F]_e}{dt} = K_D \cdot [F]_i \qquad (2.5.1)$$

where [F] is the concentration of fluorescein, K_D is the diffusion constant, and where e and i refer to extracellular and intracellular respectively. This result was determined with a fluorescence microscope by observing the fluorescent intensity from single cells as a function of time. The results from a typical study are shown in Figure 9. Because of varying membrane properties, cells from the same population exhibit a great degree of heterogeneity with respect to diffusion constants. It is difficult to account for this in any analytical model and only an average diffusion constant can be assumed for a large number of cells.

In Appendix C, it is shown that the total fluorescent intensity can be expressed by euqation (C.1.2) as $I_t = I_{\parallel} + 2I_{\perp}$, and since I_t is proportional to the total concentration of fluorescein

$$I_t = I_{\parallel} + 2I_{\perp} \propto [F]_t \qquad (2.5.2)$$

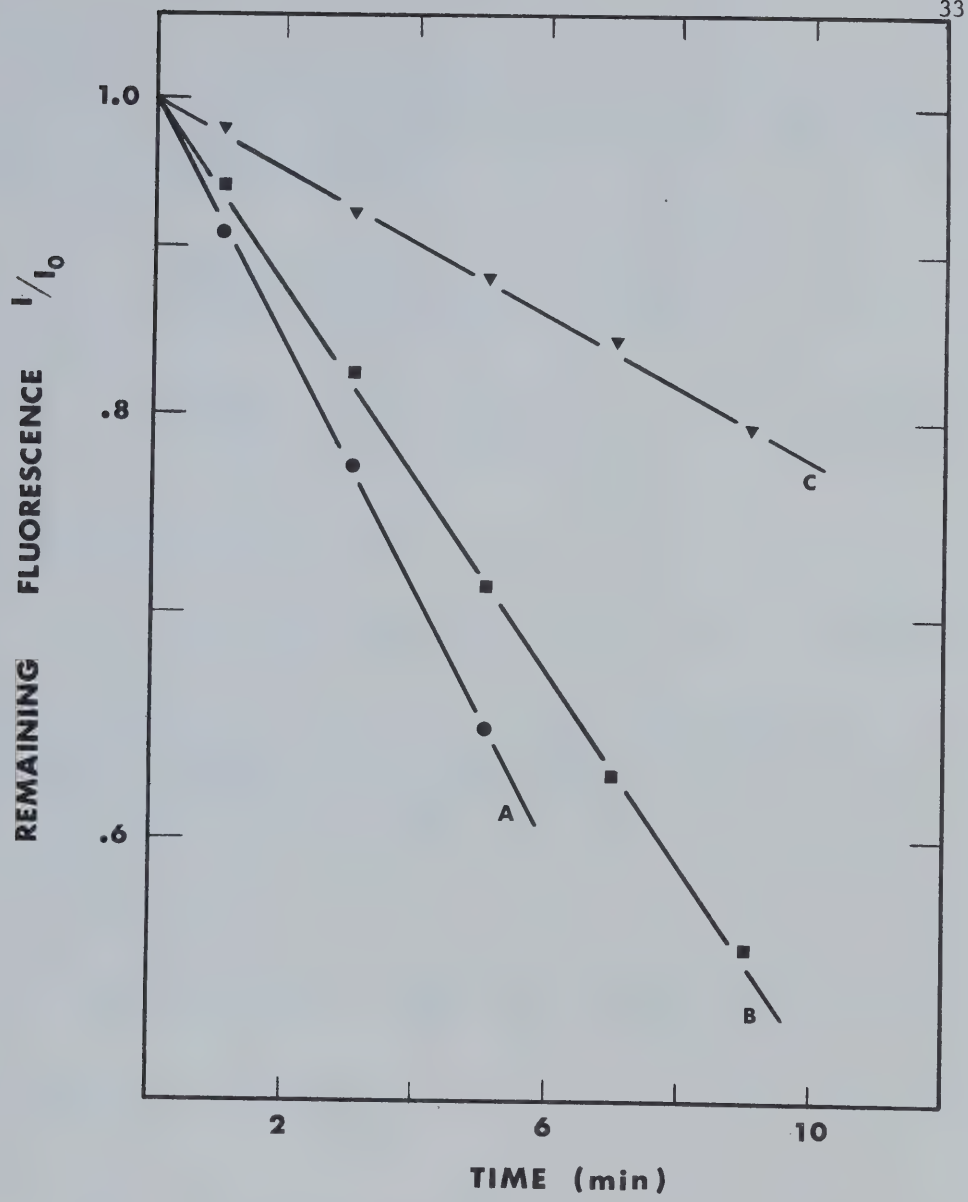

FIGURE 9. Release of intracellular fluorescein. A,B and C represent measurements taken from single mouse lymphoma cells (ML 388) in PBS at 23° C . (After Rotman and Papermaster (37)).

The total fluorescein concentration is the sum of the extracellular and intracellular concentrations and using $[F]_t = [F]_e + [F]_i$ equation (2.5.1) can be rewritten as:

$$\frac{d[F]_e}{dt} = K_D \cdot [F]_i = K_D \cdot ([F]_t - [F]_e)$$

or:

$$\frac{d[F]_e}{dt} + K_D \cdot [F]_e = K_D \cdot [F]_t \qquad (2.5.3)$$

Following equation (2.5.2):

$$I^e = I^e_{\parallel} + 2I^e_{\perp} \propto [F]_e \qquad (2.5.4)$$

and since equations (2.5.2) and (2.5.4) have the same constant of proportionality (assuming that the fluorescence efficiency of intracellular and extracellular fluorescein is the same), equation (2.5.3) can be expanded to give:

$$\frac{d}{dt}(I^e_{\parallel} + 2I^e_{\perp}) + K_D \cdot (I^e_{\parallel} + 2I^e_{\perp}) = K_D \cdot (I_{\parallel} + 2I_{\perp}) \qquad (2.5.5)$$

This equation may be rearranged as:

$$\frac{dI^e_{\parallel}}{dt} + K_D \cdot I^e_{\parallel} - K_D \cdot I_{\parallel} + 2\left(\frac{dI^e_{\perp}}{dt} + K_D \cdot I^e_{\perp} - K_D \cdot I_{\perp}\right) = 0$$

which yields the two simultaneous equations:

$$\frac{dI^e_{\parallel}}{dt} + K_D \cdot I^e_{\parallel} = K_D \cdot I_{\parallel} \qquad (2.5.6)$$

$$\frac{dI^e_{\perp}}{dt} + K_D \cdot I^e_{\perp} = K_D \cdot I_{\perp} \qquad (2.5.7)$$

As stated in Section 2.3, the best least squares fit for both $I_{\parallel}$ and $I_{\perp}$ was a quadratic polynomial and thus, for a lymphocyte system, equations (2.5.6) and (2.5.7) can be solved for $I^e_{\parallel}$ and $I^e_{\perp}$. Since $I_{\parallel}$ and $I_{\perp}$ can be expressed generally as:

$$I_{\parallel}(t) = A_0 + A_1 t + A_2 t^2 \qquad (2.5.8)$$

a particular solution for (2.5.6) is:

$$P_{I^e_{\parallel}}(t) = (A_0 + A_1 t + A_2 t^2) - \frac{(A_1 + 2A_2 t)}{K_D} + \frac{2A_2}{K_D^2} \qquad (2.5.9)$$

The complementary solution to the equation $\frac{dI^e_{\parallel}}{dt} + K_D \cdot I^e_{\parallel} = 0$ is:

$$c_{I^e_{\parallel}}(t) = Ae^{-K_D t} \qquad (2.5.10)$$

and the general solution to equation (2.5.6) is given by the sum of (2.5.9) and (2.5.10). At $t = 0$, $I^e_{\parallel}(0) = A_0$, and therefore

$$A + A_0 - A_1/K_D + 2A_2/K_D^2 = A_0 \qquad (2.5.11)$$

Solving for A:

$$A = A_1/K_D - 2A_2/K_D^2 \qquad (2.5.12)$$

and the general solution can then be written:

$$I^e_{\parallel}(t) = \frac{A_1}{K_D} - \frac{2A_2}{K_D^2} e^{-K_D t} + (A_0 + A_1 t + A_2 t^2) - \frac{(A_1 + 2A_2 t)}{K_D} + \frac{2A_2}{K_D^2} \qquad (2.5.13)$$

A similar expression can be derived for $I_{\perp}^{e}(t)$.

Equation (2.5.13) suggests an interesting method for calculating both P_c and K_D simultaneously. By using equation (2.4.6), P_c is given by:

$$P_c(K_D,t) = \frac{(I_{\parallel} - I_{\parallel}^{e}) - (I_{\perp} - I_{\perp}^{e})}{(I_{\parallel} - I_{\parallel}^{e}) - (I_{\perp} - I_{\perp}^{e})} \qquad (2.5.14)$$

and an analytical expression for $P_c(t)$ can be obtained by simply providing a value for K_D. However, since the experimental conditions are well defined (pH = 7.4, isotonic media, constant temperature = 27° C), P_c should remain constant and therefore K_D should be chosen so that $\frac{dP_c}{dt} = 0$. This condition was impossible to achieve experimentally and K_D was chosen so that there was a minimum variation in P_c. This was accomplished by calculating the average polarization $\langle P_c \rangle$ for several values of K_D and finding the one with the minimum standard deviation. Because of the tedious nature of these calculations a computer program was drafted to determine the optimum value for $\langle P_c \rangle$. The program was written in Fortran and is listed in Appendix D. For simplicity, a block diagram demonstrating the main features is shown in Figure 10. The program is designed to calculate and list the average polarizations, $\langle P_c \rangle$, and the standard deviations, σ_P, for a range of diffusion constants supplied by the user. To eliminate random estimation of K_D, a subroutine CLCD1 was constructed which calculates K_D from a value of $I_{\parallel}^{e}$ or $I_{\perp}^{e}$ at a particular time. With this subprogram the user can initiate a search at a fictitious time of filtration and let the computer work its way through a range of possible filtrates ($I_{\parallel}^{e}$ and $I_{\perp}^{e}$) without interruption. The optimum value of $\langle P_c \rangle$ can then be chosen from the computer printout.

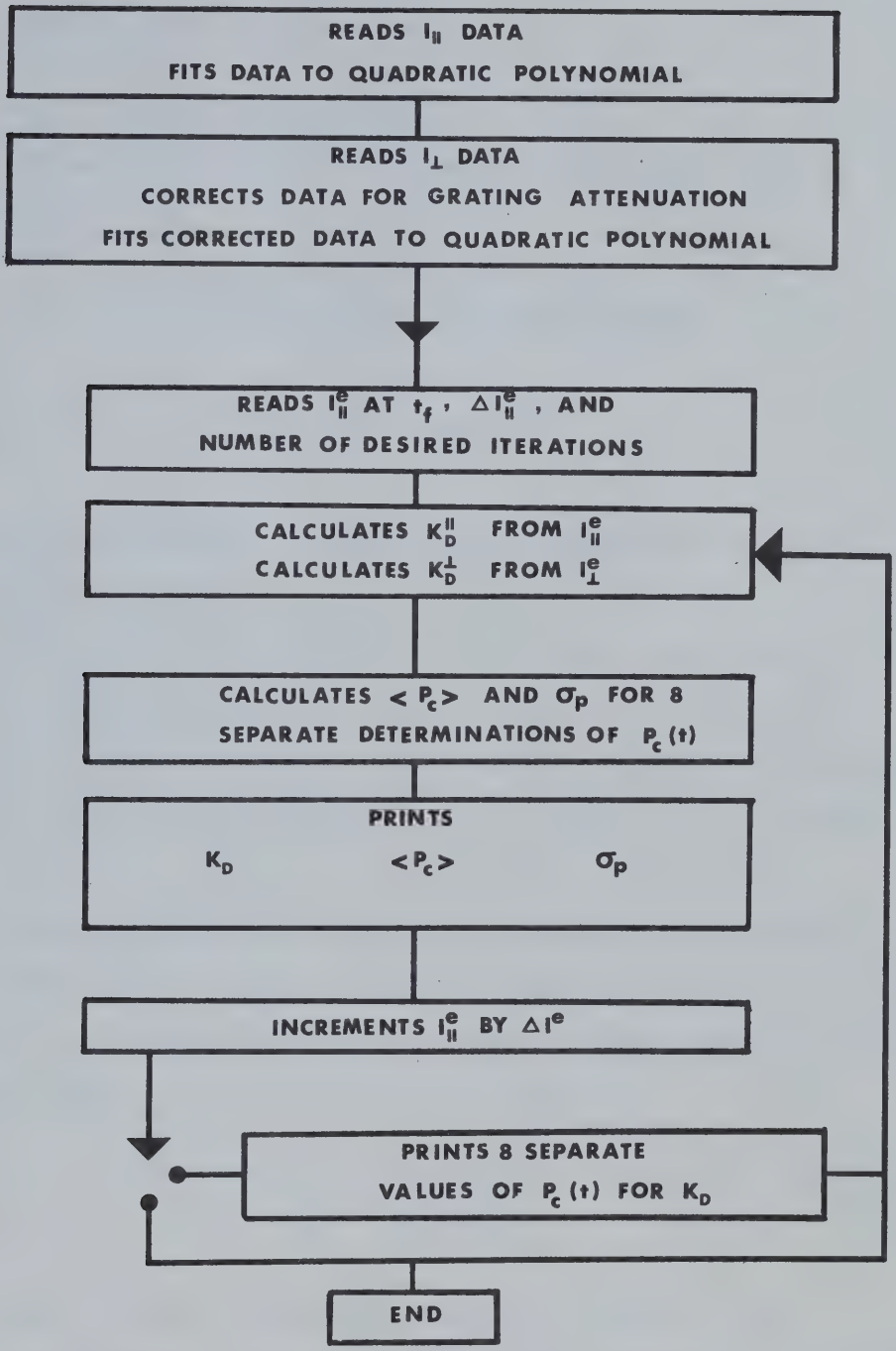

FIGURE 10 . Flow diagram of computer program for calculating P_c .

2.6 EVALUATION OF THE ANALYTICAL MODEL

2.6.1 Testing the Assumptions

The analytical method for determining P_c is based on two assumptions:

$$(1)\quad \frac{d[F]_e}{dt} = K_D[F]_i \quad \text{(equation (2.5.1))}$$

$$(2)\quad \frac{dP_c}{dt} = 0 \quad (P_c = \text{constant}) \qquad (2.6.1)$$

To check the experimental validity of these assumptions two separate tests can be performed.

Because $I^e_{\parallel}$ and $I^e_{\perp}$ are derived from separate quadratic polynomials, each function contains a distinct value for K_D ($K^{\parallel}_D$ and $K^{\perp}_D$). However, according to equations (2.5.6) and (2.5.7), $K^{\parallel}_D$ and $K^{\perp}_D$ should be identical, and therefore this criterion can be used to verify equation (2.5.1).

The second test that can be performed concerns the background polarization. Since the supporting medium is well defined (2.8 ml 2.5 μM FDA/PBS + .2 ml Medium 199 at 27° C), P_b should remain constant. Knowing $I^e_{\parallel}$ and $I^e_{\perp}$ this can be checked from the equation:

$$P_b(t) = \frac{I^e_{\parallel} - I^e_{\perp}}{I^e_{\parallel} + I^e_{\perp}} \qquad (2.6.2)$$

The constancy of P_b is a direct verification of equation (2.6.1).

The "K_D" and "P_b" tests are a good means of evaluating a particular selection of $\langle P_c \rangle$ and were therefore incorporated into the computer

program. The "K_D" test proved to be very useful as large differences in the values of $K_D^{\parallel}$ and $K_D^{\perp}$ were directly related to large magnitudes of σ_P. In contrast, the "P_b" test was less significant because of the extremely low background polarization (P_b = .015).

2.6.2 A Typical Analysis

To demonstrate the complete function of the computer program the numerical and graphical results from a typical run are shown in Figure 11 and Table II.

Figure 11 shows the variation in P_c (equation (2.5.14)) for three values of K_D and demonstrates how the optimum value for $\langle P_c \rangle$ is analytically determined. The total polarization (P) and the background polarization (P_b) are also shown.

From the numerical results in Table II, the optimum polarization was $\langle P_c \rangle$ = .186 with a standard deviation of σ_P = .002. On the basis that the per cent difference in $K_D^{\parallel}$ and $K_D^{\perp}$ was 9.9% and that P_b = .014 ± .004 it can be concluded that .186 is a reasonable value for $\langle P_c \rangle$.

Also shown in Table II is the intracellular component ratio C_i from equation (2.4.5). These data indicate that after a four-minute incubation about 50% of the total fluorescent intensity is from the cytoplasm of the cells. Since $P_c >> P_b = 0$, equations (2.4.4) and (2.4.5) can be approximated by:

$$R_i \simeq P/P_c \tag{2.6.3}$$

$$C_i \simeq \frac{P \cdot (3 - P_c)}{P_c \cdot (3 - P)} \tag{2.6.4}$$

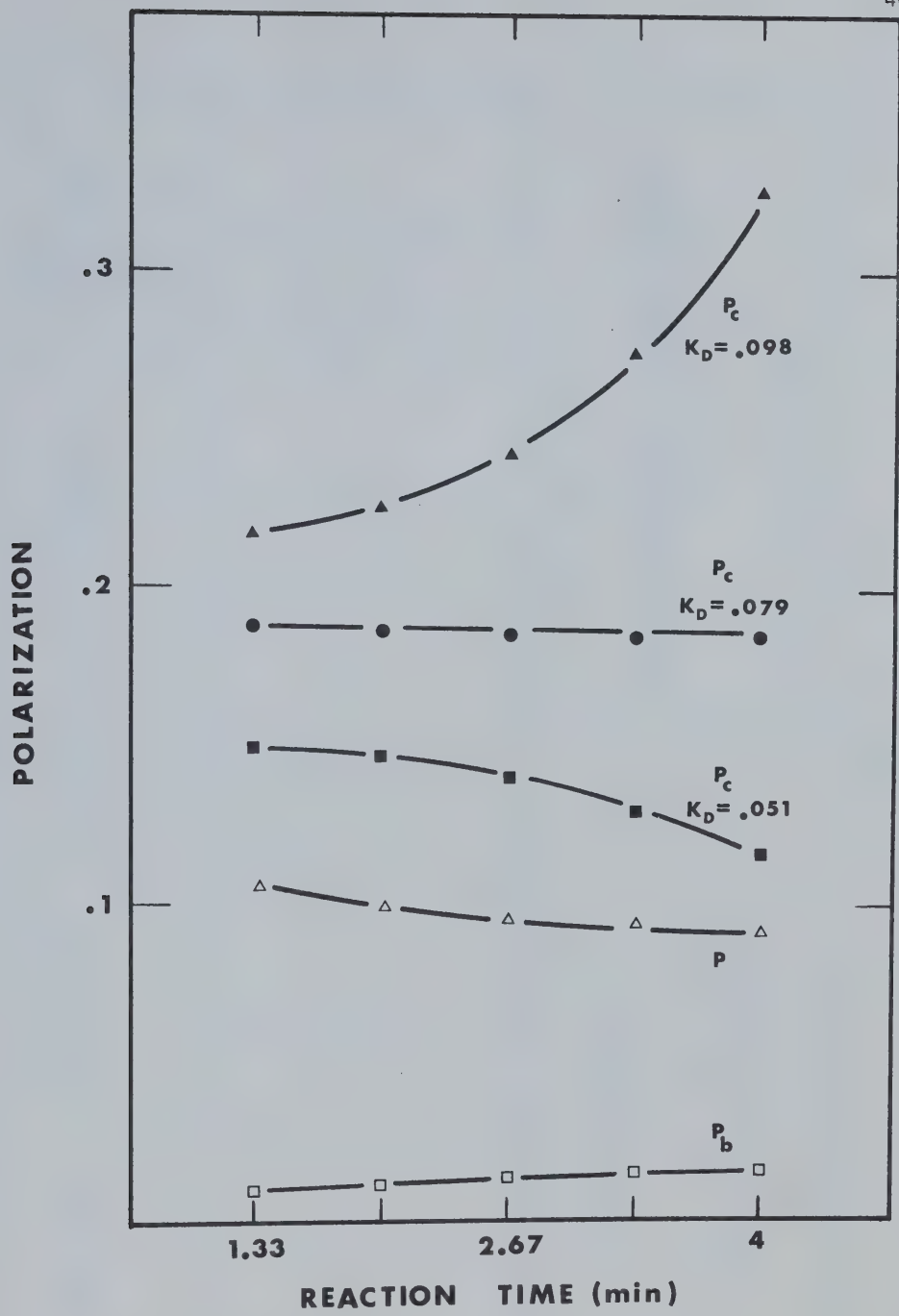

FIGURE 11 . Graphical results from a typical run.

NUMERICAL DATA CORRESPONDING TO FIGURE 11

REACTION TIME (MIN)	POLARIZATION FROM THE CYTOPLASM P_c	TOTAL POLARIZATION P	BACKGROUND POLARIZATION P_b	FRACTION OF INTRACELLULAR FLUORESCENCE $C_i = I^i/I_t$
1.33	.188	.105	.010	.519
2.00	.187	.100	.012	.487
2.67	.186	.096	.014	.463
3.33	.185	.094	.016	.447
4.00	.184	.092	.018	.431

RESULTS FROM NUMERICAL ANALYSIS:

DIFFUSION CONSTANTS FROM $I_{\parallel}$ AND $I_{\perp}$ DATA:

$K_D^{\parallel} = .087$; $K_D^{\perp} = .071$

AVERAGE DIFFUSION CONSTANT:

$K_D = .079 \pm 9.9\ \%$

BACKGROUND POLARIZATION:

$P_b = .014 \pm .004$

AVERAGE POLARIZATION FROM THE CTOPLASM CORRESPONDING TO THE MINIMUM STANDARD DEVIATION:

$< P_c > = .186$

MINIMUM STANDARD DEVIATION:

$\sigma_p = .002$

TABLE II

Equations (2.6.3) and (2.6.4) show that the time dependence of C_i and R_i is approximately the same as for the total polarization. The fact that C_i gradually decreases can be explained by a steady-state intracellular concentration of fluorescein. When this occurs, I^i = constant, and since I_t is continually increasing, $I^i/I_t = C_i$ must decrease. From the data in Table II, the steady-state concentration is reached within the first minute of incubation.

CHAPTER THREE

RESULTS AND DISCUSSION

3.1 NORMAL RANGE FOR P_c

To establish the normal variation in P_c for human lymphocytes, a total of 17 donors were tested. Data were compiled by calculating the average polarization (P_c) and standard deviation ($\sigma_{experimental}$) from approximately five runs for each donor. In all, 87 separate determinations of P_c were done and the results of the study are shown in Table III. The overall average polarization was calculated by weighting the individual averages according to their contribution to the total number of runs. This value is given at the bottom of the table as $\overline{P}_c = .199 \pm .004$. The overall standard deviation was calculated assuming a Normal distribution in the data and using an average standard deviation of .015.

Havind determined the normal variation in P_c, equation (C.3.27) was applied to determine the approximate range for the average microviscosity of the cytoplasm. Assuming that:

(a) the principal polarization of fluorescein is

$P_0 = 1/2$ (Appendix C.1)

(b) the excited lifetime of fluorescein is

$\tau = 4.5 \times 10^{-9}$ seconds (48)

(c) the molar volume of fluorescein is

$V_m = 500$ ml (including solvation shell (35))

equation (C.3.27) reduces to (at 27° C):

NORMAL RANGE OF POLARIZED FLUORESCENCE FROM THE CYTOPLASM OF HUMAN LYMPHOCYTES		
DONOR	$P_c \pm \sigma_{experimental}$	NUMBER OF RUNS
1	.210 ± .015	4
2	.180 ± .017	4
3	.190 ± .020	5
4	.201 ± .022	5
5	.185 ± .015	5
6	.214 ± .012	5
7	.187 ± .016	4
8	.191 ± .021	5
9	.186 ± .011	6
10	.205 ± .017	5
11	.212 ± .019	5
12	.191 ± .016	5
13	.190 ± .014	7
14	.216 ± .017	6
15	.211 ± .014	5
16	.203 ± .016	6
17	.210 ± .013	5
	$\overline{P_c}$ = .199 ± .004	87

TABLE III

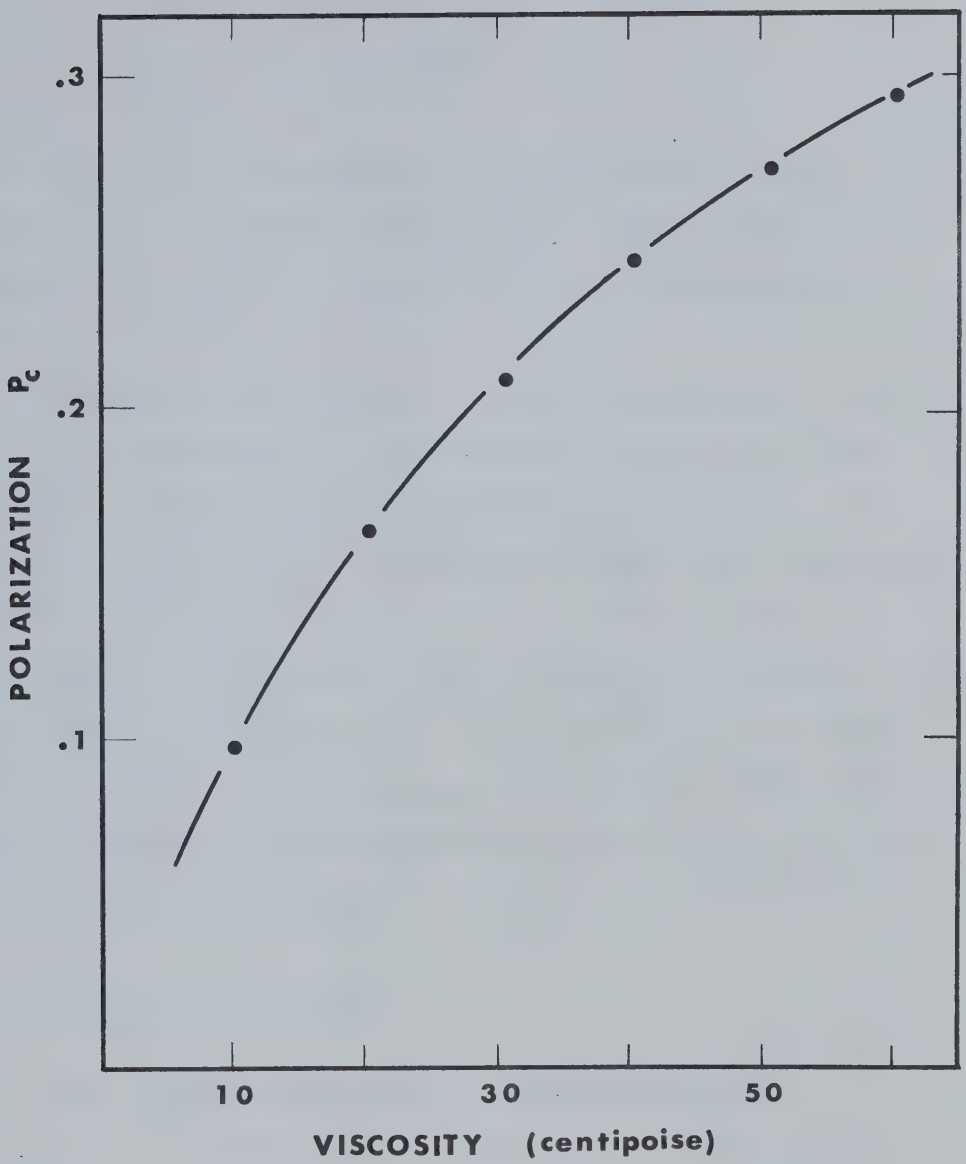

FIGURE 12 . Variation of the polarization of fluorescence from the cytoplasm of lymphocytes with the average microviscosity (27° C).

$$\frac{1}{P_c} = 2.000 + .832 \frac{1}{\bar{\eta}} \qquad (3.1.1)$$

From a graph of this equation shown in Figure 12, the value of $\bar{P}_c = .199$ corresponds to an average microviscosity of $\bar{\eta} \simeq 30$ centipoise (1 poise = 1 dyne sec/cm^2). This value is about 30 x more viscous than water at 20° C.

An average standard deviation of .015 represents about 8% of the value of $\bar{P}_c$. From Figure 12, this represents a range in the average microviscosity between 25 and 35 centipoise. Although part of the standard deviation was due to fluctuations in tonicity and pH (Sections 3.2.3 and 3.2.4), some of it was due to the analytical method for determining P_c. For the data in Table III, the "K_D" test showed that the majority of the % differences in $K_D^{\parallel}$ and $K_D^{\perp}$ were in the 7-11% range. This corresponded to a variation in σ_p between .002 and .010 and it was therefore estimated that the average contribution to $\sigma_{experimental}$ from the analytical method was ±.006.

3.2 EXTERNAL FACTORS AFFECTING P_c

3.2.1 The pH and Osmolarity of the Supporting Medium

In order to sustain mammalian cells "in vitro" such factors as the temperature, pH, tonicity and nutritional content of the supporting medium must be carefully controlled. Optimum cell growth can generally be attained by matching these parameters as closely as possible with those of the original cellular environment (extracellular fluid). The actual chemical compositions of the extracellular and intracellular fluids

are quite different and are shown in Table IV.

To maintain a pH in the vicinity of 7.4, the supporting medium is provided with a buffer system which consists of a weak acid in equilibrium with its salt. According to the Henderson-Hasselbach equation (31) the pH of a buffered medium can be described by:

$$pH = pK_a + \log \frac{[BA]}{[HA]} \qquad (3.2.2)$$

where the acid dissociates as:

$$HA \overset{K_a}{\rightleftharpoons} H^+ + A^- \text{ (weak dissociation)}$$

and the salt dissociates as:

$$BA \rightleftharpoons B^+ + A^- \text{ (complete dissociation)}$$

As equation (3.2.2) shows, the pH of the medium will fluctuate around the value of pK_a depending on the relative proportions of salt and acid.

Medium 199 (Table VI) employs a bicarbonate/carbonic acid buffer which is the most widely used system for culture media. This system consists of a liquid-gas equilibrium described by the reactions:

$$CO_2\ (g) + H_2O \rightleftharpoons H_2CO_3 \overset{K_a}{\rightleftharpoons} H^+ + HCO_3^-$$

(where $pK_a = 6.1$ at 25° C (31)) and:

$$NaHCO_3 \rightleftharpoons Na^+ + HCO_3^-.$$

Applying equation (3.2.2) to these reactions:

$$pH = 6.1 + \log \frac{[NaHCO_3]}{[CO_2]}$$

CHEMICAL COMPOSITION OF EXTRACELLULAR AND INTRACELLULAR FLUIDS (FROM GUYTON (22))

COMPONENT	EXTRACELLULAR FLUID pH=7.4	INTRACELLULAR FLUID pH=7.0
Na^{+}	142 mEq/l	10 mEq/l
K^{+}	5 mEq/l	141 mEq/l
Ca^{++}	5 mEq/l	<1 mEq/l
Mg^{++}	3 mEq/l	58 mEq/l
Cl^{-}	103 mEq/l	4 mEq/l
HCO_3^{-}	28 mEq/l	10 mEq/l
PHOSPHATES	4 mEq/l	75 mEq/l
SO_4^{--}	1 mEq/l	2 mEq/l
GLUCOSE	90 mgm %	0 - 20 mgm %
AMINO ACIDS	30 mgm %	200 mgm %
CHOLESTEROL PHOSPHOLIPIDS NEUTRAL FAT	.5 gm %	2 - 95 gm %

1 mEq = 10^{-3} Equivalent Weight

1 mgm % = 10^{-3} gm/100 ml blood or plasma

TABLE IV

and can be controlled by adjusting the partial pressure of CO_2. A $[NaHCO_3]/[CO_2]$ ratio of 20 to 1 provides a pH of 7.4.

PBS (Table V) employs a phosphate/phosphoric acid buffer which is self-adjusting and is designed for short-term incubations. This system is described by the reactions:

$$KH_2PO_4 \overset{K_a}{\rightleftharpoons} K^+ + H^+ + HPO_4^{--}$$

(where $pK_a = 6.7$ at 23° C (31)) and:

$$Na_2HPO_4 \rightleftharpoons 2Na^+ + HPO_4^{--}.$$

From Table V, $[Na_2HPO_4]/[KH_2PO_4] = 4.59$, and applying equation (3.2.2), pH = 7.4. The phosphate/phosphoric acid buffer has an advantage over the bicarbonate/carbonic acid system in that the value of pK_a is closer to 7.4.

The simplest quantitative description of the tonicity of a solution is provided by the osmolarity (osmolality). The osmolarity is defined as the number of osmols per liter of solution where 1 osmol represents one mole of dissolved particles. (For example, 1×10^{-3} moles of completely dissociated $CaCl_2$ represents an osmolarity of 3 milliosmols.) In calculating the osmilarity of concentrated solutions an osmotic coefficient must be introduced to allow for solute interaction (38). A 154 mM solution of NaCl (isotonic saline) has an osmolarity of only .283 osmols because the osmotic coefficient at this concentration is .92.

Although all the components in the supporting medium contribute to the tonicity, the osmotic pressure is mainly controlled by NaCl. For a solution of PBS the total osmolarity is .288 osmols while the osmolarity due to NaCl is .252 osmols.

CHEMICAL COMPOSITION OF PHOSPHATE BUFFERED SALINE pH = 7.4 (FROM PAUL(34))	
INORGANIC SALT	mg/l
$CaCl_2$	100.0
KCl	200.0
KH_2PO_4	200.0
$MgCl_2 \cdot 6H_2O$	100.0
NaCl	8000.0
$Na_2HPO_4 \cdot 2H_2O$	1150.0

TABLE V

MEDIUM 199

Component		*mg/L*
AMINO ACIDS		
DL-Alpha-Alanine		50.000
L-Arginine HCl		70.000
DL-Aspartic acid		60.000
L-Cysteine HCl·H_2O		0.110
L-Cystine	26.00 (2 HCl)(a)	20.000
DL-Glutamic acid·H_2O		150.000
L-Glutamine		100.000
Glycine		50.000
L-Histidine HCl·H_2O		21.880
L-Hydroxyproline		10.000
DL-Isoleucine		40.000
DL-Leucine		120.000
L-Lysine HCl		70.000
DL-Methionine		30.000
DL-Phenylalanine		50.000
L-Proline		40.000
DL-Serine		50.000
DL-Threonine		60.000
DL-Tryptophan		20.000
L-Tyrosine	57.88 (2 Na)(a)	40.000
DL-Valine		50.000
VITAMINS		
Ascorbic acid		0.050
d-Biotin		0.010
Calciferol		0.100
Ca pantothenate		0.010
Choline chloride		0.500
Folic acid		0.010
i-Inositol		0.050
Menadione		0.010
Niacin		0.025
Niacinamide		0.025
Para-aminobenzoic acid		0.050
Pyridoxal HCl		0.025
Pyridoxine HCl		0.025
Riboflavin		0.010
Thiamine HCl		0.010
Vitamin A (acetate)(c)		0.140

Component		*mg/L*
INORGANIC SALTS		
$CaCl_2$ (anhyd.)		140.00
$Fe(NO_3)_3 \cdot 9H_2O$		0.72
KCl		400.00
KH_2PO_4		60.00
$MgSO_4 \cdot 7H_2O$		200.00
	(anhyd.)(a)	97.72
NaCl		8000.00
$NaHCO_3$(b)		350.00
$NaH_2PO_4 \cdot H_2O$		
$Na_2HPO_4 \cdot 7H_2O$		60.00
	(anhyd.)(a)	47.70

OTHER COMPONENTS		
Adenine sulfate		10.000
Adenosinetriphosphate (Disodium salt)		1.000
Adenylic acid		0.200
alpha tocopherol phosphate (sodium salt)		0.010
Cholesterol		0.200
Deoxyribose		0.500
Glucose		1000.000
Glutathione		0.050
Guanine HCl (Free base)		0.300
Hypoxanthine	(.354 Na salt)(a)	0.300
Phenol red		20.000
Ribose		0.500
Sodium acetate		50.000
Thymine		0.300
Tween 80 *Atlas Powder Co.*		20.000
Uracil		0.300
Xanthine	(.344 Na salt)(a)	0.300

Remarks:
(a)As supplied in powdered media
(b)Omitted from 10X preparations and powdered media
(c)Values established by the Tissue Culture Standards Committee.

TABLE VI . The chemical composition of TC Medium 199 .

(From GIBCO catalogue, 1976)

3.2.2 Physical State of H_2O in the Cytoplasm

Two theories have been proposed to explain how the cell maintains the component distribution shown in Table IV. These are the membrane theory and the association-induction hypothesis (30).

The membrane theory assumes that the membrane is the universal rate-limiting barrier to the traffic of water and all solutes between the cell and the external environment. Hypothetical pumps, located in the cell membrane are suggested to be responsible for excluding sugars and Na^+ or Cl^- ions from the cell. This theory also assumes that the bulk of cell water is normal and that the intracellular K^+ ions are in the free state.

According to the association-induction hypothesis, a living cell represents a protein-aqueous fixed-charge system in which a high degree of molecular association exists among water, solutes and protein. This theory proposes that the component distribution in Table IV is maintained by metastable equilibrium which requires no direct energy expenditure. K^+ ions are believed to be selectively adsorbed on protein anionic side chains and the bulk of cell water is presumed to exist as polarized multilayers.

Recent NMR and diffusion studies (29) have provided strong evidence that the association-induction hypothesis is the most plausible of the two theories. The fact that the degree of polarization of fluorescence from the cytoplasm of lymphocytes is greater than 10X the polarization from the supporting medium is irrefutable evidence that the organization of the cytoplasm involves a high degree of molecular association. This result also suggests that the ratio of free to bound

water in the cytoplasm is an important factor in determining the average microviscosity and hence P_c.

3.2.3 The Effect of Osmolarity on P_c

It is an established fact that the osmotic pressure of the supporting medium controls the amount of intracellular water. To determine the effect of the osmolarity on P_c, the same procedure was followed as in Chapter 2.4 except that FDA/PBS solutions of varying osmolarity were used. Hypotonic and hypertonic solutions of PBS were prepared using NaCl concentrations of 4 g/l (.159 osmols) and 16 g/l (.545 osmols) respectively. Solutions of isotonic PBS contained 8 g/l NaCl (.288 osmols). Approximately five determinations of P_c were done for each osmolarity and the results are shown in Figure 13.

In the hypertonic environment, where there is a net flow of water from the cells into the supporting medium, P_c was found to increase to .223 ± .010 at an osmolarity of .545 osmols. An opposite effect occurred for a hypotonic environment and P_c decreased to .138 ± .011. For isotonic solutions of PBS, P_c = .186 ± .011.

These results clearly indicate that the intracellular concentration of H_2O is a critical factor in determining the polarization of fluorescence from the cytoplasm. Similar data have been reported by Cercek (16).

To determine the effect of small changes in the osmolarity a similar experiment was conducted by varying the concentration of $CaCl_2$ in PBS. Hypotonic and hypertonic solutions were prepared using $CaCl_2$ concentrations of 0 and 2×10^{-3} M respectively. Isotonic solutions of PBS contained $\simeq 1 \times 10^{-3}$ M $CaCl_2$. Again, approximately five determinations of P_c were done for each osmolarity and the results are shown in Figure 14.

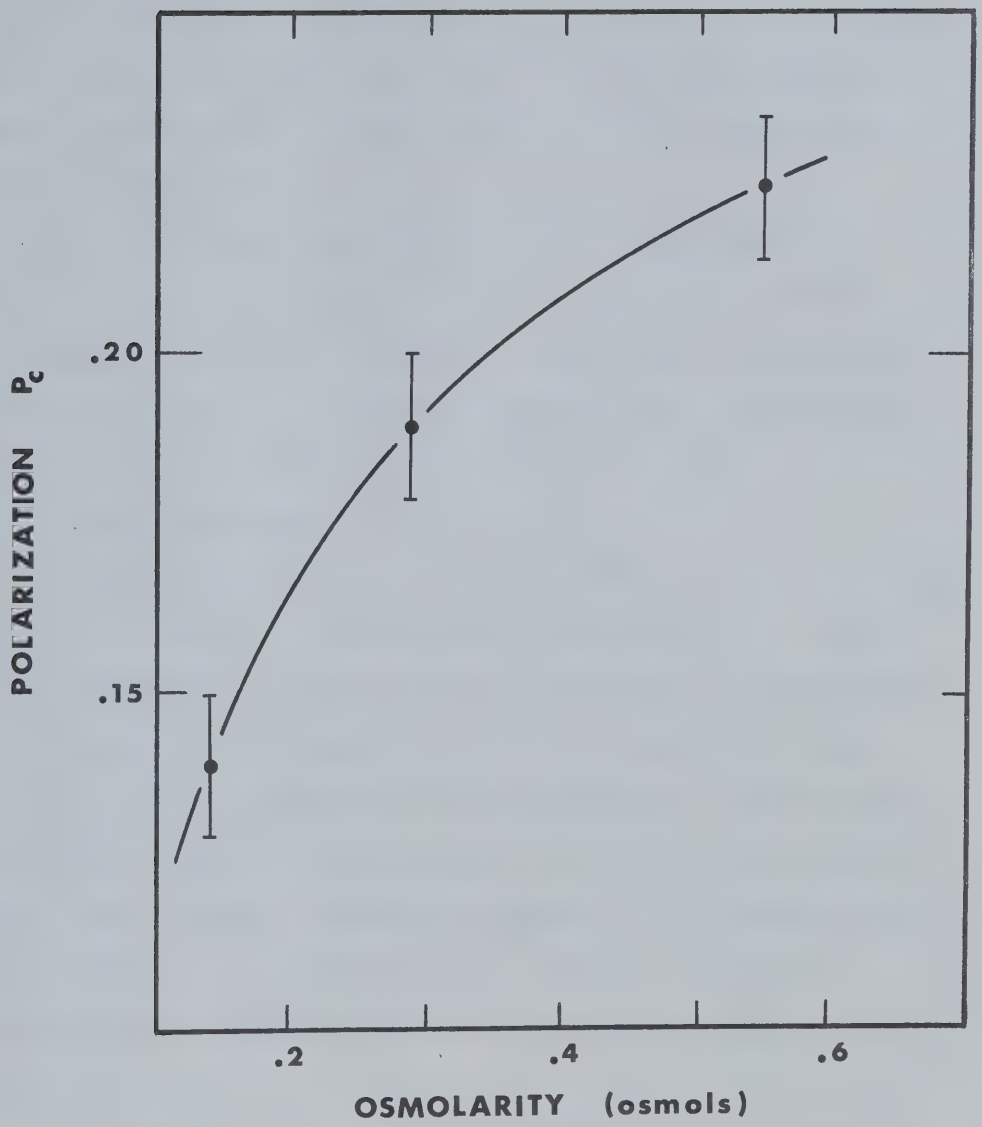

FIGURE 13 . Variation of the polarization of fluorescence from the cytoplasm with the osmolarity of the supporting medium. The osmolarity of isotonic PBS is .288 osmols .

Because the variation in the concentration of $CaCl_2$ did not significantly affect the total number of osmols in PBS (2×10^{-3} M $CaCl_2$ corresponds to a change in the osmolarity of .0027), the units of the x axis of Figure 14 are shown as concentration.

For a $CaCl_2$ concentration of 2×10^{-3} M, P_c was found to be $.192 \pm .012$ while for zero concentration $P_c = .170 \pm .011$. The value of P_c corresponding to isotonic PBS was $P_c = .184 \pm .011$. Although these results indicate that P_c is sensitive to extremely small changes in the osmolarity it should be pointed out that there is considerable overlap in P_c for all three osmolarities.

It was interesting to note in these experiments that the percentage difference in $K_D^{\shortparallel}$ and $K_D^{\perp}$ for the individual determinations of P_c was in the same 7-11% range as for the normal study (Table III). This indicated that the exchange of H_2O between the cells and the supporting medium occurred within the first minute of incubation in PBS. If the exchange occurred over a period of several minutes, it would be expected that P_c would not remain constant (violation of equation (2.6.1)) and that there would be unusually large differences in $K_D^{\shortparallel}$ and $K_D^{\perp}$. It should be emphasized that the analytic method for determining P_c depends on the validity of equation (2.6.1).

During an experiment, it is unlikely that the osmolarity of the supporting medium changes appreciably. It can therefore be concluded that fluctuations in the osmolarity can only account for a small percentage of $\sigma_{experimental}$. It is possible, however, that changes in the osmolarity on a day to day basis could account for a significant variation in the magnitude of P_c.

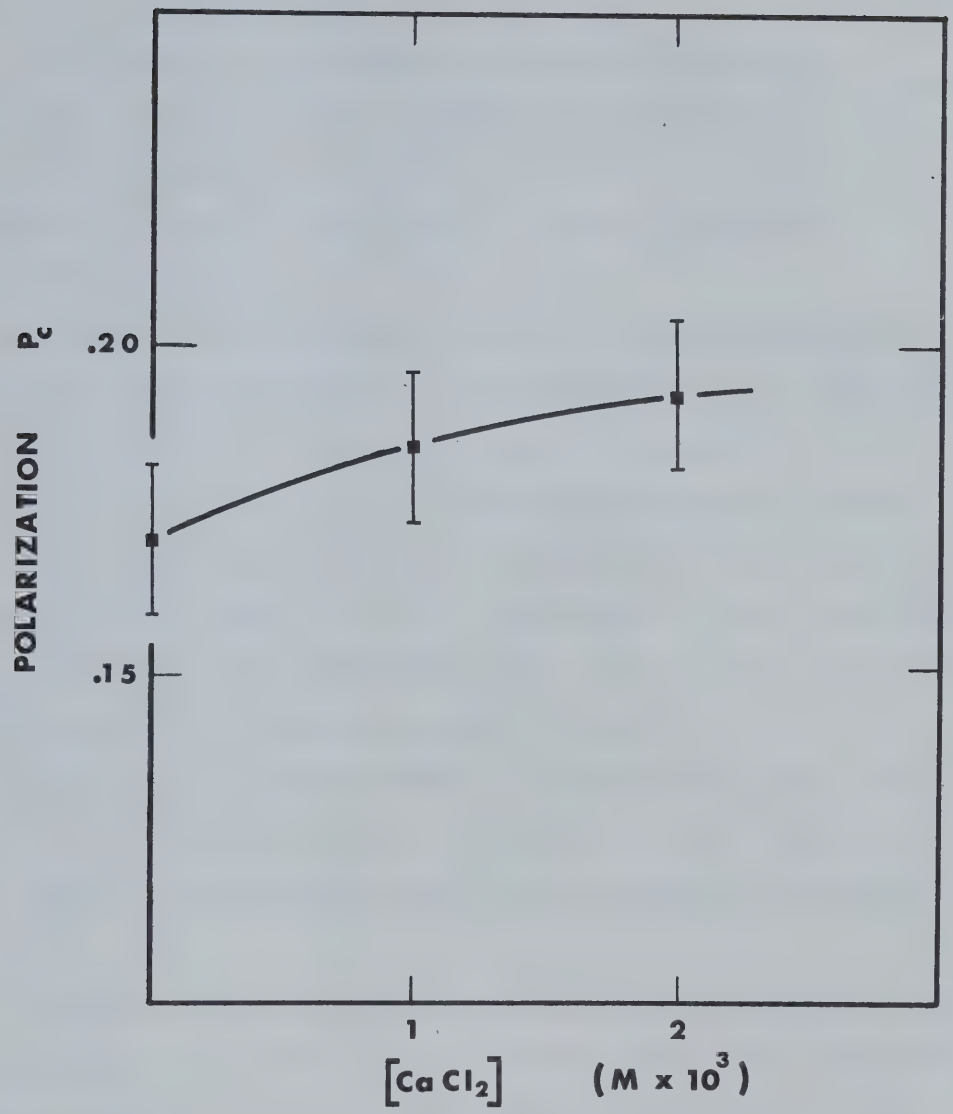

FIGURE 14 . Variation of the polarization of fluorescence from the cytoplasm with the concentration of $CaCl_2$ in the supporting medium. The concentration of $CaCl_2$ in isotonic PBS is $\simeq 1 \times 10^{-3}$ M.

3.2.4 The Effect of pH on P_c

Since changes in the tonicity of the supporting medium can significantly affect P_c, it was expected that variation in the pH would produce similar results. To study this effect, the same procedure was followed as in Chapter 2.4 except that the cells were immersed in isotonic PBS of varying pH.

The effect of increased pH could not be determined because FDA is unstable under these conditions (pH > 7.4) and decomposes into fluorescein.

The effect of decreased pH was studied by using three solutions of PBS with pH's of 7.4, 6.5, and 5.5. The acidic solutions were prepared by adding .1 N HCl dropwise to isotonic PBS until the pH stabilized at the appropriate values. These were read on a Radiometer pH meter/28 and were accurate to within ±.05. Approximately seven runs were done at each pH and the results of the experiment are shown in Figure 15.

As the pH of the medium decreases, P_c decreases from .186 ± .014 at pH = 7.4 to .175 ± .010 at pH = 6.5 and finally to .141 ± .011 at pH = 5.5. Figure 15 also indicates that P_c does not increase significantly for pH > 7.4.

Although the pH effect on P_c appears to be similar to the hypotonic effect described in Section 3.2.3, the exact mechanism is more complicated. Legge and Shortman (39) have previously reported that erythrocytes and thymic lymphocytes swell when immersed in acidic media. These authors proposed a mechanism for this process whereby HCO_3^- and Cl^- ions first enter the cell according to Gibbs-Donnan equilibria and are then followed by an influx of water in response to a hypertonic intracellular fluid. The data in Figure 15 are compatible with this mechanism and demonstrate

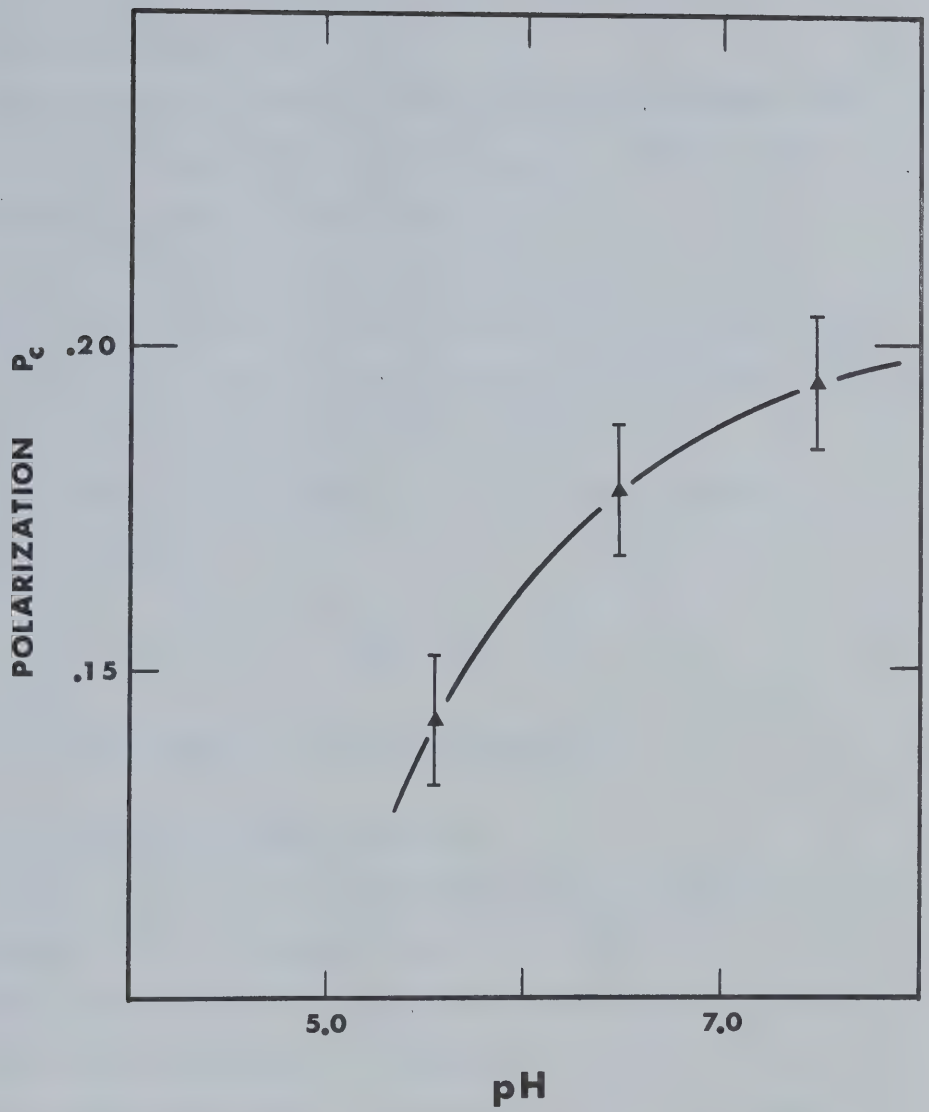

FIGURE 15 . Variation of the polarization of fluorescence from the cytoplasm with the pH of the supporting medium.

again the importance of intracellular H_2O in determining the average microviscosity and hence P_c.

The percentage difference in $K_D^{\parallel}$ and $K_D^{\perp}$ for this experiment was also in the 7-11% range which indicated that the analytical method for determining P_c is valid for acidic media.

Because the pH is the most difficult parameter to control experimentally it is highly probable that most of $\sigma_{experimental}$ is due to fluctuations in the pH of the supporting medium. The pH effect could also account for day to day variation in the magnitude of P_c.

The effect of pH and osmolarity on P_c can be summarized by equation (C.3.27) as:

$$\frac{1}{P_c} \propto \frac{1}{\bar{\eta}}$$

where $\bar{\eta}$ = f (pH, osmolarity) at constant temperature.

3.2.5 Effect of Temperature on P_c

Prior to this section, no explanation has been given as to why P_c was measured at 27° C. At temperatures >28° C, the kinetics for the hydrolysis of FDA are extremely unpredictable and sporadic increases in the fluorescent intensity make it impossible to accurately fit $I_{\parallel}$ and $I_{\perp}$ data to analytical curves. At temperatures <28° C, the kinetics are uniform but the efficiency of enzymatic hydrolysis (and hence the magnitude of the $I_{\parallel}$ and $I_{\perp}$ components) decreases with decreasing temperature. Therefore, an intermediate temperature of 27° C was chosen.

To simulate "in vivo" metabolism, the lymphocytes were kept at 37° C prior to their immersion in FDA/PBS. It should be mentioned that prolonged incubation (>1½ hr) at 37° C caused the cell medium to turn

alkaline and resulted in non-uniform kinetics.

From the best data that could be obtained, it was found that the temperature dependence of P_c follows that predicted by equation (C.3.27),

i.e., $$\frac{1}{P_c} \propto \frac{T}{\bar{\eta}}$$

where $\bar{\eta}$ = f (T) decreases slowly with increasing temperature. For a temperature = 30° C, P_c was determined to be 7% less than the average of .199 while at room temperature (23° C), P_c was consistently 5% higher than .199.

Because the temperature was controlled to within ±.6° C (including a temperature gradient in the cuvette) it can be concluded that the experimental variation in temperature does not account for a significant part of $\sigma_{experimental}$.

CHAPTER FOUR

SUMMARY AND CONCLUSION

In 1974, Cercek et al. (5) reported that they could reliably distinguish cancer patients from those suffering from non-malignant disorders with the SCM test. The SCM test is performed on lymphocytes and employs the principle that stimulatory molecules, interacting with receptors on the cell membrane, induce changes in the average microviscosity of the cytoplasm. Such changes can be detected indirectly by measuring changes in the average polarization of fluorescence from fluorescein molecules in the cytoplasm (P_c).

The original objective in this study was to investigate applications of the SCM test but sufficient difficulty was encountered establishing a well defined control that the emphasis has been on the methodology. Although the SCM test was originally performed with a fluorescence spectrophotometer, this study suggests that such a method is unreliable for detecting changes in the average polarization of fluorescence from the cytoplasm. The principal evidence supporting this claim is that the filtrate fluorescence ($I^e_{\parallel}$ and $I^e_{\perp}$) was found to vary with the method of filtration (Chapter 2.4.4). Since the Cerceks' procedure for determining P_c depends on the extracellular or filtrate fluorescence, it is clear that the method is inconsistent. In addition to the filtration problem, fluctuating pH and data extrapolation are also significant sources of error in determining P_c.

In an attempt to circumvent the filtration difficulties, a semi analytical method was developed for determining P_c (Chapter 2.5). It

should be emphasized that the method is limited to systems where P_c remains constant and where the rate of diffusion of fluorescein across the cell membrane is directly proportional to the intracellular concentration. For antigen/mitogen stimulated systems it is questionable as to whether these constraints are applicable. Applying the method to unstimulated lymphocytes, the average polarization of fluorescence from the cytoplasm (isotonic PBS at 27° C) was determined to be $P_c = .199 \pm .004$. This value is in accord with that determined by the Cerceks and corresponds (Perrin equation) to an average microviscosity of $\bar{\eta} \simeq 30$ cp. The analytical method can also be used to demonstrate that P_c is extremely sensitive to variation in the pH or osmolarity of the supporting medium (Chapter 3). This indicates that the intracellular water content is a key factor in determining the average polarization of fluorescence from the cytoplasm. According to the Cerceks' data, the value of P_c decreases by approximately 20% as the result of antigen or mitogen stimulation. It is interesting to note that the same decrease can also be achieved by suspending the cells in a medium with a pH $\simeq$ 5.5 or with an osmolarity of about .2 osmols. These facts suggest there are two separate mechanisms by which P_c can decrease. First, by changes in the intracellular water content as the result of osmosis, and second, by molecular rearrangement or structural transformation within the cytoplasm following antigen/mitogen stimulation.

It should be pointed out that this study does not directly refute the antigen/mitogen-induced effects reported by the Cerceks. To properly evaluate such phenomena, a different technique than the cell suspension method (spectrophorometer) must be used. Although the limitations of

alternative instrumentation were discussed in Chapter 2.1, it appears that a highly sensitive fluorimeter with a built-in flow system is the only feasible solution. Because of the obvious potential associated with the SCM test such systems must be investigated in the near future.

BIBLIOGRAPHY

1. Azumi, T., McGlynn, S. P. Polarization of the luminescence of phenanthrene. J. Chem. Phys. 37: 2413-2420, 1962.

2. Bellanti, J. A. Immunology. Chapters 1-3. W. B. Saunders Co., Toronto, Ont., 1971.

3. Bevington, P. R. Data Reduction and Error Analysis for the Physical Sciences. Chapter 11. McGraw-Hill Book Co., New York, 1969.

4. Bowen, E. G., Seaman, D. Luminescence of Organic and Inorganic Material. Edited by Kallman, H. and Spruch, G. M. P. 153. Wiley & Sons, New York, 1962.

5. Cercek, L., Cercek, B., Franklin, C. I. V. Biophysical differentiation between lymphocytes from healthy donors, patients with malignant diseases, and other disorders. Br. J. Cancer 29: 345-352, 1974.

6. Cercek, L., Cercek, B. Changes in the SCM response ratio (RR_{SCM}) after surgical removal of malignant tissue. Br. J. Cancer 31: 250-251, 1975.

7. Cercek, L., Cercek, B. Apparent tumor specificity with the SCM test. Br. J. Cancer 31: 252, 1975.

8. Cercek, L., Cercek, B., Garrett, J. V. Biophysical differentiation between normal human and chronic lymphocytic leukemia lymphocytes. P. 553 in Lymphocyte Recognition and Effector Mechanisms. Edited by Lindahl-Kiessling, K. and Osoba, K. Academic Press, New York, London, 1974.

9. Cercek, L., Cercek, B., Ockey, C. H. Cell membrane permeability during the cell generation cycle in Chinese hamster ovary cells. Biophysik 10: 195-197, 1973.

10. Cercek, L., Cercek, B. Effect of centrifugal forces on the structuredness of cytoplasm in growing yeast cells. Biophysik 9: 105-108, 1973.

11. Cercek, L., Cercek, B. Relationship between changes in the structuredness of cytoplasm and rate constants for the hydrolysis of FDA in saccharomyces cerevisiae. Biophysik 9: 109-112, 1973.

12. Cercek, L., Cercek, B., Ockey, C. H. Structuredness of the cytoplasmic matrix and Michaelis-Menten constants for the hydrolysis of FDA during the cell cycle in Chinese hamster ovary cells. Biophysik 10: 187-194, 1973.

13. Cercek, L., Cercek, B. Studies on the structuredness of cytoplasm and rates of enzymatic hydrolysis in growing yeast cells: I. Changes induced by ionizing radiation. Int. J. Rad. Biol. 21: 5, 445-453, 1972.

14. Cercek, L., Cercek, B. Studies on the structuredness of cytoplasm and rates of enzymatic hydrolysis in growing yeast cells: II. Changes induced by ultra-violet light. Int. J. Rad. Biol. 22: 6, 539-544, 1972.

15. Cercek, L., Cercek, B. Changes in the structuredness of cytoplasm matrix (SCM) in human lymphocytes induced by PHA and cancer basic protein as measured in single cells. Br. J. Cancer 33: 539-543, 1976.

16. Cercek, L., Cercek, B. Effects of osmomolarity, calcium, and magnesium ions on the structuredness of cytoplasmic matrix (SCM). Rad. Environ. Biophys. 13: 9-12, 1976.

17. Chen, R. F., Bowman, R. L. Fluorescence polarization: Measurement with ultraviolet-polarizing filters in a spectrofluoremeter. Science 147: 729-732, 1965.

18. Feofilov, P. P. Physical Basis of Polarized Emission. Chapters 1 & 4. Consultants Bureau, New York, 1961.

19. Feofilov, P. P., Sveshnikoff, B. J. Journal of Physics, U.S.S.R. 3: 493, 1940.

20. Field, E. J., Caspary, E. A., Smith, K. S. Macrophage electrophoretic mobility (MEM) test in cancer: A critical evaluation. Br. J. Cancer 28: Suppl. I, 208-214, 1973.

21. Guilbault, G. G., Kramer, D. N. Fluorometric determination of lipase, acylase, α and γ chymotrypsin and inhibitors of these enzymes. Analyt. Chem. 36: 409-412, 1964.

22. Guyton, A. C. Textbook of Medical Physiology. Chapters 4, 9 & 10. W. B. Saunders Co., Philadelphia, 1971.

23. Harris, R., Ukaekiofo, E. O. Tissue typing using a routine one-step lymphocyte separation technique. Br. J. Haematol. 18: 229-235, 1970.

24. Jablonski, A. Z. Physik 96: 236, 1935.

25. Jackson, J. D. Classical Electrodynamics. John Wiley & Sons, New York, 1962.

26. Jenkins, F. A., White, H. E. Fundamentals of Optics. Third Edition. McGraw-Hill Book Co., New York, 1967.

27. Kasha, M. Theory of molecular luminescence. In Fluorescence: Theory, Instrumentation, and Practice. Edited by Guilbault, G. G. Marcel Dekker, Inc., New York, 1967.

28. Klein, M. V. Optics. Chapters 10 & 11. John Wiley & Sons, Inc., New York, 1970.

29. Ling, G. N. Hydration of macro-molecules. P. 692 in Water and Aqueous Solutions: Structure, Thermodynamics, and Transfer Processes. Edited by Horn, R. A. Wiley-Interscience, New York, 1971.

30. Ling, G. N. A Physical Theory of the Living State. Ginn-Blaisdell, New York, 1962.

31. Mazur, A., Harrow, B. Textbook of Biochemistry. Chapter 4. W. B. Saunders Co., Philadelphia, 1971.

32. Norman, A. Department of Radiology, University of California, Los Angeles, Calif. Direct correspondence.

33. Parker, C. A. Photoluminescence of Solutions. Chapters 1 & 2. Elsevier Publishing Co., New York, 1968.

34. Paul, J. Cell and Tissue Culture. P. 91. E. & S. Livingstone, Edinburgh and London, 1970.

35. Perrin, F. La fluorescence des solutions. Annales de Physiques, Paris, 12: 169, 1929.

36. Pringsheim, P. Fluorescence and Phosphorescence. Chapter 4. Interscience Publishers, Inc., New York, 1949.

37. Rotman, B., Papermaster, B. W. Membrane properties of living mammalian cells as studied by enzymatic hydrolysis of fluorogenic esters. Proc. Natl. Acad. Sci. U.S. 55: 134-141, 1966.

38. Ruch, T. C., Patton, H. D. Physiology and Biophysics. Chapter 43. W. B. Saunders Co., Philadelphia, 1965.

39. Shortman, K., Legge, D. G. The effect of pH on the volume, density and shape of erythrocytes and thymic lymphocytes. Br. J. Haematol. 3: Vol. 14, 1968.

40. Shurcliff, W. A. Polarized Light: Production and Use. Harvard University Press, Cambridge, Mass., 1962.

41. Singer, S. J. Molecular biology of cellular membranes with applications to immunology. In Advances in Immunology. Vol. 19. Edited by Dixon, F. J., Kunkel, H. G. Academic Press, New York, 1974.

42. Soleillet, P. Ann. Phys. X, 12: 23, 1929.

43. Udenfriend, S., Zaltzman-Nirenberg, P., Guroff, G. A study of cellular transport with the fluorescent amino acid aminonaphthylalanine. Arch. Biochem. Biophys. 116: 261-270, 1966.

44. Warner, N. L. Membrane immunoglobulins and antigen receptors on B and T lymphocytes. In Advances in Immunology. Vol. 19. Edited by Dixon, F. J. and Kunkel, H. G. Academic Press, New York, 1974.

45. Weber, G. Dependence of the polarization of fluorescence on the concentration. Trans. Faraday Soc. 50: 552, 1954.

46. Weber, G. Photoelectric method for the measurement of the polarization of the fluorescence of solutions. J. Optical Soc. Am. 46: 962-970, 1956.

47. Weber, G. Polarization of the fluorescence of macromolecules. Biochemistry 51: 145-155, 1952.

48. Weber, G. Rotational Brownian motion and polarization of the fluorescence of solutions. In Advances in Protein Chemistry, 8: 416. Academic Press, New York, 1953.

49. Wehry, E. L. Structure and environmental factors in fluorescence. In Fluorescence: Theory, Instrumentation, and Practice. Edited by Guilbault, G. G. Marcel Dekker, Inc., New York, 1967.

APPENDIX A

POLARIZED LIGHT

Light, or electromagnetic radiation, can be described as the superposition of plane waves.[1] These consist of sinusoidally varying electric and magnetic fields aligned perpendicular to each other and to the direction of propagation (Figure 16).

To facilitate the discussion and pictorial representation of these waves it is customary to refer to only one of the two fields and usually the electric. Knowing either of the fields the other may be deduced from Maxwell's equations.

A.1 Pure Polarized Light

For a single monochromatic plane wave travelling in the positive z direction with respect to an xyz Cartesian coordinate system, the

---

[1]As derived from Maxwell's equations, the three-dimensional wave equations governing the behavior of the electric and magnetic fields in linear isotropic nonconducting media are:

$$\nabla^2 \vec{E} - \frac{1}{v^2} \frac{\partial^2 \vec{E}}{\partial t^2} = 0; \quad \nabla^2 \vec{B} - \frac{1}{v^2} \frac{\partial^2 \vec{B}}{\partial t^2} = 0$$

with $v = c/n$; $n = (\varepsilon\mu)^{\frac{1}{2}}$; $\vec{D} = \varepsilon\vec{E}$; $\vec{B} = \mu\vec{H}$
where c is the wave speed in a vacuum, v is the phase velocity, and where n, ε and μ are the index of refraction, dielectric constant, and magnetic permeability of the medium respectively.

Analytic plane wave solutions to these equations (25) are:

$$\vec{E} = \vec{E}_0 \, e^{i(\omega t - \vec{k}\cdot\vec{r})}; \quad \vec{B} = \vec{B}_0 \, e^{i(\omega t - \vec{k}\cdot\vec{r})}$$

with $k = |\vec{k}| = \omega/v$, where ω is the frequency of oscillation of the fields.

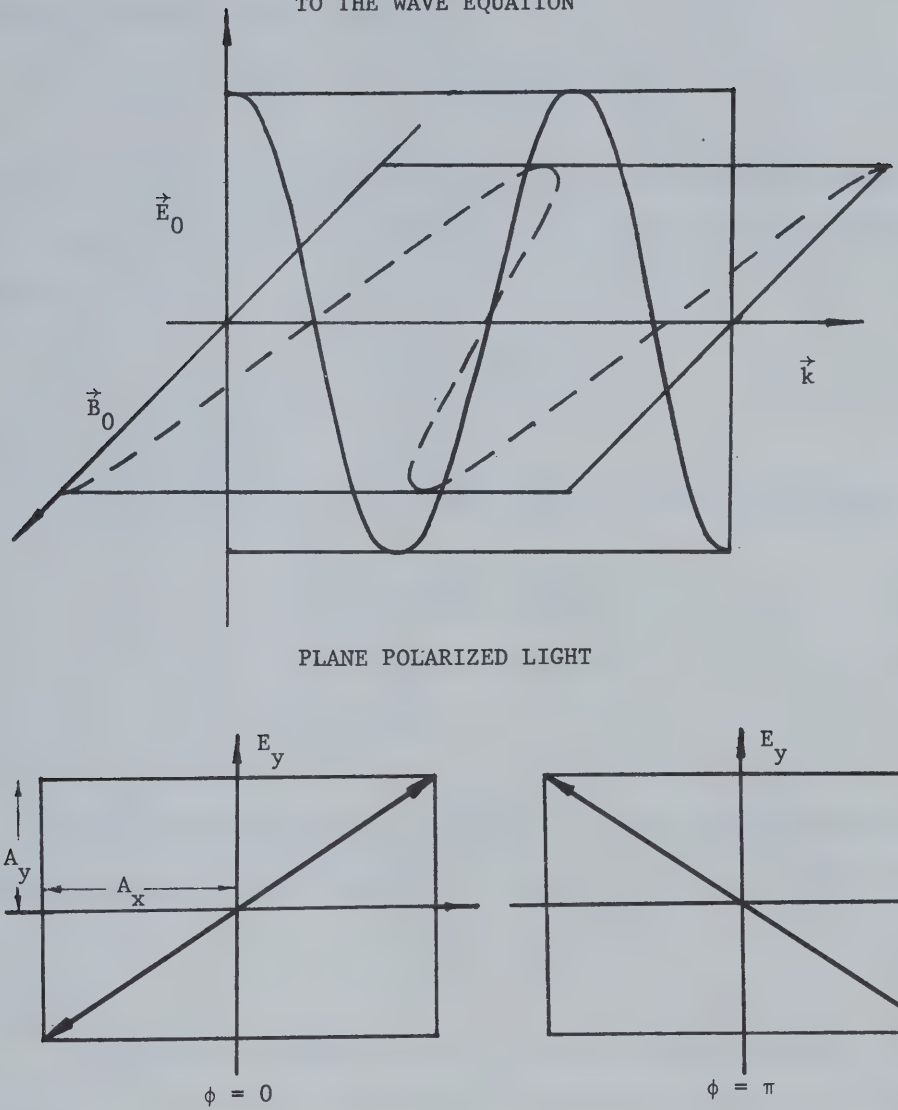

FIGURE 16 . Spatial and temporal cross sections for plane polarized light.

physical electric field is given by:

$$\vec{E}(x,y,z,t) = \mathrm{Re}\{\vec{E}_0 e^{i(\omega t - kz)}\} \qquad (A.1.1)$$

where Re{ } and Im{ } represent the real and imaginary parts respectively of a complex number, and where $\vec{E}_0$ is a vector in the xy plane that may be complex;

$$\text{i.e.,} \qquad \vec{E}_0 = (\bar{E}_x, \bar{E}_y, 0) \qquad (A.1.2)$$

where $\bar{E}_x = A_x e^{i\phi x}$ and $\bar{E}_y = A_y e^{i\phi y}$.

The individual components of the total electric field are therefore:

$$E_x = A_x \cos(\omega t - kz + \phi_x) \qquad (A.1.3a)$$

$$E_y = A_y \cos(\omega t - kz + \phi_y) \qquad (A.1.3b)$$

$$E_z = 0 \qquad (A.1.3c)$$

Different types of pure polarized light are distinguished by the relative sizes of A_y and A_x and on the phase difference ϕ defined by:

$$\phi = \phi_y - \phi_x \qquad (A.1.4)$$

In general the quantities A_y, A_x and ϕ assume arbitrary value and the light is elliptically polarized. From a fixed point on the z axis the electric field vector traces out an ellipse in the xy plane with an angular speed ω. The ellipse is contained in a rectangle whose sides are parallel to the coordinate axes and whose dimensions are $2A_y$ by $2A_x$. The eccentricity of the ellipse ε depends on the magnitude of ϕ while the helicity, or sense of rotation about z, depends on the sign. If $\phi > 0$ then the sense of rotation is clockwise (negative helicity) and the light is defined to be right elliptically polarized (REP). Conversely, for

$\phi < 0$ the rotation is counterclockwise (positive helicity) and the light is left elliptically polarized (LEP). For fixed t the electric vector traces out a helix along an elliptical cylinder parallel to the z axis with a cross section identical to the ellipse referenced above for fixed z. The sense of rotation of this helix about the z axis is opposite to that of the electric vector for fixed z. These features are shown in Figure 17.

Plane polarized light occurs for $\phi = 0$ or $\phi = \pi$ and the electric field components from (A.1.3) are given by:

$$E_y = \pm \frac{A_y}{A_x} E_x \qquad \text{(A.1.5)}$$

where E_y is positive for $\phi = 0$ and negative for $\phi = \pi$.
For either of these cases the eccentricity of the ellipse describing the electric field is a maximum ($\varepsilon = 1$) and for fixed z the electric field undergoes simple harmonic motion along the diagonal of the rectangle (Figure 16). At a given time, the electric field undergoes simple harmonic motion in a plane containing the diagonal of the rectangle and running parallel to the z axis.

When $\phi = \pm \frac{\pi}{2}$ and $A_y \neq A_x$ the eccentricity of the ellipse is a minimum ($0 < \varepsilon < 1$) and the major axis of the ellipse lies along the x axis.

For $\phi = \pm \frac{\pi}{2}$ and $A_y = A_x$ the eccentricity is zero and the light is right or left circularly polarized (RCP or LCP). In these cases the electric field components from (A.1.3) are:

$$E_x = A_x \cos(\omega t - kz + \phi_x) \qquad \text{(A.1.6a)}$$

$$E_y = \pm A_x \sin(\omega t - kz + \phi_x) \qquad \text{(A.1.6b)}$$

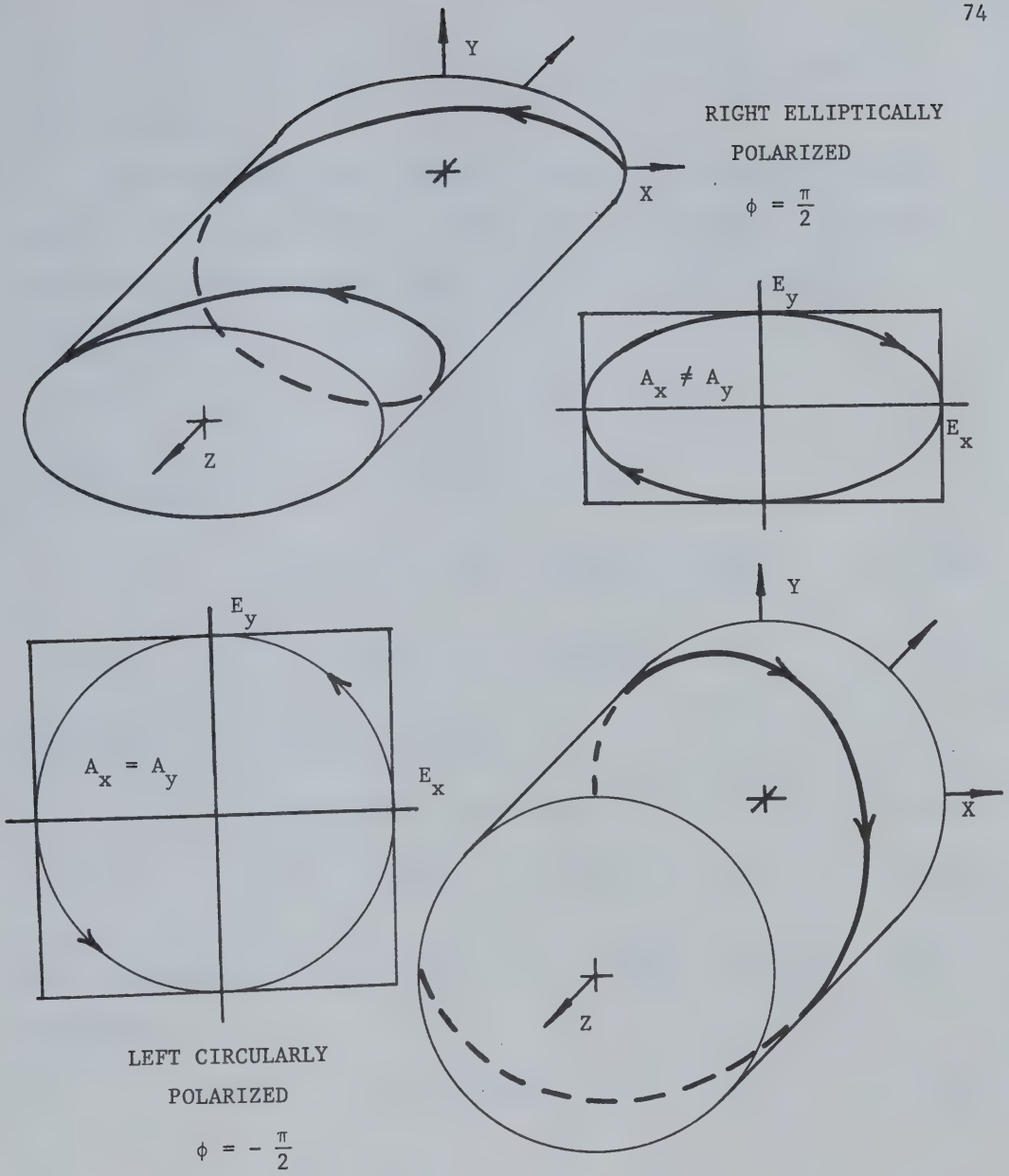

FIGURE 17 . Spatial and temporal cross sections for elliptically and circularly polarized light.

where E_y is positive for $\phi = -\frac{\pi}{2}$ and negative for $\phi = +\frac{\pi}{2}$. This is shown in Figure 17.

Although elliptically polarized light may be described as the superposition of two orthogonal plane polarized components an equally valid depiction is the superposition of left and right circularly polarized components (28). Defining θ:

$$\theta = \omega t - kz \tag{A.1.7}$$

the LCP components from (A.1.6) can be written:

$$E_x = A_+ \cos(\theta + \phi_+) = \mathrm{Re}\{A_+ e^{i\theta} e^{i\phi_+}\} \tag{A.1.8a}$$

$$E_y = A_+ \sin(\theta + \phi_+) = \mathrm{Im}\{A_+ e^{i\theta} e^{i\phi_+}\} \tag{A.1.8b}$$

and similarly for the RCP components:

$$E_x = A_- \cos(\theta - \phi_-) = \mathrm{Re}\{A_- e^{-i\theta} e^{i\phi_-}\} \tag{A.1.9a}$$

$$E_y = -A_- \sin(\theta - \phi_-) = \mathrm{Im}\{A_- e^{-i\theta} e^{i\phi_-}\} \tag{A.1.9b}$$

With equations (A.1.8) and (A.1.9) the total analytical electric field is written:

$$\bar{E} = E_x + iE_y = A_+ e^{i\phi_+} e^{i\theta} + A_- e^{i\phi_-} e^{-i\theta} \tag{A.1.10}$$

By defining α and β such that:

$$\beta = \phi_- + \phi_+ \tag{A.1.11a}$$

$$\alpha = \phi_- - \phi_+ \tag{A.1.11b}$$

equation (A.1.10) can be written:

$$\bar{E} = e^{i\beta/2}(A_+ e^{i(\theta - \alpha/2)} + A_- e^{-i(\theta - \alpha/2)}) \qquad (A.1.12)$$

Equation (A.1.12) completely defines the general case of elliptically polarized light. For $\theta = \alpha/2$,

$$\bar{E} = e^{i\beta/2}(A_+ + A_-) \qquad (A.1.13)$$

and the magnitude $A_+ + A_-$ (which is the physical electric field) is the major axis of the ellipse making an angle $\beta/2$ with the x axis. For $\theta = \alpha/2 + \pi/2$,

$$\bar{E} = e^{i(\beta/2 + \pi/2)}(A_+ - A_-) \qquad (A.1.14)$$

and the magnitude $A_+ - A_-$ is the minor axis making an angle $\beta/2 + \pi/2$ with the x axis. These features are shown in Figure 18.

Finally, the essential parameters from both the plane polarized and circularly polarized superpositions are related by:

$$\sin 2\eta = \sin 2\chi \sin \phi \qquad (A.1.15a)$$

$$\tan \beta = \tan 2\chi \cos \phi \qquad (A.1.15b)$$

where $\tan \beta$ is positive for REP and negative for LEP, and where:

$$\chi = \tan^{-1}\left(\frac{A_y}{A_x}\right) \qquad (A.1.16)$$

$$\eta = \tan^{-1}(|A_+ - A_-|/(A_+ + A_-)) \qquad (A.1.17)$$

A.2 Partially Polarized Light

In Section A.1 pure polarized states were described for single monochromatic waves. Since light can be described as the superposition of

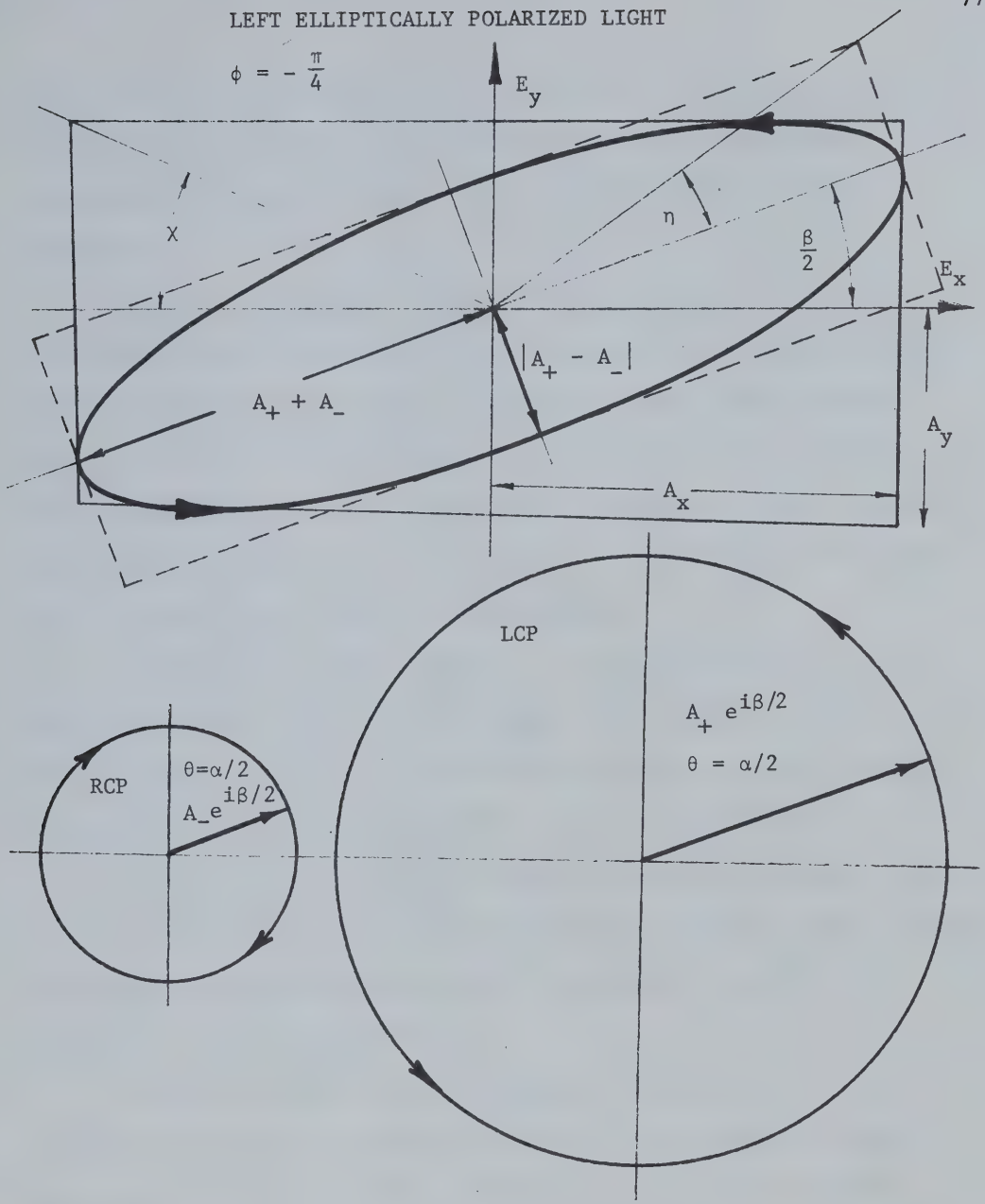

FIGURE 18 . Elliptically polarized light as the superposition of left and right circularly polarized light. (After Klein (28)).

such waves, the polarization characteristics of a macroscopic beam of monochromatic light can be defined in terms of the time averages of two perpendicular field components and the mutual coherence of these components.

However, in contrast with pure polarized states, where there is a well defined phase difference between two perpendicular field components, the superposition of many waves can produce a phase difference that changes rapidly over the period of observation and remains undefined. When this occurs, the time average of any two electric field components (in a plane perpendicular to the direction of propagation) will be the same, and the light is said to be unpolarized.

If unpolarized light combines with pure polarized light the resulting mixture is partially polarized. To characterize partially polarized light the degree of polarization is defined as the ratio of the intensity of the polarized part to the total intensity (26).

To physically determine the state of pure polarized light or the degree of polarization in the case of partially polarized light, a plane polarizing filter and a phase shifter are ordinarily needed. This procedure is described in Section A.3.

A plane polarizing filter converts unpolarized light to plane polarized by transmitting only the electric field components aligned in a particular direction. This is referred to as the pass direction. Polarizers are usually made with a dichroic material or less commonly with birefringent (doubly refracting) crystals (40).

A phase shifter, or compensator, acts on a normally incident beam by retarding the phase of all electric field components aligned perpendicular to a fixed axis relative to the field components aligned

parallel to the axis. The direction along which the field components are retarded is called the slow axis while the fixed axis is called the fast axis. A compensator imposing a phase shift of $\pi/2$ is called a quarter-wave plate. By positioning the fast axis of a quarter-wave plate along the direction of the major axis of elliptically polarized light the light is converted to plane polarized. This follows from the fact that the resultant phase difference between field components parallel and perpendicular to the major axis will be 0 or π depending on the helicity of the incident light. Compensators are made from uniaxial birefringent crystals (40).

A.3 A Coherency Matrix

Recalling equation (A.1.1), the analytic electric field components at a particular point in space are given by:

$$\bar{E}_x = A_x e^{i(\omega t + \phi_x)} \tag{A.3.1a}$$

$$\bar{E}_y = A_y e^{i(\omega t + \phi_y)} \tag{A.3.1b}$$

By placing a compensator in the light with its fast axis along the x axis the field components become:

$$\bar{E}_x = A_x e^{i(\omega t + \phi_x)} \tag{A.3.2a}$$

$$\bar{E}'_y = A_y e^{i(\omega t + (\phi_y - \delta))} = e^{-i\delta} \bar{E}_y \tag{A.3.2b}$$

where δ is the amount that ϕ_y is retarded relative to ϕ_x.

If the resulting beam then passes through a polarizer with its pass direction inclined at an angle α to the x axis, the emerging signal

will be the sum of the projections of $\bar{E}_x$ and $\bar{E}_y'$ along α:

$$\bar{E}(\alpha,\delta) = \bar{E}_x \cos\alpha + e^{-i\delta}\,\bar{E}_y \sin\alpha \qquad \text{(A.3.3)}$$

The intensity[2] can then be expressed:

$$I(\alpha,\delta) = \langle \bar{E}(\alpha,\delta)\,\bar{E}^*(\alpha,\delta) \rangle \qquad \text{(A.3.4)}$$

where the notation $\langle\ \rangle$ and * represent time average and complex conjugate respectively.

Expanding (A.3.4) in terms of (A.3.3) the intensity becomes:

$$I(\alpha,\delta) = \langle \bar{E}_x\bar{E}_x^* \rangle \cos^2\alpha + \langle \bar{E}_y\bar{E}_y^* \rangle \sin^2\alpha + (\langle \bar{E}_x\bar{E}_y^* \rangle e^{i\delta} + \langle \bar{E}_x^*\bar{E}_y \rangle e^{-i\delta}) \sin\alpha\cos\alpha \qquad \text{(A.3.5)}$$

Following a similar derivation by Klein (28), the four time averages appearing in (A.3.5) may be described as the elements of a 2 x 2 matrix

---

[2]Although not technically correct, the intensity is described:

$$I = |\vec{E}_0|^2$$

which is an abbreviated form of the mean irradiance. The irradiance, or electromagnetic flux density, associated with the plane waves described above is given by (25):

$$\vec{S} = \vec{E} \times \vec{H}$$

where $\vec{S}$ is Poynting's vector. The mean irradiance can be written:

$$S = \langle \vec{S} \rangle = \frac{n}{2\mu} |\vec{E}_0|^2$$

where the factor of ½ evolves from averaging a $\cos^2$ function of time.

Since the derivation of the degree of polarization involves the ratio of two irradiances, the expression for I as given above may be used. I is only used to simplify the derivation. More physically correct:

$$I \propto |\vec{E}_0|^2$$

(MKS units have been used in the discussion above.)

called the coherency matrix:

$$C = \begin{pmatrix} C_{xx} = \langle \bar{E}_x \bar{E}^*_x \rangle & C_{xy} = \langle \bar{E}_x \bar{E}^*_y \rangle \\ C_{yx} = \langle \bar{E}^*_x \bar{E}_y \rangle & C_{yy} = \langle \bar{E}_y \bar{E}^*_y \rangle \end{pmatrix} \qquad \text{(A.3.6)}$$

Since $C^*_{xy} = C_{yx}$, these quantities may be expressed as:

$$C_{xy} = |C_{xy}| \, e^{-i\phi} \qquad \text{(A.3.7a)}$$

$$C_{yx} = |C_{xy}| \, e^{i\phi} \qquad \text{(A.3.7b)}$$

Equation (A.3.5) can then be simplified:

$$I(\alpha,\delta) = C_{xx} \cos^2\alpha + C_{yy} \sin^2\alpha + 2|C_{xy}| \sin\alpha \cos\alpha \cos(\delta - \phi) \qquad \text{(A.3.8)}$$

When (A.3.8) is averaged over α:

$$\langle I(\alpha,\delta) \rangle_\alpha = 1/2 \, (C_{xx} + C_{yy}) = 1/2 \, I_t \qquad \text{(A.3.9)}$$

where I_t is the total intensity of the beam. The total intensity can be written:

$$I_t = C_{xx} + C_{yy} = \text{Tr } C \qquad \text{(A.3.10)}$$

where Tr indicates the trace or sum of the diagonal elements of a matrix. Using equations (A.3.1), the coherency matrix for arbitrary elliptically polarized light is written:

$$C = \begin{pmatrix} \langle A_x^2 \rangle & e^{-i\phi} \langle A_x A_y \rangle \\ e^{i\phi} \langle A_x A_y \rangle & \langle A_y^2 \rangle \end{pmatrix} \qquad \text{(A.3.11)}$$

and using equation (A.1.16) with $I_t = \langle A_x^2 \rangle + \langle A_y^2 \rangle$:

$$C = I_t \begin{pmatrix} \cos^2\chi & e^{-i\phi} \sin\chi \cos\chi \\ e^{i\phi} \sin\chi \cos\chi & \sin^2\chi \end{pmatrix} \qquad \text{(A.3.12)}$$

Examining C shows that det $C = 0$ for all pure polarized states where det $C = C_{xx} C_{yy} - C_{yx} C_{xy}$.

For unpolarized light there is no coherence between the x and y components and therefore $C_{xy} = C_{yx} = 0$. Also, since the time averages of any two perpendicular components must be equal, $\langle A_x \rangle = \langle A_y \rangle$, and the coherency matrix for unpolarized light is written:

$$C = \frac{I_t}{2} \begin{pmatrix} 1 & 0 \\ 0 & 1 \end{pmatrix} \qquad \text{(A.3.13)}$$

These matrices are used to calculate the degree of polarization of partially polarized light.

A.4 The Degree of Polarization

An arbitrary coherency matrix may be written as the sum of a polarized and an unpolarized matrix:

$$C = \begin{pmatrix} a & 0 \\ 0 & a \end{pmatrix} + \begin{pmatrix} b & d \\ d^* & c \end{pmatrix} = C^u + C^p \qquad \text{(A.4.1)}$$

where u and p indicate unpolarized and polarized light respectively.

C may also be expressed:

$$C = \begin{pmatrix} C_{xx} = a + b & C_{xy} = d \\ C_{yx} = d^* & C_{yy} = c + a \end{pmatrix} \qquad (A.4.2)$$

From section A.3, det $C^p = 0$ so that:

$$bc - d^*d = 0 \qquad (A.4.3)$$

Substituting $b = C_{xx} - a$, and $c = C_{yy} - a$ from (A.4.2) into equation (A.4.3) yields:

$$a^2 - a\,(C_{xx} + C_{yy}) + C_{xx}\,C_{yy} - C_{xy}\,C_{yx} = 0 \qquad (A.4.4)$$

or restating (A.4.4) in terms of the trace and determinant of C:

$$a^2 - a\ \mathrm{Tr}\ C + \det C = 0 \qquad (A.4.5)$$

Following Klein (28), the only meaningful solution to (A.4.5) is:

$$a = \frac{\mathrm{Tr}\ C - ((\mathrm{Tr}\ C)^2 - 4 \det C)^{\frac{1}{2}}}{2} \qquad (A.4.6)$$

Solving for b and c in (A.4.2) yields:

$$b = \frac{C_{xx} - C_{yy} + ((\mathrm{Tr}\ C)^2 - 4 \det C)^{\frac{1}{2}}}{2} \qquad (A.4.7)$$

$$c = \frac{C_{yy} - C_{xx} + ((\mathrm{Tr}\ C)^2 - 4 \det C)^{\frac{1}{2}}}{2} \qquad (A.4.8)$$

Since $I_t = \mathrm{Tr}\ C$ from (A.3.10):

$$I_p = \mathrm{Tr}\ C^p \qquad (A.4.9a)$$

$$I_u = \mathrm{Tr}\ C^u \qquad (A.4.9b)$$

and the degree of polarization P can be written:

$$P = \frac{I_p}{I_t} = \frac{\text{Tr } C^p}{\text{Tr } C} = \left(\frac{1 - 4 \det C}{(\text{Tr } C)^2} \right)^{\frac{1}{2}} \qquad \text{(A.4.10)}$$

Although the four real elements of an arbitrary coherency matrix (C_{xx}, C_{yy}, $|C_{xy}|$, ϕ) can be determined with several combinations of polarizer and compensator readings, the following method is the most accepted.

A.5 Experimental Determination of P

Rewriting equation (A.4.1) in terms of (A.3.12) and (A.3.13):

$$C = \frac{I_u}{2} \begin{pmatrix} 1 & 0 \\ 0 & 1 \end{pmatrix} + I_p \begin{pmatrix} \cos^2\chi & e^{-i\phi}\sin\chi\cos\chi \\ e^{i\phi}\sin\chi\cos\chi & \sin^2\chi \end{pmatrix} \qquad \text{(A.5.1)}$$

If a compensator is used to shift the phase of E_y relative to E_x by an amount $\delta = -\phi$, C^u remains the same and C^p changes to:

$$C^p = I_p \begin{pmatrix} \cos^2\chi & \sin\chi\cos\chi \\ \sin\chi\cos\chi & \sin^2\chi \end{pmatrix} \qquad \text{(A.5.2)}$$

This represents plane polarized light where $\phi = 0$ or π. C may then be written:

$$C = \frac{I_u}{2} \begin{pmatrix} 1 & 0 \\ 0 & 1 \end{pmatrix} + I_p \begin{pmatrix} \cos^2\chi & \sin\chi\cos\chi \\ \sin\chi\cos\chi & \sin^2\chi \end{pmatrix} \qquad \text{(A.5.3)}$$

By inserting a polarizer in the light with its pass direction oriented at an angle α with the x axis, the intensity can be described from

equation (A.3.5):

$$I(\alpha) = \frac{I_u}{2} + I_p \cos^2(\chi - \alpha) \qquad (A.5.4)$$

When $\alpha = \chi$, $I(\alpha)$ becomes a maximum:

$$I_{max} = \frac{I_u}{2} + I_p \qquad (A.5.5)$$

Conversely, when $\alpha = \chi + \pi/2$, $I(\alpha)$ is a minimum:

$$I_{min} = \frac{I_u}{2} \qquad (A.5.6)$$

Finally, the degree of polarization can be written:

$$P = \frac{I_p}{(I_u + I_p)} \quad \frac{I_{max} - I_{min}}{I_{max} + I_{min}} \qquad (A.5.7)$$

The only experimental difficulty using equation (A.5.7) is imposing a phase shift $\delta = \phi$ in the original light. As explained in Section A.2 this can be done with a quarter-wave plate. The major axis of the elliptically polarized part is first located by rotating a polarizer in the incident light. Then, by placing a quarter-wave plate along the direction of the major axis the elliptically polarized fraction is converted to plane polarized. The maximum and minimum intensities of the emerging light are determined with a polarizer and the degree of polarization is calculated from (A.5.7). In some cases the directions of maximum intensity are known *a priori*. Equation (A.5.7) is then directly applicable without the need of a compensator.

APPENDIX B

FLUORESCENCE

B.1 Fluorescence

As a consequence of the energy differences between electronic states certain molecules in solution will absorb electromagnetic radiation from the visible and ultraviolet parts of the spectrum. Several processes compete for the excess energy of an excited molecule and the relative kinetics of these processes are determined by the electronic structure of the molecule and its interaction with the surrounding medium.

At room temperature most molecules occupy the lowest vibrational level of the ground electronic state and by absorbing light can be excited to higher vibrational levels of secondary electronic states. Sometimes the absorbed energy is sufficient to cause photochemical reactions such as dissociation but in most cases the excess enrgy is lost by emission or by collision with other molecules.

Two electrons occupying the same ground state molecular orbital must satisfy the Pauli exclusion principle and have opposite spin. Hence, the total angular momentum from electron spin in this state is zero. In the excited state, however, an electron raised to an upper level can have the same spin alignment as the one remaining in the original orbital. This configuration is called the triplet state because there are three possible angular momenta associated with the total electron spin. Accordingly, the triplet state has a spin multiplicity of three and the ground state, or singlet, has a spin multiplicity of one.

There are two radiative processes by which an electronically excited molecule can return to the ground state: fluorescence and phosphorescence.

Fluorescence is the most probable of these and is defined as the radiative transition between two states of the same multiplicity. The most common fluorescent transitions are from the first excited singlet to the ground state singlet and the average lifetime between absorption and fluorescence is approximately 10^{-9} seconds.

Phosphorescence is a more intricate process than fluorescence and is defined as the radiative transition between two states of different multiplicity. Such transitions are theoretically forbidden and only occur as the result of spin-orbit coupling (33). Because of spin-orbit coupling a molecule in a low vibrational level of an excited singlet can transfer to a high vibrational level of the corresponding excited triplet. This process is known as intersystem crossing (33). Spin-orbit coupling then enables the excited triplet to decay to the ground state singlet with the emission of light. Since the transition probability is very low, the lifetime of phosphorescence is rarely less than 10^{-4} seconds and can be as much as one second. Phosphorescence is rarely observed from solutions because of various quenching mechanisms and can only be obtained from rigid media (49). The combined processes of fluorescence and phosphorescence are referred to as luminescence.

During the lifetime of the excited state molecules in solution undergo many collisions and rapidly lose their excess vibrational energy. As a result the molecule relaxes to the lowest vibrational level of the excited singlet and the wavelength of subsequent emission is longer than that of the light originally absorbed. This feature is prominent in the

emission spectra of solutions and is referred to as Stoke's law (33).

Another important process competing for the energy of an excited molecule is internal conversion. This occurs when a molecule transfers from a low vibrational level of an excited state to a high vibrational level of a lower state of the same multiplicity. Again, the excess energy is lost in collisions and the process is non radiative.

The main features of a luminescing molecule are shown in Figure 19. The diagram is drawn for diatomic molecules but is generally applicable. Due to spin-orbit coupling the triplet state of an atom consists of three closely spaced energy levels. These are not usually distinguished in molecules (33) and the triplet is illustrated as one level. In the triplet state there is less Coulomb repulsion between electrons and therefore this state lies below the corresponding singlet on a potential energy scale.

From the Franck-Condon principle, light absorption takes place within the period of vibration of the light wave ($\simeq 10^{-15}$ sec) and during this time there is no appreciable nuclear motion. The transitions in the diagram are therefore drawn as vertical lines from the most probable nuclear configurations. In the scale of the diagram the energy spacing of the rotational levels is too small to be shown clearly and only the vibrational levels have been drawn. These are represented with horizontal lines.

The shape of the potential energy curve of an electronic level to which a transition is taking place determines the general features of an absorption or emission spectrum. The vertical lines in Figure 19 represent the most probable transitions and correspond to the wavelengths

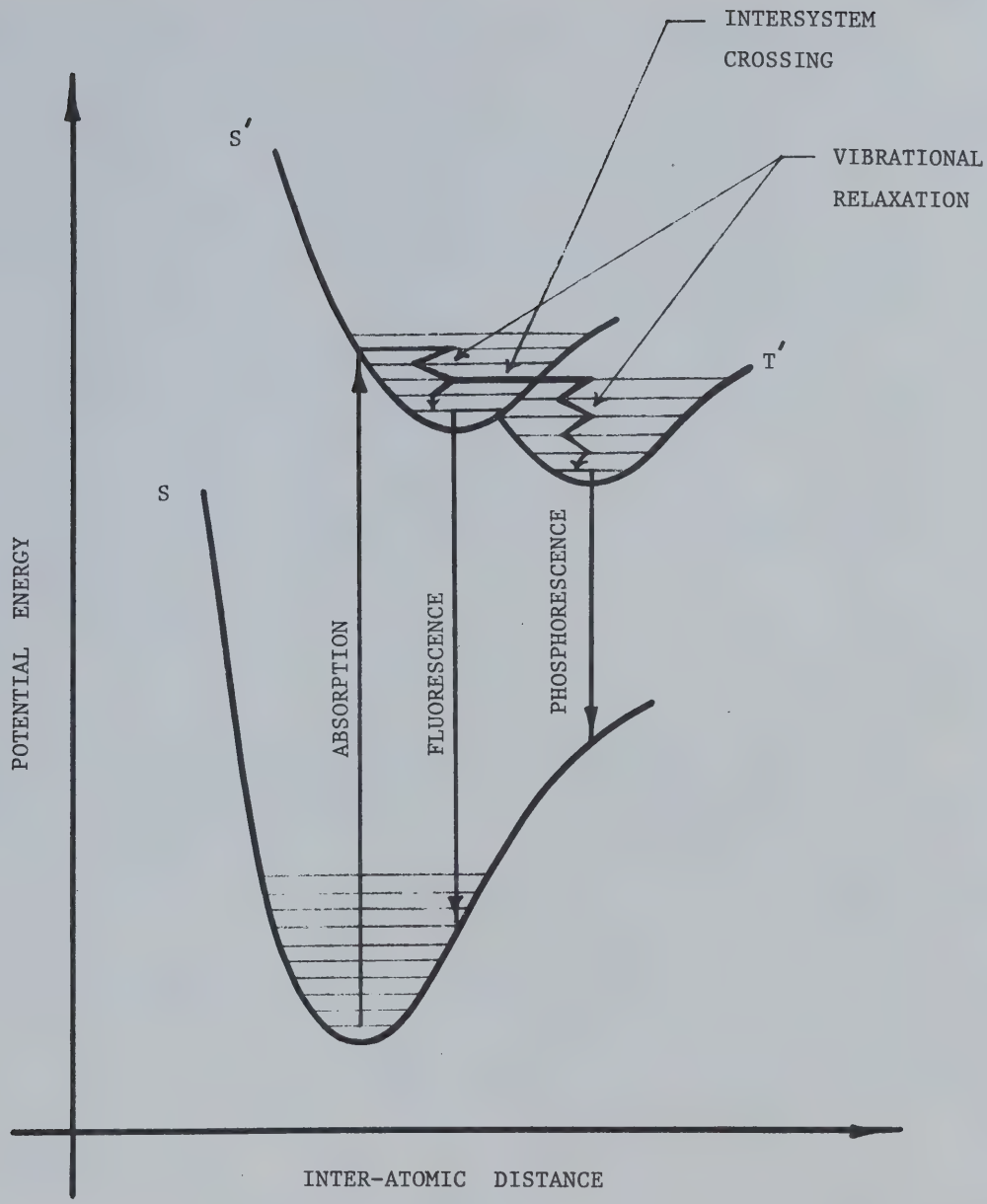

FIGURE 19 . Franck-Condon principle applied to the luminescence of a diatomic molecule . The electronic levels shown are the ground state singlet (S) , the first excited singlet (S') , and the first excited triplet (T') .

at which absorption or emission is a maximum. For absorption, the potential energy curve of the excited singlet (S´) is steeper to the left of the most probable transition and therefore the absorption spectrum will be broader to the shorter wavelength side of the maximum. If the vibrational energy spacing of the excited singlet is similar to that of the ground state singlet, the opposite is true for fluorescence and the emission spectrum is a mirror image of the absorption spectrum.

Unless a luminescing system is continually excited the intensity of fluorescence decays exponentially. This follows from the fact that the number of molecules emitting per unit time is proportional to the number excited at that time; i.e.,

$$\frac{d}{dt}n = k \cdot n \qquad \text{(B.1.1)}$$

where n is the number of excited molecules at any time. Letting n_0 be the number of excited molecules at t = 0 and integrating yields

$$n = n_0 \cdot e^{-kt} \qquad \text{(B.1.2)}$$

The rate of emission of light, Q, is given by:

$$Q = -\frac{d}{dt}n = k \cdot n_0 \cdot e^{-kt} \qquad \text{(B.1.3a)}$$

or defining $k = 1/\tau$:

$$Q = \frac{n_0 \cdot e^{-t/\tau}}{\tau} \qquad \text{(B.1.3b)}$$

where τ is the mean radiative lifetime of fluorescence.

The above formulation assumes that every excited molecule undergoes fluorescence. In general, because of the many processes competing with fluorescence a fluorescence yield, ϕ_F, must be defined.

$$\phi_F = \frac{\text{einsteins of light emitted as fluorescence}}{\text{einsteins of light absorbed}} \qquad \text{(B.1.4)}$$

where one einstein is an Avogadros number of photons. This does not affect the basic assumption of equation (B.1.1) and the decay of fluorescence remains exponential.

B.2 Fluorescence and Electronic Structure

Fluorescence is nearly always associated with the π electron system of an unsaturated molecule (33). In the theory of atomic orbitals the electronic transition of lowest energy usually corresponds to the excitation of an electron from a π orbital (bonding) to an upper π^* orbital (antibonding). However, for some molecules containing atoms with lone pair electrons, the transition of lowest energy corresponds to exciting an electron from a lone pair orbital to a π^* orbital. These transitions have been classified by Kasha (27) according to whether the lone pair electrons conjugate fully, partially, or not at all with the π electron system to which an electron is being excited. If the lone pair orbital is located perpendicular to the nodal plane of the π electron system then full conjugation is possible and the lowest energy transition is $\pi \rightarrow \pi^*$. For lone pair orbitals located parallel to the nodal plane no conjugation is possible and the lowest energy transition is from the non-bonding orbital to a π^* orbital written as $n \rightarrow \pi^*$. Located at intermediate angles, electrons from a lone pair can partially conjugate and

are only partially bonding. This absolves any strict planarity with respect to π electron configuration and the lowest energy transition is from the lone pair orbital to an antibonding orbital of π origin written as $1 \rightarrow a_{\pi}$.

Fluorescence associated with these absorption transitions is strongest from molecules excited by $\pi \rightarrow \pi^*$ and $1 \rightarrow a_{\pi}$ mechanisms. Molecules excited by $n \rightarrow \pi^*$ transitions show relatively weak fluorescence. According to Wehry (49), there are two reasons for this. For (n,π^*) excited states the radiative lifetime is usually longer than for (π,π^*) states and therefore non-radiative processes competing with fluorescence such as internal conversion are more significant. Also, since the energy differences between the first excited singlet and corresponding triplet are considerably less for (n,π^*) states compared to (π,π^*) states, intersystem crossing and phosphorescence are more probable.

Because of their high degree of π orbital conjugation most unsubstituted aromatic hydrocarbon solutions exhibit intense fluorescence yield increases and fluorescence energies decrease as the length of a conjugated system increases. The most intensely fluorescent aromatic molecules are characterized by rigid, planar structures. The principal effect of increasing molecular rigidity is to decrease vibrational amplitudes which reduces the efficiency of intersystem crossing and internal conversion and thus increases the fluorescent yield (49). Figure 20 relates electronic structure and fluorescence for several aromatic molecules.

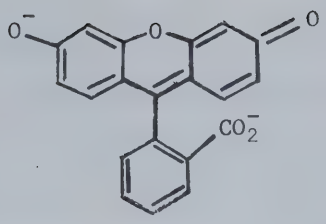

FLUORESCEIN

FLUORESCENT RIGID
PLANAR STRUCTURE

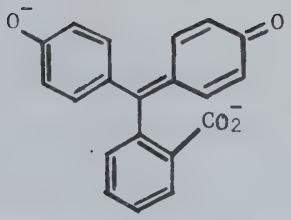

PHENOLPHTALEIN

NON FLUORESCENT
NON PLANAR STRUCTURE

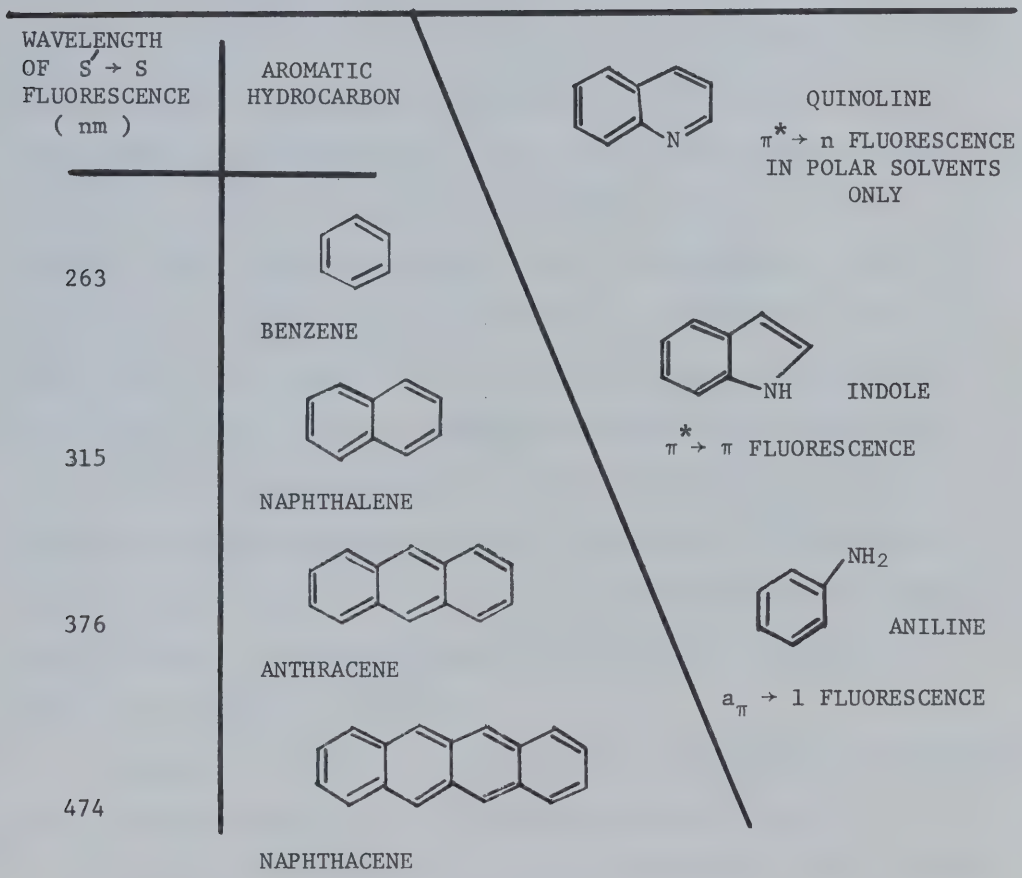

FIGURE 20 . Fluorescence and electronic structure.

B.3 External Effects on Fluorescence

When light absorption takes place, a molecule immediately (10^{-15} sec) possesses an excited, geometrically extended electronic distribution. Because of the high inertia of the constituent nuclei the nuclear configuration cannot change in 10^{-15} seconds and remains essentially the same as that of the ground level. This transitory structure is called the Franck-Condon excited state. During its radiative lifetime (10^{-9} sec) the excited molecule subsequently relaxes to an extended more stable nuclear geometry. Simultaneously the surrounding solvent molecules relax to a new configuration consistent with the electronic distribution and the geometry of the excited molecule. This "equilibrium" excited state is considerably lower in energy than the Franck-Condon excited state and all fluorescence originates from this level. Upon emission, the excited electronic distribution contracts to the ground state distribution leaving the nuclei in the excited configuration. This intermediate structure is called the Franck-Condon ground state. The molecule then undergoes structural and solvent reorientation and drops to the equilibrium ground state from which it originally absorbed. The energy relations of the four states are shown in Figure 21.

External effects on the fluorescence of a molecule are determined by the chemical properties of the equilibrium excited state.

Because the electron distribution in the excited state is less rigidly bound than in the ground state the excited molecule is usually more polarisable and therefore more easily solvated. Thus, by increasing solvent polarity the stability of (π,π^*) excited states increases relative

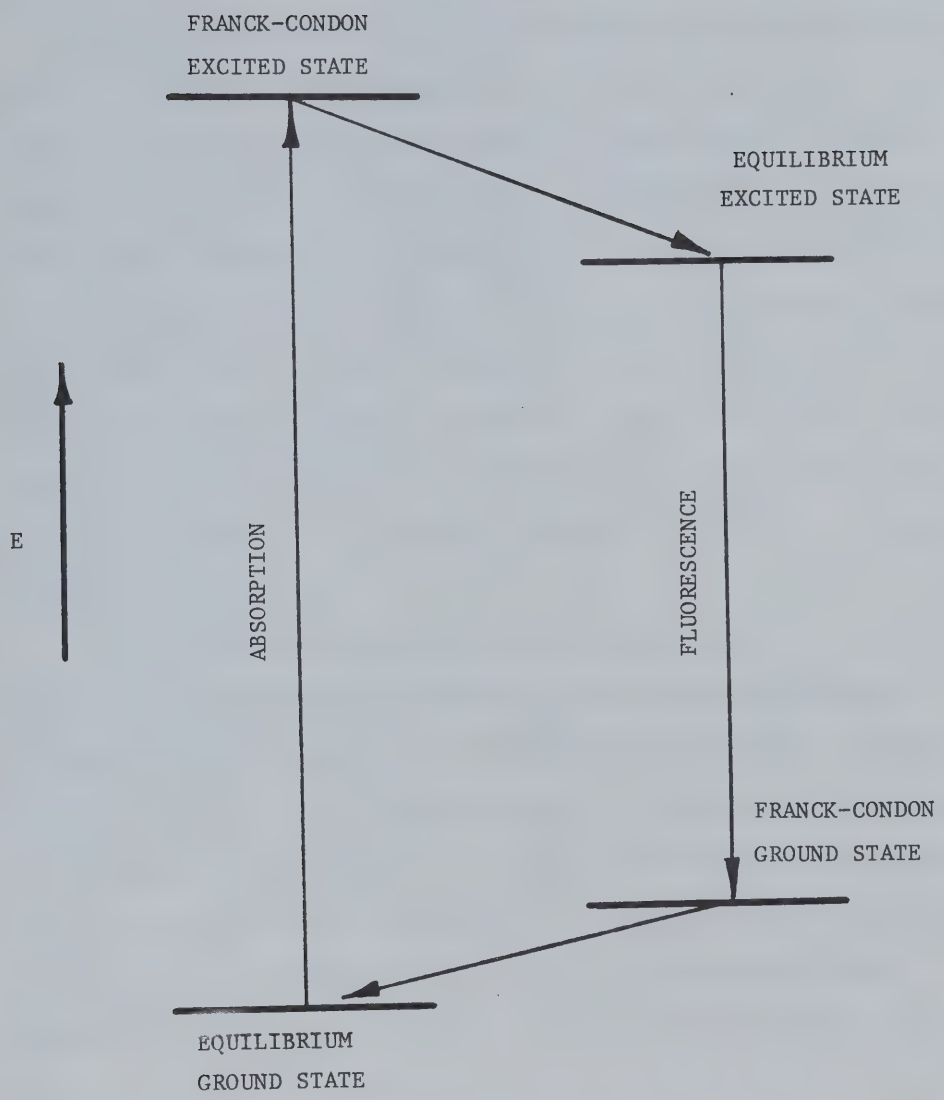

FIGURE 21 . Effect of solvation on the absorption and fluorescence of a luminescent molecule.

to the ground state and $\pi^* \rightarrow \pi$ fluorescence shifts to longer wavelengths.

For molecules containing highly electronegative atoms such as oxygen or nitrogen, the ground state is more easily solvated. In the excited state the charge density around the electronegative atoms is lowered and the resulting dipole moment is considerably less than in the ground state. Increasing the hydrogen bond capacity or the polarity of the solvent in which these molecules are dissolved causes the stability of the ground state to increase relative to the excited state and therefore the absorption wavelength decreases. Since (n,π^*) lowest excited states are commonly associated with fluorescent molecules containing nitrogen or oxygen, $n \rightarrow \pi^*$ absorption incurs a blue shift as solvent polarity is increased.

The influence of external pH on the fluorescence of a molecule containing acidic or basic functional groups is often drastically different from that observed for its absorption spectrum. In order for acid-base reactions in the excited state to perturb fluorescence spectra it is necessary for protolytic dissociation to be appreciably more rapid than the rate constants for fluorescence. Brönsted acidity differences between ground and excited states of organic molecules are large, ranging from 4 to 9 pK_a units (49).[1] As an example of the effect of

---

[1]The pH of a solution is defined as the negative logarithm (base 10) of the hydrogen ion concentration; i.e., $pH = - \log[H^+]$. For one liter of water at 23° C the dissociation $H_2O \rightleftharpoons H^+ + OH^-$ produces a H^+ concentration of 10^{-7} M/l. Thus, neutral pH is 7 and pH values less than or greater than 7 are acidic or basic respectively.

According to the law of mass action the dissociation of a weak acid can be described by an equilibrium constant:

$$K_a = \frac{[H^+]\ [A^-]}{[HA]}$$

external pH, fluorescein exhibits a brilliant yellow-green fluorescence in alkaline solutions and a weaker blue-green fluorescence in acidic solutions (36).

There are two important types of processes by which a solvent or extraneous solute can quench the fluorescence of a molecule in solution.

The first type of process is an interaction between solute and solvent that increases the rates of radiationless processes in the excited state. Most noteworthy of these is the quenching of fluorescence by molecular oxygen. Because O_2 is paramagnetic in the ground state (i.e., triplet ground state) it can induce intersystem crossing in excited solutes and thus decreases the fluorescence yield.

The second of these processes is the direct transfer of the electronic energy from solute to quencher. Direct transfer occurs in one of three ways. If the absorption spectrum of the solvent overlaps in the fluorescence spectrum of the solute then it is possible for the solvent to quench fluorescence by direct absorption. However, unless conditions are ideal this will not occur to any great extent. A more important process involving direct energy transfer is collisional transfer. Collisions are diffusion-controlled and the efficiency of collisional transfer depends on the viscosity of the solvent. The third direct transfer mechanism is known as "long range resonant transfer" or Förster transfer (33). This is a non-radiative intermolecular dipole-dipole transition that does not require close approach of donor and

---

where $HA \rightleftharpoons H^+ + A^-$. The pK_a of an acid is the negative logarithm (base 10) of K_a and thus represents the degree of dissociation.

acceptor. The efficiency of this mechanism can be expressed in terms of a critical separation distance at which the probability of transfer is equal to that of spontaneous decay. This process is only efficient when there is large overlap between emission and absorption spectra of donor and acceptor molecules respectively, and when the fluorescence yield of the donor is high.

The last external influence treated in this section is temperature. In the absence of quenchers, fluorescence efficiency is usually a maximum around room temperature and decreases slowly with increasing temperature. This is because the probability of internal conversion and intersystem crossing increases at higher temperatures which reduces the fluorescence yield. At low temperature the probability of these processes reaches a limiting value corresponding to internal conversion and intersystem crossing from the lowest vibrational level of S'. The variation of fluorescence yield can frequently be represented by the equation (4):

$$\frac{1}{\phi_F} - 1 = A\, e^{-E/RT} \qquad \text{(B.3.1)}$$

APPENDIX C

POLARIZED FLUORESCENCE

C.1 Polarized Fluorescence

As discussed in Appendix B.2 absorption and fluorescence in the visible or near ultraviolet are usually associated with π electron systems. Electron conjugation in most molecules defines fixed axes along which absorption and fluorescence preferentially occur and such molecules may be treated as electric dipole oscillators (19).

The most general classical model of a fluorescent molecule consists of an emission oscillator E and an absorption oscillator A which have different frequencies but are coupled together so that light absorbed along A is reemitted along E. The directions of E and A can coincide but generally intersect at some angle β. Polarized fluorescence is a direct consequence of totally anisotropic (linear) oscillators.

If the emission axes from a group of excited molecules are randomly oriented in solution it follows from symmetry that the subsequent fluorescence will be unpolarized. Thus, in order to produce polarized fluorescence it is necessary that the excited molecules retain a non-random orientation relative to a fixed axis. This is normally a difficult requirement because during the lifetime of the excited state molecular rotation and energy transfer tend to depolarize fluorescence. However, by using a sufficiently viscous solvent and a low enough solute concentration these effects can be minimized (Sections C.2 and C.3). When depolarization from rotation and energy transfer are negligible the degree of polarization of fluorescence depends on three factors; the

method of excitation, the direction of observation, and the coupling angle between A and E in the individual molecules.

The simplest system to analyze is shown in Figure 22 where it is assumed that depolarizing effects are unimportant and where A and E coincide. If this system is irradiated with vertically polarized light ($\vec{E}_0$ along OZ) then for any oscillator the projection of A along $\vec{E}_0$ is proportional to $\cos\theta$ and the probability of excitation is equal to $\cos^2\theta$. Absorption preferentially occurs when A is parallel or nearly parallel to the Z axis and since A and E coincide the same $\cos^2\theta$ dependence applies to fluorescence. Thus for a given number of excited molecules the fluorescence intensity viewed through a plane polarizing filter will be a maximum when the pass direction is oriented parallel to the Z axis and a minimum when oriented perpendicular to the Z axis. This is shown in Figure 22 where the Y axis has been chosen as the direction of observation. For vertically polarized excitation the Z axis is an axis of symmetry and viewed along any direction in the XY plane $I_{\parallel}$ and $I_{\perp}$ remain constant. Equation (A.5.7) is directly applicable and the degree of polarization of fluorescence is given by:

$$P = \frac{I_{max} - I_{min}}{I_{max} + I_{min}} = \frac{I_{\parallel} - I_{\perp}}{I_{\parallel} + I_{\perp}} \qquad (C.1.1)$$

where the subscripts $\parallel$ and $\perp$ refer to directions parallel and perpendicular to the axis of symmetry defined by $\vec{E}_0$ of the exciting light. When equation (A.3.10) is extended to three dimensions the total emitted intensity can be described as the sum of three orthogonal components and because of the symmetry resulting from vertically polarized excitation

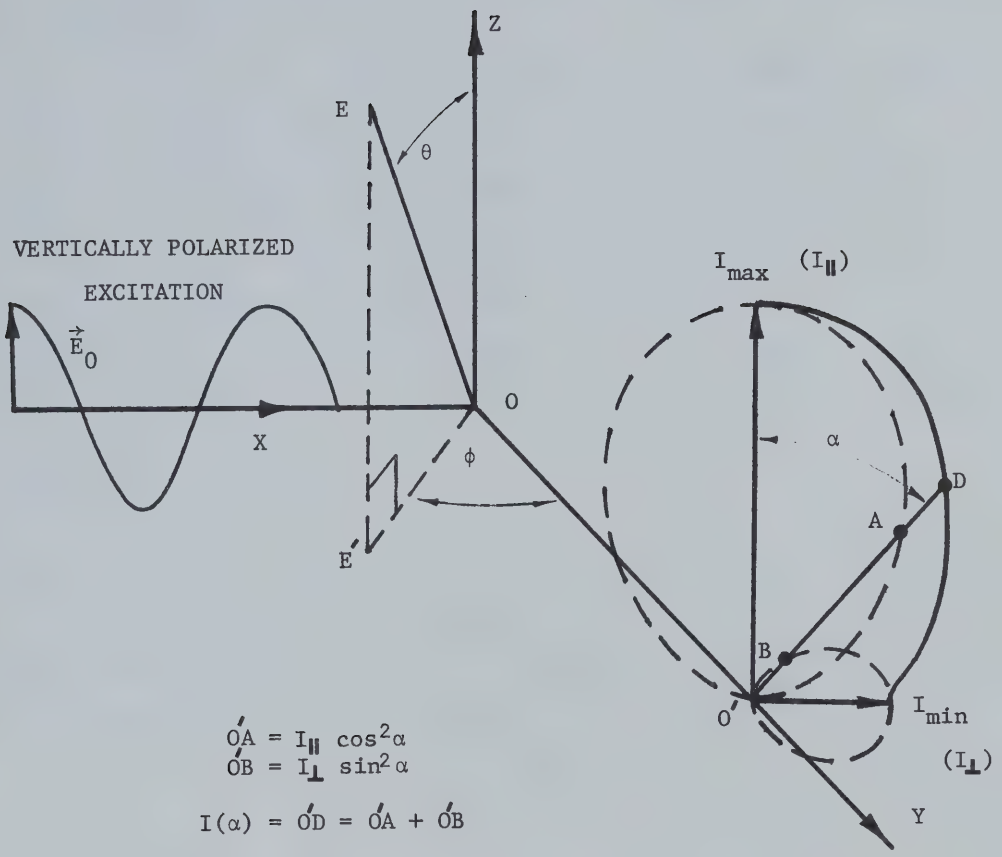

FIGURE 22 . Absorption and emission of a randomly oriented electric dipole oscillator. Absorption and emission axes coincide along OE . If the direction of observation is along the Y axis , the fluorescent intensity viewed through a plane polarizing filter will vary with the orientation of the pass direction α as shown.

$$I_t = I_{\parallel} + 2I_{\perp} \qquad (C.1.2)$$

where $I_{\parallel}$ is the component directed along the Z axis and the two equal $I_{\perp}$ components are in the XY plane.

Equation (C.1.1) employs only one of the $I_{\perp}$ components because the remaining component is parallel to the direction of observation. However, if the direction of observation is inclined at an angle γ to the XY plane (Figure 23) I_{max} becomes the sum of the projections of $I_{\parallel}$ and the second $I_{\perp}$ component along a direction perpendicular to OP and in the plane OPY'. As γ increases the projection of $I_{\parallel}$ is reduced by the factor $\cos^2\gamma$ and that of $I_{\perp}$ is increased by the factor $\sin^2\gamma$. I_{max} can therefore be written:

$$I_{max}(\gamma) = I_{\parallel} \cos^2\gamma + I_{\perp} \sin^2\gamma \qquad (C.1.3)$$

I_{min} is also perpendicular to OP but lies in the XY plane and is therefore independent of γ. From symmetry:

$$I_{min}(\gamma) = I_{\perp} \qquad (C.1.4)$$

and the degree of polarization of fluorescence becomes:

$$P(\gamma) = \frac{(I_{\parallel} \cos^2\gamma + I_{\perp} \sin^2\gamma) - I_{\perp}}{(I_{\parallel} \cos^2\gamma + I_{\perp} \sin^2\gamma) + I_{\perp}} \qquad (C.1.5)$$

From equation (C.1.5) P is a maximum when viewed in the XY plane ($\gamma = 0$) and decreases with increasing γ until the direction of observation coincides with the Z axis and P = 0. Thus for vertically polarized excitation P is normally measured along the Y axis as in Figure 22.

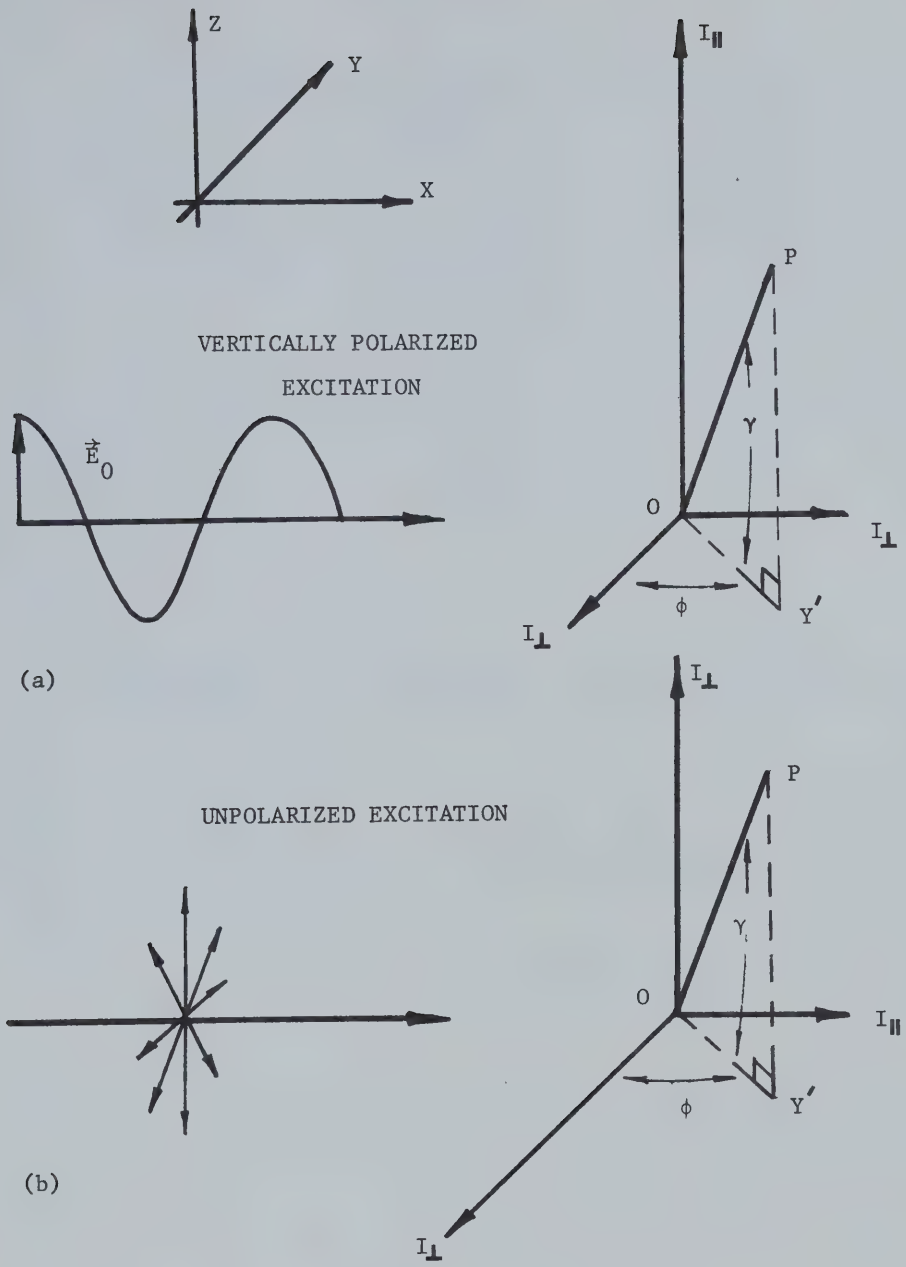

FIGURE 23 . Fluorescent intensity components and symmetries from systems excited by (a) vertically polarized light directed along the X axis (b) unpolarized light directed along the X axis

Polarized fluorescence can also be produced by excitation with unpolarized light. If the same system is excited by a beam of unpolarized light directed along OX then with respect to absorption and fluorescence the X axis will become an axis of symmetry. Equation (C.1.2) can again be applied but for unpolarized excitation the two $I_{\perp}$ components lie in the ZY plane while the $I_{\parallel}$ component lies along the X axis (Figure 23). Because there are two unequal components in the XY plane the degree of polarization does not follow the same format of equation (C.1.5). The method for calculating P is the same however and viewed along OP as in Figure 23:

$$P(\phi,\gamma) = \frac{[(I_{\perp}\cos^2\phi + I_{\parallel}\sin^2\phi)\sin^2\gamma + I_{\perp}\cos^2\gamma] - (I_{\parallel}\cos^2\phi + I_{\perp}\sin^2\phi)}{[(I_{\perp}\cos^2\phi + I_{\parallel}\sin^2\phi)\sin^2\gamma + I_{\perp}\cos^2\gamma] + (I_{\parallel}\cos^2\phi + I_{\perp}\sin^2\phi)} \qquad (C.1.6)$$

where the subscripts refer to directions relative to the axis of symmetry. When $\phi = \gamma = 0$ the direction of observation coincides with the Y axis and equation (C.1.6) reduces to:

$$P = \frac{I_{\perp} - I_{\parallel}}{I_{\perp} + I_{\parallel}} \qquad (C.1.7)$$

This is the maximum value of P obtainable from equation (C.1.6) and therefore for unpolarized excitation, the Y axis is the preferred direction of observation. Although unpolarized excitation is of theoretical interest the degree of polarization of fjuorescence is always greater from systems excited with plane polarized light and for this reason plane polarized excitation is normally used.

In the absence of depolarizing effects and for a given method of excitation, the maximum polarization that may be produced from a system

is referred to as the principal polarization and is designated by P_0. Referring again to Figure 22, the vertical and horizontal intensity components from a single oscillator are given by:

$$I_{\parallel} \propto \cos^2\theta \qquad \text{(C.1.8)}$$

$$I_{\perp} \propto \sin^2\theta \cdot \sin^2\theta \qquad \text{(C.1.9)}$$

If equations (C.1.8) and (C.1.9) are weighted to include the probability of excitation and integrated over θ and ϕ, P_0 can be determined from equations (C.1.1) and (C.1.7). For systems irradiated with vertically polarized light the probability of excitation varies as $\cos^2\theta$ and $P_0 = (I_{\parallel} - I_{\perp})/(I_{\parallel} + I_{\perp}) = 1/2$. If the exciting light in unpolarized $P_0 = (I_{\perp} - I_{\parallel})/(I_{\perp} + I_{\parallel}) = 1/3$. These limiting polarizations can also be obtained by a less formal method. Weber (47) has shown that for n individual oscillators, P may be expressed by:

$$\frac{1}{P} \pm \frac{1}{3} = \frac{1}{\sum_{i=1}^{n} \frac{f_i}{\frac{1}{P_i} \pm \frac{1}{3}}} \qquad \text{(C.1.10)}$$

where the plus sign refers to unpolarized excitation and the minus sign refers to vertically polarized excitation. In equation (C.1.10) P_i is the polarization from the "i"th oscillator and f_i is the contribution from the "i"th oscillator to the total fluorescent intensity, i.e.:

$$f_i = I_i/I_t, \text{ where } \sum_{i=1}^{n} f_i = 1 \qquad \text{(C.1.11)}$$

Since f can represent the probability of excitation and P can be calculated for a given θ and ϕ, equation (C.1.10) can be summed over over

all θ and ϕ to give 1/2 or 1/3 depending on the method of excitation.

The principal polarizations of 1/2 and 1/3 apply only to systems containing molecules whose absorption and emission axes coincide. Jablonski (24) has shown that if the angle between the absorption and emission oscillators is β, the principal polarization can be described by:

$$P_0 = (3 \cos^2\beta - 1)/(\cos^2\beta + 3) \qquad \text{(C.1.12)}$$

for vertically polarized excitation, and

$$P_0 = (3 \cos^2\beta - 1)/(7 - \cos^2\beta) \qquad \text{(C.1.13)}$$

for unpolarized excitation. Because β can only vary between 0 and $\pi/2$, P will lie between the limits of +1/2 and -1/3 for equation (C.1.12) or +1/3 and -1/7 for equation (C.1.13).

The importance of equations (C.1.12) and (C.1.13) is experimentally demonstrated by the variation of the degree of polarization of fluorescence with exciting wavelength. Figure 24 shows the absorption and polarization spectra of a basic glycerol solution of fluorescein.[1]

---

[1]The polarization spectrum, or polarized excitation spectrum, shown in Figure 24 was constructed with data obtained from a Perkin-Elmer MPF-4 spectrophotometer. A description of the instrument is given in Chapter Two. To obtain a polarized excitation spectrum, a sample is irradiated with plane polarized light and the fluorescence intensities parallel and perpendicular to the electric vector of the exciting light are analyzed through a plane polarizing filter. The fluorescence components are observed at a fixed emission wavelength, λ_{em}, while the exciting wavelength is varied from the near ultraviolet through to the visible. The polarization at any exciting wavelength is given by:

$$P(\lambda) = \frac{I_{\parallel}(\lambda) - G \cdot I_{\perp}(\lambda)}{I_{\parallel}(\lambda) + G \cdot I_{\perp}(\lambda)}$$

where G is the grating correction due to the polarization from the

The various peaks in the polarization spectrum correspond to different absorption transitions within the molecule and in accordance with vertically polarized excitation the curve varies between the limits of +1/2 and -1/3. These limiting polarizations cannot be reached experimentally however, and as shown in Figure 24 the maximum and minimum polarizations are .43 and -.23 respectively. Feofilov (18) contends that this is due to incomplete anisotropy in the oscillators and represents a breakdown of the classical model in completely describing polarization phenomenon. Because of incomplete anisotropy, P_0 can never be accurately determined and therefore equation (C.1.12) has limited experimental application. Feofilov has alleviated this problem somewhat by deriving an expression which relates various limiting polarizations to molecular symmetry (18). With this formulation many polarization spectra can be resolved.

C.2 Depolarization by Energy Transfer

In sufficiently viscous solutions where rotational depolarization is minimal Feofilov and Sveshnikoff (19) empirically found that P varies inversely with solute concentration, i.e.:

$$\frac{1}{P} = \frac{1}{P_0} + A \cdot c \cdot \tau \qquad (C.2.1)$$

where τ is the lifetime of the excited state, c is the solute

---

emission monochromator.

For the fluorescein solution, depolarization effects were minimal, and Figure 24 depicts the variation of the principal polarization (P_0) with the exciting wavelength. The wavelength of maximum emission was λ_{em} = 515 nm, and λ_{ex} was varied from 250 nm to 550 nm. At an emission bandwidth of 10 nm (slit width = 3 mm), G was calculated from the method of Azumi and Mclynn (1) to be G = .454. This spectrum agrees with that previously published by Chen and Bowman (17).

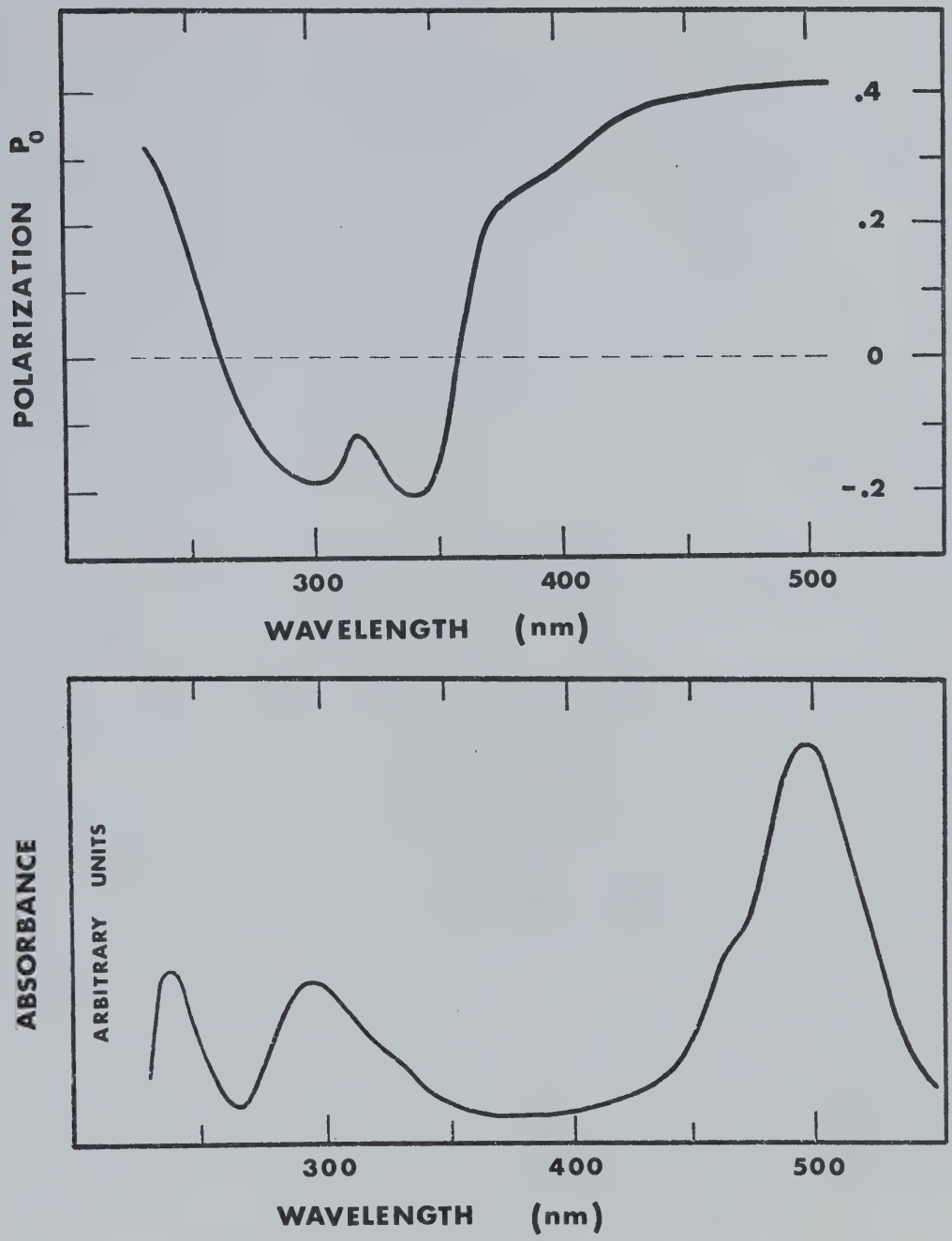

FIGURE 24 . Absorption and polarization spectra of fluorescein , 5×10^{-6} M in 95% glycerol and 5% 0.10 N NaOH by volume, recorded at 10° C.

concentration and P_0 is the principal polarization.

As an example, the polarization from basic glycerol solutions of fluorescein begins to decrease at concentrations > .3 mM and falls to 0 at approximately .03 M. At these concentrations the average intermolecular distance between solute molecules is about three times their kinetic radii and energy transfer can only be explained by Förster transfer (18, Appendix B.3). By considering the probability of long-range energy transfer between two dipole oscillators Weber (45) has derived a concentration-dependent polarization. According to Weber:

$$\frac{1}{P} \pm \frac{1}{3} = \left(\frac{1}{P_0} \pm \frac{1}{3} \right) \cdot \left(1 + \frac{4\pi \cdot N \cdot R_c^6 \cdot 10^{-3}}{15 \cdot (2a)^3} \cdot c \right) \qquad (C.2.2)$$

where the plus sign refers to unpolarized excitation and the minus sign refers to vertically polarized excitation. In equation (C.2.2) P_0 is the principal polarization, N is Avogadro's number, R_c is the critical radius between parallel dipoles at which the probability of emission equals the probability of transfer, 2a is the molecular diameter, and c is the solute concentration in moles/liter.

Applying this result to the data of Feofilov and Sveshnikoff, Weber has calculated a critical radius of 26 Å for fluorescein. By keeping the concentration sufficiently low that the average distance between solute molecules is greater than the critical radius, concentration-dependent polarization can be minimized.

C.3 Rotational Depolarization

When concentration effects are negligible depolarization of fluorescence depends only on the interval between excitation and emission

and on the speed of molecular rotation. Various models have been formulated to describe rotational depolarization and all have been derived from the classical theory of Brownian motion. This theory assumes that equipartition of energy (kT/2 average rotational energy per degree of freedom) applies to the motion of the molecules and that molecular interaction can be described by macroscopic properties. The first analytical description of rotational depolarization was done for spherical molecules by Perrin (35). This was later revised by Soleillet (42), and more recently Weber (48) has extended the theory to include ellipsoidal mollecular geometries.

Following the description by Weber, the angular speed of a molecule rotating in a viscous medium is given by:

$$\omega = \omega_0 \, e^{-(f_r/I)t} \qquad \text{(C.3.1)}$$

where ω_0 is the initial angular speed, I is the moment of inertia of the molecule, and f_r is the damping coefficient which is a function of η the viscosity of the medium and the geometry of the molecule. From equation (C.3.1) it can be shown that the average angle rotated by the molecule in a time interval Δt is:

$$< \Delta\alpha^2 > = 4 \cdot < E > \Delta t / f_r \qquad \text{(C.3.2)}$$

where < > indicates time average and where <E> is the average rotational energy of the molecule. Equation (C.3.2) is a fundamental property of Brownian motion.

The diagram below shows two successive rotations of a molecule about independent axes. The position of a direction rigidly bound to a

sphere lies successively along OA, OB and OC making angles α, β and γ as shown.

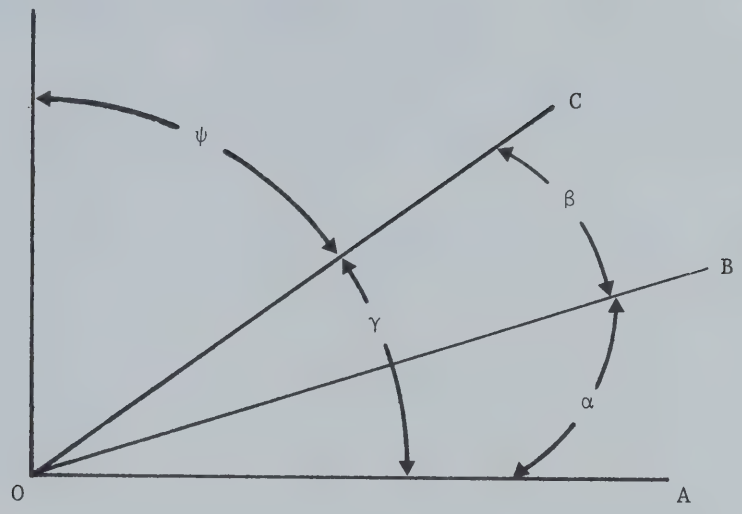

ψ is the azimuth of OC about the plane AOB

From elementary geometry:

$$\cos \gamma = \cos \alpha \cdot \cos \beta + \sin \alpha \cdot \sin \beta \cdot \cos \psi \qquad \text{(C.3.3)}$$

Averaging equation (C.3.3) for a large number of molecules that have undergone two successive rotations:

$$\langle \cos \gamma \rangle_\gamma = \langle \cos \alpha \rangle_\alpha \cdot \langle \cos \beta \rangle_\beta + \langle \sin \alpha \rangle_\alpha \cdot \langle \sin \beta \rangle_\beta \cdot \langle \cos \psi \rangle_\psi \qquad \text{(C.3.4)}$$

If the molecules undergo isotropic rotation all values of ψ are equally probable so that $\langle \cos \psi \rangle_\psi = 0$ and $\langle \cos^2 \psi \rangle_\psi = 1/2$. Thus, by squaring equation (C.3.4):

$$\langle\cos^2\gamma\rangle_\gamma = \langle\cos^2\alpha\rangle_\alpha \cdot \langle\cos^2\beta\rangle_\beta + \frac{\langle\sin^2\alpha\rangle_\alpha \cdot \langle\sin^2\beta\rangle_\beta}{2} \qquad \text{(C.3.5)}$$

or by trigonometric rearrangement:

$$\frac{3\langle\cos^2\gamma\rangle_\gamma - 1}{2} = \frac{3\langle\cos^2\alpha\rangle_\alpha - 1}{2} \cdot \frac{3\langle\cos^2\beta\rangle_\beta - 1}{2} \qquad \text{(C.3.6)}$$

Equation (C.3.6) describes γ as the product of two angular impulses and the effect of any number of individual impulses may be computed in the same way.

For a small rotation α, $\cos^2\alpha = 1 - \sin^2\alpha \simeq 1 - \alpha^2$, and using equation (C.3.2):

$$\cos^2\alpha = 1 - 4 \cdot \langle E\rangle \cdot \Delta t / f_r \qquad \text{(C.3.7)}$$

or

$$\frac{3\cos^2\alpha - 1}{2} = 1 - 6 \cdot \langle E\rangle \cdot \Delta t / f_r \qquad \text{(C.3.8)}$$

The value of $\langle\cos^2\gamma\rangle_\gamma$ at any time t may be calculated by dividing t into an arbitrary number of small intervals and applying equations (C.3.6) and (C.3.8). Thus,

$$\frac{3\langle\cos^2\gamma(t)\rangle_\gamma - 1}{2} = (1 - 6 \cdot \langle E\rangle \cdot \Delta t / f_r)^{t/\Delta t} \qquad \text{(C.3.9)}$$

and for $t/\Delta t \ll 1$:

$$\frac{3\langle\cos^2\gamma(t)\rangle_\gamma - 1}{2} = 1 - e^{-6 \cdot \langle E\rangle \cdot t / f_r} \qquad \text{(C.3.10)}$$

Equation (C.3.10) was derived for isotropic rotation and in general is only applicable to spherical molecules. Since there are two degrees of freedom for the rotational motion of a sphere about two independent axes, the average rotational energy is given by $\langle E \rangle = kT$, where k is Boltzmann's constant and T is the absolute temperature. In addition, the damping coefficient for a sphere rotating in a viscous medium is given from basic hydrodynamics (Kirchoff) as $f_r = 8 \cdot \pi \cdot \eta \cdot r^3$, where r is the radius of the sphere and η is the viscosity of the medium. Substituting these values in equation (C.3.10) and defining:

$$\rho_0 = 4 \cdot \pi \cdot \eta \cdot r^3 / k \cdot T \qquad \text{(C.3.11)}$$

as the rotational relaxation time,

$$\langle \cos^2 \gamma(t) \rangle_\gamma = 1/3 + 2/3 \, e^{-3t/\rho_0} \qquad \text{(C.3.12)}$$

The concept of isotropic rotation is useful because if the average angle of the emission oscillator with a given axis is known at t = 0 the average angle at any further time can be calculated from equation (C.3.6).

From Figure 22 the fluorescent intensity components from a single oscillator were given by equations (C.1.8) and (C.1.9) as $I_\parallel = \cos^2\theta$ and $I_\perp = \sin^2\theta \cdot \sin^2\phi$. For systems irradiated with vertically polarized light all values of ϕ are equally probable and $\langle \sin^2\phi \rangle_\phi = 1/2$. Thus, for all oscillators making an angle θ with the Z axis the contribution to the total perpendicular component is given by:

$$I_\perp = \frac{\sin^2\theta}{2} \qquad \text{(C.3.13)}$$

and the polarization from these oscillators becomes:

$$P_\theta = \frac{I_\parallel - I_\perp}{I_\parallel + I_\perp} = \frac{3\cos^2\theta - 1}{\cos^2\theta + 1} \qquad \text{(C.3.14)}$$

or

$$\frac{1}{P_\theta} - \frac{1}{3} = \frac{2/3}{\frac{3\cos^2\theta - 1}{2}} \qquad \text{(C.3.15)}$$

Using equation (C.1.10), the polarization from all oscillators making variable angles θ is:

$$\frac{1}{P} - \frac{1}{3} = \frac{1}{\sum_{\theta=0}^{\theta=\pi/2} \frac{f(\theta)}{\frac{1}{P_\theta} - \frac{1}{3}}} = \frac{1}{\sum_{\theta=0}^{\theta=\pi/2} f(\theta) \cdot \frac{3\cos^2\theta - 1}{2}} \qquad \text{(C.3.16)}$$

and since $\sum_{\theta=0}^{\theta=\pi/2} f(\theta) = 1$:

$$\frac{1}{P} - \frac{1}{3} = \frac{2/3}{\frac{3\langle\cos^2\theta\rangle_\theta - 1}{2}} \qquad \text{(C.3.17)}$$

The temporal dependence of equation (C.3.17) can be determined by considering the separate polarizations at times 0 and t after excitation. At t = 0:

$$\frac{1}{P_0} - \frac{1}{3} = \frac{2/3}{\frac{3\langle\cos^2\theta(0)\rangle_\theta - 1}{2}} \qquad \text{(C.3.18)}$$

and at time t after excitation:

$$\frac{1}{P_t} - \frac{1}{3} = \frac{2/3}{\frac{3\langle\cos^2\theta(t)\rangle_\theta - 1}{2}} \qquad \text{(C.3.19)}$$

If the rotations are isotropic:

$$\frac{3\langle\cos^2\theta(t)\rangle_\theta - 1}{2} = \frac{3\langle\cos^2\theta(0)\rangle_\theta - 1}{2} \cdot \frac{3\langle\cos^2\alpha(t)\rangle_\alpha - 1}{2} \tag{C.3.20}$$

where $\alpha(t)$ is the angle swept by the emission axes between times 0 and t, and by substituting equation (C.3.20) into (C.3.19):

$$\frac{1}{P_t} - \frac{1}{3} = \left(\frac{1}{P_0} - \frac{1}{3}\right) \cdot \left(\frac{2}{3\langle\cos^2\alpha(t)_\alpha\rangle - 1}\right) \tag{C.3.21}$$

Although equation (C.3.21) expresses P as a function of time, it does not take into account that the number of molecules emitting at any time are distributed according to when they were excited and thus according to the average angle they have rotated relative to their original positions. To calculate the polarization observed at any time after excitation, equation (C.1.10) can be used again giving:

$$\frac{1}{P} - \frac{1}{3} = \frac{1}{\sum_{t=0}^{t=\infty} \frac{f(t)}{\frac{1}{P_t} - \frac{1}{3}}} = \left(\frac{1}{P_0} - \frac{1}{3}\right) \cdot \left(\frac{2}{\sum_{t=0}^{t=\infty} 3\langle\cos^2\alpha(t)\rangle_\alpha \cdot f(t) - 1}\right) \tag{C.3.22}$$

where f(t) is the fraction of the total intensity due to molecules emitting t seconds after excitation. The function f(t) is given by equation (B.1.3) and represents a constant rate of emission, i.e.,

$$f(t) = \frac{e^{-t/\tau}}{\tau} \tag{C.3.23}$$

where τ is the lifetime of the excited state. In the denominator of

equation (C.3.22):

$$\sum_{t=0}^{t=\infty} \langle \cos^2\alpha(t)\rangle_\alpha \cdot f(t) = \int_0^\infty \langle \cos^2\alpha(t)\rangle_\alpha \cdot \frac{e^{-t/\tau}}{\tau}\, dt \qquad \text{(C.3.24)}$$

and since $\langle \cos^2\alpha(t)\rangle_\alpha = 1/3 + 2/3\ e^{-3t/\rho_0}$ for spherical molecules, equation (C.3.24) can be integrated and inserted in equation (C.3.22) giving:

$$\frac{1}{P} - \frac{1}{3} = \left(\frac{1}{P_0} - \frac{1}{3}\right) \cdot \left(1 + \frac{3\tau}{\rho_0}\right) \qquad \text{(C.3.25)}$$

Thus, derived from the classical theory of Brownian motion, rotational depolarization depends on the ratio of the average excited lifetime and the rotational relaxation time of the molecular oscillators.

Equation (C.3.25) has been derived for vertically polarized excitation and a similar derivation for unpolarized excitation yields:

$$\frac{1}{P} + \frac{1}{3} = \left(\frac{1}{P_0} + \frac{1}{3}\right) \cdot \left(1 + \frac{3\tau}{\rho_0}\right) \qquad \text{(C.3.26)}$$

As they appear, equations (C.3.25) and (C.3.26) are difficult to verify experimentally. Since the volume of a molecular sphere of radius r is given by $V = 4/3\pi r^3$, equation (C.3.25) can be modified giving:

$$\frac{1}{P} - \frac{1}{3} = \left(\frac{1}{P_0} - \frac{1}{3}\right) \cdot \left(1 + \frac{kT}{V\eta}\tau\right) \qquad \text{(C.3.27)}$$

Perrin (35) and Pringsheim (36) have verified equation (C.3.27) for several solutions by obtaining a straight line for graphs of $1/P$ against T/η. Although this method is somewhat limited in that it assumes V and

τ are independent of T/η, the experimental evidence corroborates the classical derivation of rotational depolarization.

APPENDIX D

COMPUTER PROGRAM FOR DETERMINING $\dot{P}_c$

The computer program for calculating P_c was written in Fortran and was executed by an Artronix PC-12 interactive system. The system compiler did not accept logical IF statements and therefore the arithmetic IF statement was used. PGCTL is a "system" subprogram for controlling the oscilloscope display and can be deleted for operation on other computers. A minimum memory of 16 K is required to run the program.

The main features of the program are shown by a flow diagram in Figure 10. To provide a least squares fit to $I_{\parallel}$ and $I_{\perp}$ data, a subroutine CURF was used which is a modification of a program originally designed by Bevington (3). The important variables in the program are given in the following list.

X = reaction time

Y = $I_{\parallel}$ and $I_{\perp}$ data

G = grating correction factor

S = standard deviation in the $I_{\parallel}$ and $I_{\perp}$ points

R = corrected ratio of $\parallel$ and $\perp$ background components

BB = $\parallel$ background component (Figure 8)

TF = fictitious time of filtration

C = least squares fit to quadratic polynomial for $I_{\parallel}$ data

B = least squares fit to quadratic polynomial for $I_{\perp}$ data

FB = starting filtrate ($I_{\parallel}^{e}$) for the search for optimum P_c

DFB = $\Delta I_{\parallel}^{e}$

MNM = number of iterations

CLCD1 = subprogram which calculates K_D from a value of $I_{\parallel}^{e}$ or $I_{\perp}^{e}$ at a particular time

DB = $K_D^{\parallel}$

DC = $K_D^{\perp}$

PT = total polarization P(t)

PC = polarization from the cytoplasm $P_c(K_D,t)$

PF = background polarization $P_b(t)$

YET1 = equation (2.5.13) for $I_{\parallel}^{e}(t)$ and $I_{\perp}^{e}(t)$

IC = R_i from equation (2.4.4)

PVM(1) = K_D

PVM(2) = $\langle P_c \rangle$

PVM(3) = σ_p

```
      DIMENSION X(30),Y(30),SGMY(30),A(3),DLTA(3),SGMA(3),YFT(30)
      DIMENSION X1(30),Y1(30),B(3),C(3),V1(8),V2(8),V3(8),V4(8)
      DIMENSION V5(8),PVM(15,3)
      CALL PGCTL(1)
99    READ(1,1)G,BB,R,S
1     FORMAT(" "," G=",F10.4," BB=",F10.4," R=",F10.4," S=",F10.4)
      READ(1,100)TF
100   FORMAT(" "," TF=",F10.4)
      READ(1,2)NPTS,NTRMS,MODE,N
2     FORMAT(" "," NPTS=",I4," NTRMS=",I4," MODE=",I4," N=",I4)
      BC = BB*R
      DO 114 I=1,2
      DO 3 IA=1,NPTS
      READ(1,4)X(IA),Y(IA)
4     FORMAT(" "," X=",E13.5," Y=",E13.5)
      IF(I-2)6,5,5
5     Y(IA)=Y(IA)*G
6     SGMY(IA)=S
3     CONTINUE
      K=NPTS-N
      DO 7 IB=1,K
      X1(IB)=X(IB+N)
      Y1(IB)=Y(IB+N)
7     CONTINUE
      DO 8 IC=1,NTRMS
      DLTA(IC)=.005
8     CONTINUE
      A(1)=BB
      IF(I-2)9,10,10
10    A(1)=BC
9     A(2)=1.5
      A(3)=-.005
      FL=.001
11    CALL CURF(X1,Y1,SGMY,K,NTRMS,MODE,A,DLTA,SGMA,FL,YFT,CHI)
      DO 12 ID=1,NTRMS
      WRITE(1,13)A(ID)
13    FORMAT(" "," A=",E13.5)
12    CONTINUE
      WRITE(1,14)CHI
14    FORMAT(" "," CHI=",E13.5)
      READ(1,15)IE
15    FORMAT(" "," REFIT WITH NO.  .GE. 1 ",I4)
      IF(IE-1)16,11,11
16    V=YTT1(A,TF)
      IX=NPTS+1
      X(IX)=TF
      Y(IX)=V
      FL=.001
17    CALL CURF(X,Y,SGMY,IX,NTRMS,MODE,A,DLTA,SGMA,FL,YFT,CHI)
      WRITE(1,21)CHI
21    FORMAT(" "," CHI=",E13.5)
      DO 18 IG=1,NTRMS
      WRITE(1,19)A(IG),SGMA(IG)
19    FORMAT(" "," A=",E13.5," S=",E13.5)
```

```
18    CONTINUE
      READ(1,20)IH
20    FORMAT(" "," REFIT WITH NO.  .GE.  1  ",I4)
      IF(IH-1)22,17,17
22    DO 23 II=1,IX
      IF(I-2)24,25,25
25    YFT(II)=YFT(II)/G
24    WRITE(1,26)YFT(II)
26    FORMAT(" "," YFT=",E13.5)
23    CONTINUE
      DO 114 IJ=1,NTRMS
      IF(I-2)28,29,29
29    C(IJ)=A(IJ)
      GO TO 114
28    B(IJ)=A(IJ)
114   CONTINUE
C
C     CALCULATION OF POLARIZED FLUORESCENCE
C
86    READ(1,80)FB,DFB,MNM
80    FORMAT(" "," FB=",F10.4," DFB=",F10.4," MNM=",I4)
      DO 150 IS=1,MNM
      PVM(IS,1)=FB
      FC=FB*R
      CALL CLCD1(B,FB,TF,DB)
      CALL CLCD1(C,FC,TF,DC)
      SUMP=0.
      T=10.
      DO 81 IK=1,8
      P1=YTT1(B,T)
      P2=YET1(B,DB,T)
      P3=YTT1(C,T)
      P4=YET1(C,DC,T)
      PT=(P1-P3)/(P1+P3)
      PC=((P1-P2)-(P3-P4))/((P1-P2)+(P3-P4))
      PF=(P2-P4)/(P2+P4)
      V1(IK)=PT
      V2(IK)=PC
      V3(IK)=PF
      V4(IK)=1. - ((P2+P4)/(P1+P3))
      SUMP=SUMP+V2(IK)
      T=T+2.
81    CONTINUE
      PA=SUMP/8.
      PVM(IS,2)=PA
      SUMS=0.
      DO 82 J=1,8
      V5(J)=ABS(PA-V2(J))**2
      SUMS=SUMS+V5(J)
82    CONTINUE
      SP=SQRT(SUMS)
      PVM(IS,3)=SP
      FB=FB+DFB
150   CONTINUE
```

```
      WRITE(1,83)
83    FORMAT(" ",10X,"FB",15X,"PA",15X,"SP")
      DO 151 IT=1,MNM
      WRITE(1,152)PVM(IT,1),PVM(IT,2),PVM(IT,3)
152   FORMAT(" ",5X,F10.4,5X,F10.4,5X,E13.5)
151   CONTINUE
      PAUSE
      READ(1,84)IL,IM
84    FORMAT(" "," READ FLT WITH 1 ",I4," VIEW PTS WITH 1  ",I4)
      IF(IM-1)85,88,88
88    T=10.
      WRITE(1,91)
91    FORMAT(" ",7X,"T",11X,"PT",11X,"PC",11X,"PF",11X,"IC")
      DO 93 IN=1,8
      WRITE(1,90)T,V1(IN),V2(IN),V3(IN),V4(IN)
90    FORMAT(" ",2X,F10.4,2X,F10.4,2X,F10.4,2X,F10.4,2X,F10.4)
      T=T+2.
93    CONTINUE
85    IF(IL-1)89,86,86
89    GO TO 99
      STOP
      END
C
C     CURVE FITTING SUBROUTINE
C
      SUBROUTINE CURF(X,Y,SGMY,NPTS,NTRMS,MODE,A,DLTA,SGMA,FL,YFT,CHI)
      DIMENSION X(25),Y(25),SGMY(25),A(3),DLTA(3),SGMA(3),YFT(25)
      DIMENSION WT(100),ALP(10,10),BET(10),DRIV(10),ARRAY(10,10),B(10)
11    NFREE=NPTS-NTRMS
      IF(NFREE)13,13,20
13    CHI=0.
      GO TO 110
20    DO 30 I=1,NPTS
21    IF(MODE)22,27,29
22    IF(Y(I))25,27,23
23    WT(I)=1./Y(I)
      GO TO 30
25    WT(I)=1./(-Y(I))
      GO TO 30
27    WT(I)=1.
      GO TO 30
29    WT(I)=1./SGMY(I)**2
30    CONTINUE
31    DO 34 J=1,NTRMS
      BET(J)=0.
      DO 34 K=1,J
34    ALP(J,K)=0.
41    DO 50 I=1,NPTS
      CALL FDRIV(X,I,A,DLTA,NTRMS,DRIV)
      DO 46 J=1,NTRMS
      BET(J)=BET(J)+WT(I)*(Y(I)=QPOL(X,I,A))*DRIV(J)
      DO 46 K=1,J
46    ALP(J,K)=ALP(J,K)+WT(I)*DRIV(J)*DRIV(K)
50    CONTINUE
```

```
51    DO 53 J=1,NTRMS
      DO 53 K=1,J
53    ALP(K,J)=ALP(J,K)
61    DO 62 I=1,NPTS
62    YFT(I)=QPOL(X,I,A)
63    CHI1=FCHI(Y,SGMY,NPTS,NFREE,MODE,YFT)
71    DO 74 J=1,NTRMS
      DO 73 K=1,NTRMS
73    ARRAY(J,K)=ALP(J,K)/SQRT(ALP(J,J)*ALP(K,K))
74    ARRAY(J,J)=1.+FL
80    CALL MINV(ARRAY, NTRMS, DET)
81    DO 84 J=1,NTRMS
      B(J)=A(J)
      DO 84 K=1,NTRMS
84    B(J)=B(J)+BET(K)*ARRAY(J,K)/SQRT(ALP(J,J)*ALP(K,K))
91    DO 92 I=1,NPTS
92    YFT(I)=QPOL(X,I,B)
93    CHI=FCHI(Y,SGMY,NPTS,NFREE,MODE,YFT)
      IF(CHI1-CHI)95,101,101
95    FL=10.*FL
      GO TO 71
101   DO 103 J=1,NTRMS
      A(J)=B(J)
103   SGMA(J)=SQRT(ARRAY(J,J)/ALP(J,J))
      FL=FL/10.
110   RETURN
      END

C
C     REDUCED CHI SQUARE FIT FUNCTION
C
      FUNCTION FCHI(Y,SGMY,NPTS,NFREE,MODE,YFT)
      DIMENSION Y(25),SGMY(25),YFT(25)
11    CHI=0.
12    IF(NFREE)13,13,20
13    FCHI=0.
      GO TO 40
20    DO 30 I=1,NPTS
21    IF(MODE)22,27,29
22    IF(Y(I))25,27,23
23    WT=1./Y(I)
      GO TO 30
25    WT=1./(-Y(I))
      GO TO 30
27    WT=1.
      GO TO 30
29    WT=1./SGMY(I)**2
30    CHI=CHI+WT*(Y(I)-YFT(I))**2
31    FREE=NFREE
32    FCHI=CHI/FREE
40    RETURN
      END
```

```
C
C     MATRIX INVERSION AND DETERMINANT SUBROUTINE
C
      SUBROUTINE MINV(ARRAY,NORD,DET)
      DIMENSION ARRAY(10,10),IK(10),JK(10)
10    DET=1.
11    DO 100 K=1,NORD
      AMAX=0.
21    DO 30 I=K,NORD
      DO 30 J=K,NORD
23    IF(ABS(AMAX)-ABS(ARRAY(I,J)))24,24,30
24    AMAX=ARRAY(I,J)
      IK(K)=I
      JK(K)=J
30    CONTINUE
31    IF(AMAX)41,32,41
32    DET=0.
      GO TO 140
41    I=IF(K)
      IF(I-K)21,51,43
43    DO 50 J=1,NORD
      SAVE=ARRAY(K,J)
      ARRAY(K,J)=ARRAY(I,J)
50    ARRAY(I,J)=-SAVE
51    J=JK(K)
      IF(J-K)21,61,53
53    DO 60 I=1,NORD
      SAVE=ARRAY(I,K)
      ARRAY(I,K)=ARRAY(I,J)
60    ARRAY(I,J)=-SAVE
61    DO 70 I=1,NORD
      IF(I-K)63,70,63
63    ARRAY(I,K)=-ARRAY(I,K)/AMAX
70    CONTINUE
71    DO 80 I=1,NORD
      DO 80 J=1,NORD
      IF(I-K)74,80,74
74    IF(J-K)75,80,75
75    ARRAY(I,J)=ARRAY(I,J)+ARRAY(I,K)*ARRAY(K,J)
80    CONTINUE
81    DO 90 J=1,NORD
      IF(J-K)83,90,83
83    ARRAY(K,J)=ARRAY(K,J)/AMAX
90    CONTINUE
      ARRAY(K,K)=1./AMAX
100   DET=DET*AMAX
101   DO 130 L=1,NORD
      K=NORD-L+1
      J=IK(K)
      IF(J-K)111,111,105
105   DO 110 I=1,NORD
      SAVE=ARRAY(I,K)
      ARRAY(I,K)=-ARRAY(I,J)
110   ARRAY(I,J)=SAVE
```

```
111   I=JK(K)
      IF(I-K)130,130,113
113   DO 120 J=1,NORD
      SAVE=ARRAY(K,J)
      ARRAY(K,J)=-ARRAY(I,J)
120   ARRAY(I,J)=SAVE
130   CONTINUE
140   RETURN
      END

C
C     QUADRATIC POLYNOMIAL FUNCTION
C
      FUNCTION QPOL(X,I,A)
      DIMENSION X(25),A(3)
      XI=X(I)
      QPOL=A(1)+A(2)*XI+A(3)*XI**2
      RETURN
      END

C
C     DERIVATIVE OF QUADRATIC POLYNOMIAL SUBROUTINE
C
      SUBROUTINE FDRIV(X,I,A,DLTA,NTRMS,DRIV)
      DIMENSION X(25),A(3),DLTA(3),DRIV(3)
      XI=X(I)
      DRIV(1)=1.
      DRIV(2)=XI
      DRIV(3)=XI**2
      RETURN
      END

C
C     TOTAL FLUORESCENCE FUNCTION
C
      FUNCTION YTT1(A,T)
      DIMENSION A(3)
      F=A(1)
      F1=A(2)
      F2=A(3)
      YTT1=F+F1*T+F2*T**2
      RETURN
      END
```

```
C
C     BACKGROUND FLUORESCENCE FUNCTION
C
      FUNCTION YET1(A,DK,T)
      DIMENSION A(3)
      F=A(1)
      F1=A(2)
      F2=A(3)
      F3=(F1/DK-2.*F2/DK**2)*EXP(-DK*T)
      F4=F+F1*T+F2*T**2
      F5=-(F1+2.*F2*T)/DK
      F6=2.*F2/DK**2
      YET1=F3+F4+F5+F6
      RETURN
      END


C
C     DIFFUSION COEFFICIENT SUBROUTINE
C
      SUBROUTINE CLCD1(A,F,T,D)
      DIMENSION A(3)
      D=.1
9     V=YET1(A,D,T)
      IF(F-V)1,4,3
1     D=D-.01
      GO TO 9
3     D=D+.0001
      V=YET1(A,D,T)
      IF(F-V)4,43
4     WRITE(1,10)D,F,V
10    FORMAT(" "," D=",E13.5,"  F=",F8.3,"  V=",F8.3)
      RETURN
      END
```